



**KTH Architecture and
the Built Environment**

***Model Uncertainty of Design Tools to Analyze
Block Stability***

Mehdi Bagheri

Licentiate Thesis

Division of Soil and Rock Mechanics

Division of Civil and Architectural Engineering

Royal Institute of Technology

Stockholm, 2009

TRITA-JOB LIC 2014

ISSN 1650-95IX

Abstract:

Block failure is one of the most common failure modes in tunnels. Design tools have some simplifications and, therefore, they also have some model uncertainties. The purpose of this licentiate thesis is to assess the model uncertainty for different design tools in order to estimate block stability.

Different approaches of kinematic limit equilibrium (KLE) including conventional KLE, limited joint length, limited joint length and stress field consideration and probabilistic KLE were compared to that of DFN-DEM. In this approach, the results of the calibrated DFN-DEM with field mapping were considered to be of true value. The results show that the conventional KLE is overdesign due to its over simplification. By considering fracture length and stress field, the volume of predicted unstable blocks is reduced. The probabilistic approach of KLE by considering finite joint length and stress field predicts the volume of unstable blocks to be lower than DFN-DEM approach. Therefore there is a great model uncertainty of our standard design tools for block stability analysis.

The assumption made in this study is that the results from DEM were considered to have a true value; the results from analytical solution based on joint relaxation process were compared to those of DEM in a different condition of depth, K_0 , apical and friction angle, K_n and K_s value, and ratio of K_n/K_s . The comparison shows that for shallow depth with K_0 less than 1, analytical solution leads to an overestimation of block stability. The analytical solution predicts that the block is stable, while the analyses from numerical solution show the block is unstable. The analyses show that by increasing K_0 , accuracy of analytical solution also increases. Moreover, for the cases with close value of friction angle to semi-apical angle, the use of analytical solution is not recommended. As the ratio of K_n/K_s increases, the accuracy of analytical solution decreases. Increasing the angle ratio (ratio between semi-apical angle to friction angle) is one source of increasing uncertainty in the model. The analytical solution is very uncertain in cases with a low value of K_0 , and a high value of stiffness ratio and angle ratio. On the other hand, the analytical solution is more certain in conditions with a high value of K_0 and a low value of stiffness ratio and angle ratio. According to current information (K_0 , angle ratio, stiffness ratio), one can determine the value of model uncertainty by using the diagrams presented in Chapter 6 of the thesis. The analyses show that by having more information about the key parameters, the model uncertainty could be identified more precisely. However, having more information means spending more money, and this increase in cost must be compared to the cost of failure or delay in the project or overdesign.

Sammanfattning:

Blockutfall är en av de vanligaste brottformerna i tunnlar. Dimensioneringsverktyg har förenklingar och därför har de viss modellosäkerhet. Syftet med licentiat avhandlingen är att bedöma modellosäkerhet för olika dimensioneringsverktyg för att uppskatta blockstabilitet.

I Olika metoder av KLE inkluderad konventionell KLE, begränsad spricklängd och insitu spänning och sannolikhetsbaserad KLE är jämförda med DFN-DEM. I den här metoden kalibreras DFN-DEM med fältkartläggning som är betraktad som sanna värden. Resultat visar att konventionell KLE ger starkt konservativa resultat. Genom att betrakta spricklängden och spänningsfältet, så minskar volymen på uppskattade instabila block. Den sannolikhetsbaserade metoden för KLE genom att betrakta finit spricklängd, och spänningsfältet förutsätter att volymen av de instabila blocken är mindre än de som bedöms med DFN-DEM metoden. Det finns mycket osäkerhet i vår standard dimensioneringsverktyg att uppskatta block stabilitet.

Antagande som gjorts i den studien är att resultatet från DEM är betraktade som sanna värden och resultaten från analytiska lösningar baserad på sprickavlastning är jämförda med resultatet från DEM. Jämförelse visar att för grunda djup och med K_0 mindre än 1, den analytiska lösningen leder till en överestimering av blockstabiliteten. Den analytiska lösningen förutsäger att blocket är stabilt medan analys av den numeriska lösningen visar att blocket är instabilt. Analysen visar att genom en ökning av K_0 så ökar tillförlitligheten av den analytiska lösningen. Det visar sig att även att för fall med friktionsvinkel nära semitoppvinkeln så kan den analytiska lösningen inte rekommenderas. Vidare leder en ökning av förhållandet K_n/K_s till att tillförlitligheten av den analytiska lösningen minskar. En ökning av vinkelförhållandet mellan semitoppvinkeln och friktionsvinkeln är källa till en ökning av osäkerhet i modellen. En analytisk lösning är mer osäker i fall av lågt värde på K_0 och högt värde på styvhetsförhållandet och vinkelförhållandet. Å andra sidan, så är den analytiska lösningen mer säker i fall av högt värde på K_0 , och lågt värde på vinkel förhållandet och styvhetsförhållandet.

Vid given information (K_0 , styvhetsvärde och vinkel förhållande) kan man bestämma värdet på modellosäkerheten genom att använda diagrammen i avhandlingen. Analysen visar att vid ökad information om nyckelparametrarna, så kan modellosäkerheten identifieras mer exakt. Hur som helst så betyder mer tillgång till information att mer pengar måste satsas och denna kostnad måste gemföras med kostnader för blockinstabilitet eller överdesign.

Acknowledgements

This licentiate thesis concerns the model uncertainty of design tools to solve the problem of block stability. Design tools such as analytical and kinematic limit equilibrium have been compared to distinct element method, which is closer to reality.

The study was initiated and supervised by Professor Håkan Stille and conducted at the Division of Soil and Rock Mechanics at Royal Institute of Technology.

The Swedish Rock Engineering Research Foundation (BeFo) financially supported this project.

I would like to thank all those who made this research possible. Special thanks goes to Professor Håkan Stille for his fruitful discussions and unwavering encouragement. I must mention that, without his help and support, this research would not have been possible. I am, therefore, deeply indebted to him. Also I want to thank my second advisor, Staffan Hintze. I also wish to thank Tomas Franzén and Mikael Hellsten for their interest in the project. I want to thanks Eva Friedman from SveBeFo. The reference group is thanked for their comments and discussions, which made this work better. Anders Fredrikson from Golder Association, Mats Holmberg from Tunnel Engineering, Rolf Christiansson from SKB, Olle Olofsson from Banvarket, Jonny Sjöberg, Erling Nordlund and Kelvis Prez from LTU, Lars O Ericksson and Mirijam Zetterlund from Chalmers are all greatly appreciated. Dr. Baghbanan from Isfahan University of Technology is thanked for his constructive discussions. Mark Christianson from Itasca consulting group is also highly acknowledged. Karyn McGettigan is appreciated for editing the text and improving the language. Special thanks go to my parents and to my girl friend Katayoun who have always encouraged me.

Finally, my gratitude goes to all of my colleagues at Division of Soil and Rock Mechanics, especially Lena Wennerlund.

Stockholm, June 2009

Mehdi Bagheri

List of Publications

This thesis incorporates 3 papers on the subject of model uncertainty design tools to estimate block stability:

- G. Nord, M. Bagheri, A. Baghbanan and H. Stille 'Design consideration of large caverns by using advanced drilling equipments', *Felsbau* Vol 25(5) PP131-136, 2007
- M. Bagheri, A. Baghbanan, H. Stille, 'Some aspects on model uncertainty in the calculation of block stability using Kinematic Limit Equilibrium', *ARMAROCKS* 08.2008
- M. Bagheri, H. Stille, 'Some aspects of model uncertainties of block stability estimation', *ARMS2008*, Tehran, PP 675-681, 2008

Table of Contents

1 INTRODUCTION	<u>1</u>
1-1-BACKGROUND	<u>1</u>
1-2- THESIS OBJECTIVE	<u>2</u>
1-3-KEY BLOCK THEORY	<u>3</u>
1-4- DESIGN TOOLS TO ANALYZE BLOCK STABILITY	<u>6</u>
1-4- IMPORTANT PARAMETERS OF BLOCK STABILITY ANALYSIS	<u>8</u>
2 UNCERTAINTIES RELATED TO ANALYZING BLOCK FAILURE	<u>10</u>
2-1- INTRODUCTION	<u>11</u>
2-2- BLOCK GEOMETRIC UNCERTAINTY	<u>14</u>
2-3- JOINT MECHANICAL PARAMETERS UNCERTAINTIES	<u>15</u>
2-4- MODEL UNCERTAINTIES	<u>16</u>
2-5- CONCLUSIONS	<u>18</u>
3 DESIGN TOOLS USED TO ESTIMATE BLOCK VOLUME	<u>20</u>
3-1- INTRODUCTION	<u>21</u>
3-2- GENERAL ASPECTS OF KINEMATIC ANALYSIS	<u>22</u>
3-3- KINEMATIC ANALYSIS WITH INFINITE JOINT LENGTH	<u>24</u>
3-4- KINEMATIC ANALYSIS WITH FINITE JOINT LENGTH	<u>24</u>
3-4-1- DETERMINISTIC APPROACH OF KINEMATIC ANALYSIS	<u>25</u>
3-4-2- PROBABILISTIC APPROACH OF KINEMATIC ANALYSIS	<u>25</u>
3-5- DISCRETE FRACTURE NETWORK (DFN)	<u>27</u>
3-6- PROBLEM IN DFN REALIZATION	<u>28</u>
3-7- DISCUSSION AND CONCLUSION ON DESIGN TOOLS FOR BLOCK EXISTENCE AND VOLUME	<u>30</u>
4 DESIGN TOOLS USED TO SOLVE BLOCK STABILITY BASED ON LITERATURE SURVEY	<u>32</u>
4-1- INTRODUCTION	<u>33</u>
4-2- ANALYTICAL SOLUTIONS	<u>34</u>
4-2-1- ANALYTICAL SOLUTION BASED ON LIMIT EQUILIBRIUM MECHANICS	<u>34</u>
4-2-2- ANALYTICAL SOLUTION BASED ON JOINT RELAXATION	<u>37</u>
4-2-3- CONCLUSION FOR ANALYTICAL SOLUTIONS	<u>42</u>
4-3- NUMERICAL METHODS	<u>43</u>
4-3-1- DISCRETE ELEMENT METHODS	<u>44</u>
4-4- CONCLUSIONS OF NUMERICAL METHODS	<u>52</u>
4-5- CONCLUSIONS	<u>52</u>
5 MODEL UNCERTAINTY OF KINEMATIC AND LIMIT EQUILIBRIUM	<u>54</u>
5-1- INTRODUCTION	<u>55</u>
5-2- CLAB2 CAVERN AND ROCK MASS DESCRIPTION	<u>57</u>
5-3- CONVENTIONAL KINEMATIC LIMIT EQUILIBRIUM ANALYSIS	<u>61</u>
5-4- KINEMATIC ANALYSIS CONSIDERING JOINT LENGTH	<u>64</u>
5-5- KINEMATIC ANALYSIS WITH CONSIDERING JOINT LENGTH AND STRESS FIELD	<u>66</u>
5-6- PROBABILISTIC KINEMATIC ANALYSIS	<u>68</u>
5-7- DFN GENERATIONS	<u>71</u>
5-7-1- FRACTURE TRACE LENGTHS	<u>71</u>
5-7-2- ORIENTATION OF FRACTURE	<u>72</u>
5-7-3- LOCATION OF FRACTURES	<u>72</u>
5-7-4-FRACTURE GENERATION USING MONTE CARLO SIMULATION	<u>74</u>

Table of Contents

5-8- <i>CALIBRATION OF DFN</i>	<u>75</u>
5-9- <i>DFN-DEM</i>	<u>76</u>
5-10- <i>DISCUSSION</i>	<u>80</u>
5-11- <i>CONCLUSIONS</i>	<u>83</u>
6 <i>MODEL UNCERTAINTY OF BRAY-CRAWFORD SOLUTION</i>	<u>84</u>
6-1- <i>INTRODUCTION</i>	<u>85</u>
6-2- <i>METHODOLOGY USED TO ASSESS MODEL UNCERTAINTY</i>	<u>85</u>
6-2-1- <i>MONTE CARLO SIMULATION</i>	<u>87</u>
6-3- <i>PRIMARY STUDY</i>	<u>87</u>
6-4- <i>RESULTS MODEL UNCERTAINTY IN THE ABSENCE OF IN-SITU VERTICAL STRESS</i>	<u>88</u>
6-5- <i>RESULTS MODEL UNCERTAINTY IN THE PRESENCE OF IN-SITU VERTICAL STRESS</i>	<u>90</u>
6-6- <i>DETAIL STUDY OF MODEL UNCERTAINTY OF ANALYTICAL SOLUTION</i>	<u>92</u>
6-7- <i>RESULT OF SIMULATIONS</i>	<u>101</u>
6-8- <i>DISCUSSION</i>	<u>102</u>
6-9- <i>CONCLUSIONS</i>	<u>116</u>
7 <i>REMARKS AND CONCLUSIONS</i>	<u>118</u>
8 <i>REFERENCES</i>	<u>122</u>
<i>APPENDIX</i>	<u>132</u>

Chapter 1

Introduction

1Introduction

1-1 Background

Several failure modes may occur around underground openings. One of the most common observed failure modes in underground openings is block failure. Fractures cross each other in the perimeter of excavation and they make blocks with different sizes, which may have the potential to fail. The excavation alters the magnitude and direction of stress, and this creates changes in the forces that act on the located blocks in the perimeter of excavation. The potential unstable blocks could slide, fall out from the roof or rotate (Mauldon and Goodman, 1990). Stability of blocks depends on block shape, size, and stresses around the opening. Block shape and size depends on the fracture pattern. The stresses around the opening depend on the shape of the opening and in-situ stresses. In order to assess the stability of the opening, potential unstable blocks must be recognized and stresses around the opening analyzed. In the case of instability, required rock support must be estimated. The block stability includes the interactions between blocks, block geometry, forces, and support. Analyzing this type of failure mode is a complex problem.

The purpose of design of an underground opening is to predict the stability with a certain amount of confidence. The reliability of the predictions is influenced by the uncertainties involved. Three different kinds of uncertainties are normally geometric uncertainty, parameters uncertainties, and uncertainties in the design tools. Model uncertainty plays an important role in the reliability analysis and the design of rock support. One example of the influence of model uncertainty on the design could be seen in the design based on ultimate limit state. The design based on the ultimate limit state requires a definition of a performance function. Performance function is usually based on a standard deterministic design tool. Model uncertainty is associated with imperfect representation of reality and simplifications in the design tool. The designer needs to know how to properly represent model uncertainty in a limit state design. According to the Eurocode, there is no recommendation for the design of openings against block failure based on reliability analysis or observational method. Based on the author's knowledge, no publication exists on model uncertainty for block failure in underground openings. For this reason, the model uncertainty for the different block failure design tools is evaluated in this thesis.

1-2 Thesis Objectives:

The objective of this thesis is to identify the advantages and disadvantages of the different design tools used to analyze block stability, as well as to assess the model uncertainty of the different design tools. Available design tools used to analyze block failure could be divided into design tools to estimate block volume (kinematic analysis and Discrete Fracture Network) and design tools to analyze the equilibrium of the block (analytical solutions and numerical solutions).

Limitations

Model uncertainty can only be quantified either by comparison with other more involved models that exhibit a closer representation of the nature or by comparison with collected data from the field or the laboratory (Ditievsen, 1982). The author has not found any recorded case in which failed block geometry, volume, resistance parameters, stresses were measured. Therefore, the results of different design tools have been compared to those, which are more closely representative of nature.

The model uncertainty is estimated for static design tools. Effects of dynamic loading on the block stability are not considered. However, this is out of the scope of this thesis.

1-3 Key Block Theory

Key block theory is a method used to find blocks that have the potential for failure, and to secure them in order to reach to a desirable level of safety. There are two different methods used to find the key blocks. Goodman and Shi (1985) presented the first theory, which is called Key block; Warburton (1987) presented the second theory called key stone.

The theory proposed by Goodman and Shi is based on the classification of blocks into finite and infinite blocks based on the stereographical projection of opening and fracture orientations. The finite blocks are classified into non-removable and removable blocks. According to Figure 1-1, removable blocks are classified into those that are stable even without friction, stable with sufficient friction, and unstable without support.

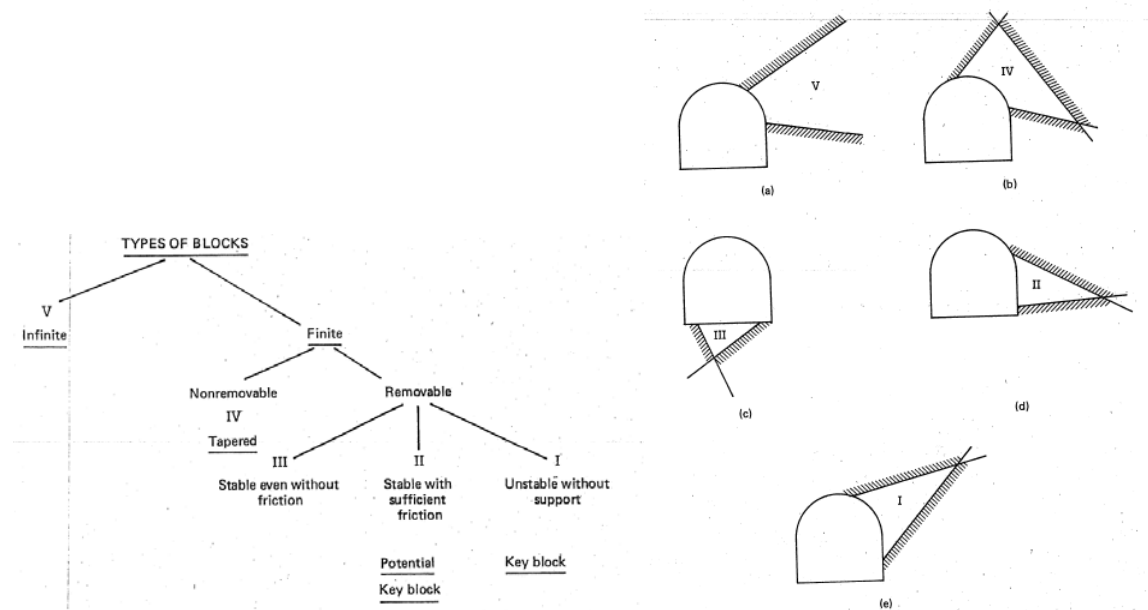


Figure1-1. Classification of blocks based on block theory (Goodman and Shi, 1985)

The infinite blocks and finite, non-removable blocks (types V and IV) don't cause any danger to the opening. The type III is stable without any friction due to the direction of the gravity force alone. Type II blocks are stable as long as the sliding force under gravitational loading is less than frictional resistance. This type of block may become unstable due to the water pressure or other types of forces; therefore, they are called potential key blocks. Type I (the key block) slides into

the opening under gravitational loading only and requires rock support in order to make it stable. Types I and II are the most dangerous and important to the tunnel stability. Forces must be analyzed in order to distinguish between types I, II, and III.

Goodman and Shi used the full sphere graphical stereographic projection and vector analysis to identify and analyze key blocks. Vector analysis is used to determine block surface, volume, and calculations of forces. In their theory, each discontinuity divides three-dimensional space into two upper and lower half spaces. The number 0 shows the upper space; number 1 shows the lower space. The blocks pass through a common origin to form a series of pyramids. The block pyramid (BP) is the assemblage of planes forming a particular set of blocks, which consists of a group of discontinuity planes called *joint pyramid* (JP) plus a group of excavation surfaces called *excavation pyramid* (EP). Theorem of finiteness is used to distinguish between type V and IV blocks.

Theorem of Finiteness:

A convex block is finite if its block pyramid is empty. Conversely, a convex block is infinite if its block is not empty.

The theorem of removability will be used to distinguish between removable and non-removable blocks.

Theorem of Removability:

A convex block is removable if its block pyramid is empty and its joint pyramid is not empty. A convex block is not removable (tapered) if its block pyramid is empty and its joint pyramid is also empty.

The condition of block pyramid empty satisfies the finiteness of block, and the condition of joint pyramid not empty satisfies the condition of removability of block. To distinguish between Types, I, II, and III of block, forces must be analyzed that are called mode analysis.

Based on an explanation given by Goodman and Shi, block theory, recognition, and analysis of key blocks are based on the three following steps:

- 1- Finding finite block by use of finiteness theorem;
- 2- Finding removable blocks by use of removability theorem; and,
- 3- Carrying out mode analysis.

The Idea behind the hemisphere analysis is to recognize the stability condition of rock blocks and wedges; these could be investigated by examining the direction of the active force vector with respect to the discontinuity direction and a generalized friction cone (Mauladon and Goodman, 1996).

According to the Goodman and Shi (1985) as long as critical blocks (key blocks) blocks are stable, the rest of the jointed domain must also remain stable. The block theory (Goodman and Shi, 1985) considered only the translation failure of blocks. The works have been conducted by Mauladon (1990) and provide an application of block theory in the rotational failure of blocks.

Another definition of keystone was defined by Warburton (1987): ***The special relationship between two adjacent blocks - that the neighbours remain stationary - as long as the keystone is held in place, but would begin to move if the keystone were removed or eliminated.*** Warburton 1981, used vector analysis to find the keystone in rock mass. One part of vector analysis is related to test the geometrical configuration, and another part is related to determine the nature and direction of the movement.

Both Warburton and Goodman and Shi analyze the key block with the assumption that its neighbors were temporarily fixed. In reality, there may be some blocks that push out the key block. Therefore, these methods tend to underestimate the number of blocks that need to support (Warburton, 1987).

According to the author opinion the following discussion will give a better definition of key blocks.

One finite and removable block in the perimeter of tunnel could be stable or unstable. The consequence of one unstable block could either be failure of that single block or failure of several blocks. In the case of just one block failure, it could be called single block failure. In the case when the failure of one block causes the failure of several blocks, the key block definition makes more sense (see figure 1-2).

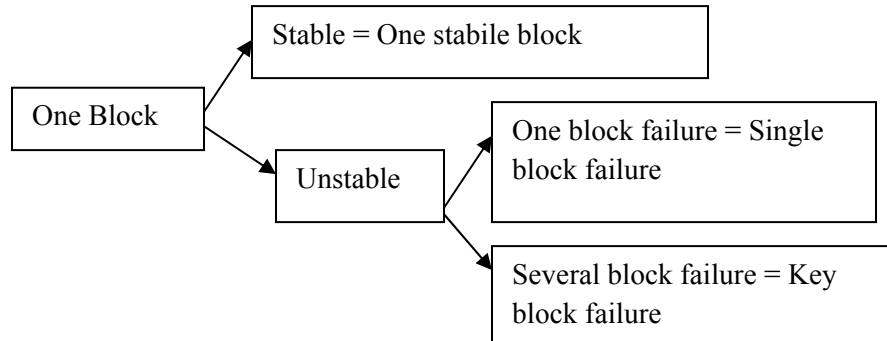


Figure 1-2. Representation of key block definition

The above definition distinguishes between single block failure and key block failure. According to Goodman and Shi's definition, one finite removable block that is unstable without support is called key block. Therefore, Goodman and Shi's definition cannot distinguish between failure of one single block and failure of key block. In another way, Goodman and Shi's definition does not take into account the relationship between the stabilizing of that block (key block) with stabilizing its neighbours.

The principal of key block theory is the identification of critical key block for a given excavation geometry. The assumption is that maintenance of the critical blocks in a stable state will guarantee stability of the entire face. Although blocks that could fill the role intended for key blocks do undoubtedly exist, there would generally not be enough information in practice to identify them (Warburton, 1987). This implies that, in practice, key block theory is not applicable due to lack of information.

1-4 Design Tools to Analyze Block Stability

In order to analyze block stability, two questions must be answered. ***Do we have any block?*** And, ***if there is one, is it stable or not?*** The first question relates to the block existence and block volume. Block volume and its existence are related to the fractures and opening orientation, and fracture length. Priest (1993) mentioned that the kinetics feasibility for a given

block can determine the potential of movement, and this is not based upon forces analysis. The second question is related to forces that act on the block. Forces acting on the block are block weight, induced stresses, dynamic loads, resistance forces from fracture friction and forces from support. To answer the first question, design tools such as kinematic analysis and DFN are available. To answer the second question, analytical solutions based on limit equilibrium and joint relaxation and numerical solutions are available. Each design tool has certain assumptions on the rock mass behaviour and some simplifications on the block geometries and presence of fractures in rock mass; it is important to understand how to use these tools efficiently and both the strengths and weaknesses of the tools (Starfield and Cundall, 1988). Table1-1 shows various combinations of different design tools to answer the question regarding block existence and analyzing forces that act upon the block.

Table 1-1. Different Design Tools to Analyze the Geometry and Stability of Blocks

<div><div>Block Volume</div><div>Estimation</div></div>			Kinematic Analysis			DFN
			Conventional Analysis	Finite Joint Length		
				Deterministic	Probabilistic	
Analytical Solution	Based on Limit Equilibrium 1	No Stress Field	A1	B1	C1	D1
		Considering Stress Field	-----	B'1	C'1	D'1
	Based on Joint Relaxation 2		A2	B2	C2	D2
DEM 3			A3	B3	C3	D3
DDA 4			A4	B4	C4	D4

In the table, alphabet (A-D) refers to the design tools used to estimate the block existence and its volume estimation. Numbers 1-4 refer to the design tools used to analyze forces around a block. In Chapter 3, a short description will be given of design tools to analyze block volume. In the Chapter 4, a short review will be given of analysis methods 1-4. Analytical solution based on joint relaxation (2 in the table) will be compared to DEM (3 in the table) in Chapter 5. A1, B1, C1, B'1 and C'1 will be applied to a site in Sweden, and they will be compared to D3 in Chapter 6.

1-5 Important Parameters for Block Stability Analysis:

The designer faces the question: *“What kind of geological information is needed to analyze the block stability?”* or in other way *“What parameters have the most influence in the block stability?”*. The first step for stability analysis of a failure mode is the recognition of important parameters. This issue was also mentioned by Strafield and Cundall (1988): *“the art of modelling lies in determining what aspects of geology are essential for a model”*. The important parameters for wedge stability analysis have been classified in Figure 1-3.

The first and important question is *what is shape and size of block?* Joint orientation, length, intensity, and tunnel geometrical configuration (orientation and shape) determine the block size and shape. Hoek and Brown (1980) noted the importance of joint set orientation regarding to the opening orientation. Priest (1980) mentioned that stability of wedges is influenced by orientation, geometry, and strength of the more extensive discontinuities within the mass. Hencher et al. 1996 pointed out the importance of discontinuities spacing, and Stead and Eberhardt (1997) pointed out the importance of discontinuities orientation on predicted failure mechanism.

The second question is about the quantity of the forces acting on a wedge; they must be defined and analyzed. Forces could be divided in two groups: driving and resisting forces. The driving forces are the weight of block, water pressure, and dynamic forces from blasting or an earthquake. Resisting forces are provided by discontinuities shear strength and confining forces from induced stresses and forces from rock support. The weight force is calculated from the volume, so the aforementioned parameters to estimate shape and size of block are important in weight force evaluation. Vaughan and Isenberg (1991) noted the importance of dynamic loads from explosion. They noted that the orientation of block relative to the tunnel and the direction of loading by wave propagation have significant effect on the block stability. Resistance forces are the result of discontinuities' resistance parameters and stresses around block. The results of Crawford and Bray (1983) show that the stability of the wedge and stress redistribution around the wedge upon excavation of an opening markedly influenced ratio of joint shear stiffness to joint normal stiffness, and the ratio of intact rock stiffness to joint normal and shear stiffness. The tangential stress around the roof depends on the magnitude of both horizontal and vertical stress field and the shape of opening. The result of considering horizontal in-situ stress is to take into account the normal stresses developed across the discontinuities that can bound the rock wedge

and enable the shear resistance of discontinuity to be mobilized; the rock wedge become wholly or partly self-supporting (Crawford, Bray, 1983). Goodman and Shi (1982) showed that the dip angle of the joint, along with stress field, have significant effects on the stability of blocks.

Hoek and Brown (1980) noted the influences of excavation sequences and the possibility of support installation before the wedge base is exposed. This gives the opportunity to support the wedge before its failure. Terzaghi (1946) mentioned the effects of the rock support distance from the face in stratified rocks.

Hammett, and Hoek (1981) and Piteau (1972) mentioned that the intact rock strength has minor effects or almost no effect on the block stability.

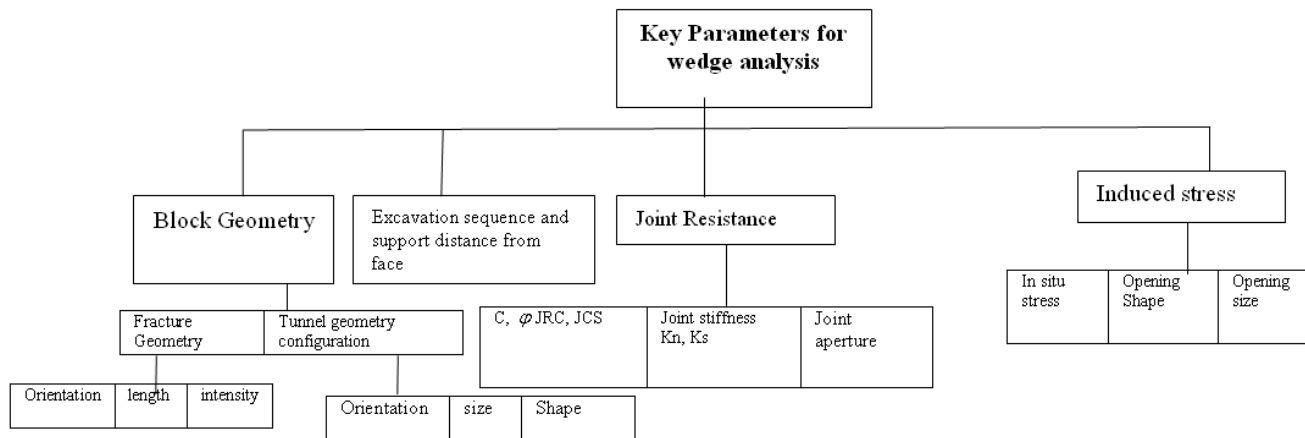


Figure 1-3. Key parameters for wedge stability analysis

Plenty of research has been conducted in this field. This type of failure mode (block failure) is a complex failure mode, and needs more research in order to understand it and assess better design tools to analyze failure. In order to evaluate design tools, having knowledge of key parameters is essential. Some of the key parameters of block stability analysis include block geometry, joint resistance, induced stress, and excavation sequence. These have been found by a literature review.

Chapter 2

Uncertainties Related to Analyzing Block Failure

2-1 Introduction

Figure 2.1 shows the design process against block failure. The design starts with some input data from a geological survey (fracture orientation, length, intensity, mechanical properties, stresses, etc.) Some of this input data have been explained as important parameters in Chapter 1. The first question in this process is: ***Can the fracture system around a tunnel form – or not form - block in the perimeter of tunnel?*** Design tools such as kinematic analysis and DFN may be used to answer to this question (see Chapter 1). If the fracture system cannot form block around tunnel, the other failure modes should be checked. In the case of forming block around tunnel, its stability must be checked. Design tools such as analytical solutions based upon limit equilibrium or joint relaxation and numerical discrete modelling (for example, DEM) may then are used. The purpose of this design is to assess certain reliability to safeguard against block failure. If this condition is satisfied, the drawing would be prepared and tunnel excavation could be started. From this stage, the observational method may be applied to adjust the design with the observed fracture pattern. However, the application of observational method to design against block failure is not within the scope of this thesis. In the design process, different types of uncertainties are involved. The purpose of this chapter is to explain uncertainties which are involved in the design process against block failure.

The word uncertain means feeling doubt about something (Longman dictionary). Uncertainty is unavoidable in engineering works. The engineering design must be robust and reliable; therefore the uncertainties must be quantified and handled. Ang and Tang (2007) divided uncertainties into two types Aleatory and Epistemic uncertainty. The first related to the randomness and variability of observed data, and the last associated with imperfect models. Although both types of uncertainties may be represented in the analyses, their respective significances may be different. Baecher and Christian (2003) divided the uncertainty into three groups. Natural variability, knowledge uncertainty and decision model uncertainty. Natural variability is equal to the aleatory uncertainty in the first classification of uncertainty; the knowledge uncertainty is based on lack of knowledge about the events and process or lack of knowledge about the true relationship between the parameters to govern the behaviour. This group of uncertainty is equal to the epistemic

uncertainty and is called subjective, internal uncertainty or structural uncertainty by Draper (1995). This group is included parameter uncertainty and model uncertainty. The third group describes inability of decision making.

As Figure 2-1 demonstrates, the design against block failure depends upon the in-data, the geometry estimation of block, and design tools. In this particular process, three different kinds of uncertainties are involved in the block failure analysis (geometric uncertainty, parameters uncertainties, and uncertainties in the design tools). Geometric uncertainties relate to uncertainties of block shape, size, and location. The description and quantification of uncertainty is important because it deals with risk and economy of project. Uncertainties are addressed by a lack of information in complex geological media. In principal, the stability analysis of blocks depends on the key parameters discussed in Chapter 1, among which the uncertainties in the structural discontinuities in the mass (Dip/Dip Direction, joint Persistency, and length) give the uncertainties in the block geometries. The uncertainties in the fracture mechanical parameters and in-situ stress estimation result in the parameters uncertainties. The outcome of model (design tool) varies from reality. This type of uncertainty is called model uncertainty.

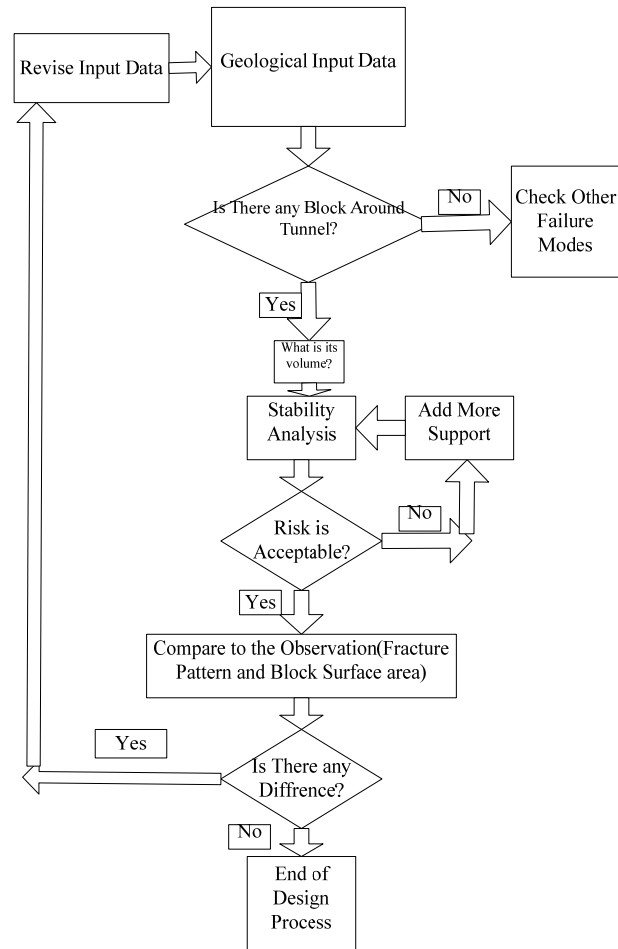


Figure 2.1. Design process against block failure

Many of these uncertainties are coupled. Starfield and Cundall (1988) mentioned the design tool simplifications due to the lack of geological data. This means that many of the assumptions that were made in the design tools are due to the lack of knowledge from the geological site description.

2-2 Block Geometric Uncertainties

Block geometric uncertainty plays an important role in the design of underground opening against block failure. If fractures in the mass could be described in three dimensional according to their locations, there was not any uncertainty about the block geometries and their locations. Unfortunately, this is not the case in rock engineering, and a full description of fracture assemblage is not possible. Therefore, there is uncertainty in the block geometry estimation. This kind of uncertainty relates to the question: *Is there any block around the opening and, if there is, what is its size and where is it located?* This type of uncertainty creates another kind of uncertainty – that of driving force and resistance force such as cohesion; it also affects the amount of required support. The joint geometry parameters such as orientation and joint length are the most important parameters when analyzing the block geometry uncertainties. Mauldon et al. (1997) compared the case of uncertainty in the block geometry to designing a masonry structure in which the sizes and shapes of bricks are unknown.

The fracture geometries and locations and, therefore, blocks geometries and locations involved the lack of knowledge. The input data comes from surface survey, boreholes or pilot tunnels. The uncertainties of fracture geometry come from the point that in the best condition there is only access to an excavation surface; there is not any access to the 3rd dimension, which is hidden behind the rock surface. As was aforementioned, some uncertainties are coupled together. For example, in this case the assumption of infinite fractures extension in kinematic analysis is coupled with a lack of measuring the fracture extension.

2-3 Joint Mechanical Parameters Uncertainties

Key parameters for block stability analysis such as joint mechanical parameters (normal and shear stiffness, friction angle and cohesion) and in-situ stress have great impact on the results of block stability analysis. The mentioned key parameters vary from point to point. Vanmarcke (1977) described the spatial variability within homogenous soil layers; the spatial variability of fracture mechanical parameters is much more complicated than the homogenous soil layer. Vanmarcke (1977) identified three different kinds of uncertainty sources in soil layers: natural heterogeneity, limited availability of information about subsurface condition, and measurement errors. Determination of exact joint mechanical properties is impossible; therefore, there are always uncertainties in the mechanical properties when the stability analysis is conducted.

The first source uncertainty is the inherent uncertainties. The natural heterogeneity of fracture parameters is caused by variation in mineral composition and stress history. The variation of mechanical parameters from mean value creates uncertainty.

The second source of uncertainty is lack of data. Fracture mechanical parameters are measured from boreholes or exposed surface in tunnel. The uncertainty that is associated with mechanical properties of fractures is due to the fact that measurements are available for only few points., The implementation of statistical methods seems inevitable for the unobserved area (Priest, 1980).

The third source of uncertainty is the measurement errors. The measured values differ from actual values because of sample disturbance, test and condition imperfections, and human errors.

2-4 Model Uncertainties

In order to design underground openings, engineers rely on idealized models. Models can never fully describe the reality, but they can give the designer insight to the rock mass behaviour (Hoek et al., 1991). Hadjigeorgiou and Gernon (2005) mentioned that the reliability of block stability analysis depends on the quality and quantity of field data and a limitation of employed design tools. The quality and quantity of field data have an effect on uncertainties of the block geometry and joint mechanical parameters. A model usually formulizes judgment about how two sets of ingredients, unknown (casual effect) and known (in-data) are related with some assumptions. In routine feature of most statistical methods is to acknowledge parametric uncertainty while a particular form of structure model has been chosen, but it is less routine to acknowledge structural uncertainty about the model itself (Draper, 1995). Different design tools such as limit equilibrium analysis, analytical solutions and numerical modelling are available to analyze block stability. Each design tool has its own assumptions and limitations. Model uncertainties (uncertainties in design tools) are related to design tool assumptions and limitations. The sources of uncertainties in design tools are their imperfect assumptions and degree of simplification in the model. The uncertainty in the prediction of unknown values (model outcome) depends both on the structural uncertainty (model uncertainty) and in data uncertainty; in other words, the model uncertainty ought to quantify in light of the value of in data (Draper, 1995).

Eurocode (EN, 1997) suggests the use of ultimate limit state design. A design based on ultimate limit state requires specifying a limit state function (performance function). A limit state function is usually based on a deterministic design tool. The design tool (model) predicts the capacities or deformations. The outcome of the model such as bearing capacity, factor of safety or the volume of unstable blocks could be represented by stochastic variables. Therefore, it must be known how to properly represent model uncertainties in limit state function where an uncertain model is included.

Model uncertainty is well explained in Ronold and Bjerager (1992) and it is of great importance in reliability analysis. The model should play two roles: First, it should have simple mathematical operations and secondly, it should predict reality. Due to their assumptions and simplification, the design tools use just few key parameters. Each of the neglected key parameters in the model generates noise in the model, which means that it generates uncertainty in the model.

Model uncertainty can only be quantified either by comparing other more involved models that exhibit a closer representation of the nature or by comparing it with collected data from the field or the laboratory (Ditlevsen, 1982). The model uncertainty factor defines the deviation between true value and predicted value by model as a stochastic value that has both a mean and a variance Ronold and Bjerager (1992). The deviation from predicted and true value is random and varying depending on case. Based on this, the relationship between true value Z and outcome of model X could be written as Eq. 2-1.

$$Z = I \bullet X \quad 2-1$$

I is the random model uncertainty factor describing the stochastic functional dependence between the true value and the outcome of the model. It is assumed to follow a probability distribution with a mean value μ_I and standard deviation of σ_I . Ronold and Bjerager (1992) assume normal and lognormal distribution for the random model uncertainty factor. The model uncertainty in the case of normal distribution could be expressed as the following:

$$\hat{\mu}_I = \frac{I}{n} \sum_{k=1}^n i_k = \frac{I}{n} \sum_{k=1}^n \frac{y_k}{x_k} \quad 2-2$$

Where y_k is the true value, x_k is the outcome of the model and n is the number of realizations. The variance of the mean value $\hat{\sigma}_I$ could be calculated from the following equation:

$$\hat{\sigma}_I = \left[\frac{I}{n-1} \sum (i_k - \hat{\mu}_I)^2 \right]^{1/2} \quad 2-3$$

$$\hat{I} = \hat{\mu}_I + T_{n-1} \hat{\sigma}_I \sqrt{1 + \frac{I}{n}} \quad 2-4$$

T_{n-1} is the student t-distribution variable with $n-1$ degree and of freedom. $\hat{\mu}_I$ is the mean value of μ_I .

2-5 Conclusions

Uncertainty deals with safety and economics of a project. This is therefore a very important issue in the design process. There are different uncertainties involved in block failure analysis such as block geometric uncertainty, model uncertainty, and parameter uncertainty. The other failure modes also deal with mechanical parameter uncertainty and model uncertainty. Geometric uncertainty makes block failure different from other types of failure modes. All aspects of uncertainties affect the results of analyses. Considering model uncertainty which is an issue that plays an important role in the design and decision-making about rock support, ignoring the model uncertainty could be very dangerous. The designer should be aware of the model uncertainty, and should correct the outcome of model regarding to the model uncertainty factor. The general aspects on the model uncertainty have been explained in this chapter. The application will be discussed in Chapter 5 and 6.

Chapter 3

Design Tools to Estimate Block Volume

3-1 Introduction

The estimation of block volume has applications other than just block stability analysis in mining and civil engineering projects. Block volume estimation is a key component of mining method selection such as sub-level caving and shrinkage stopping (Nicholas, 1981). To study the leaching potential, the estimation of rock block volume is also an important. The estimation of block volume is an important issue to determine rock mass strength and rock mass classification (Palmström, 1995, Beniaowski, 1989 and Barton et al., 1974).

There are different methods used to estimate block volume such as image processing (Kemeny et al. 1993), Discrete Fracture Network (DFN) (Dershowitz and Einstein, 1988), stereological methods such as Kinematic analysis (Dinis, 1977, Kleine, 1988, Villaescusa and Brown, 1991) and experimental equations based on RQD. Some of the methods consider the fracture length and some others do not. Generally, the block shape must be known prior to the calculation of block volume and depends on the number of joint sets and their orientation distribution within the rock mass. On the other hand, as mentioned in Chapter 2, the rock mass is not accessible in three-dimensional form, so the shape of blocks cannot be revealed. In order to solve this problem, Weibel (1980) suggested using the calliper diameter with 8-20% error. Boontun (1998) has performed sensitivity analysis on the effect of fracture parameters on key block size distribution. His results show that the number of key block increases linearly with increasing joint length; also, by increasing the joint spacing, the average of key block size increases exponentially, and the number of key block decreases exponentially. His results show that the key block size distribution shape is fixed as a reverse J-shape Weibull distribution when the concentration factor of pole vectors (K-factor) is 200 or less. As mentioned earlier, the two main methods to estimate block volume, kinematic analysis and DFN, which are based on stochastic representation of fractures, will be discussed. Each of these will be explained in the following sections. The assumptions, advantages, and disadvantages of each will be discussed.

3-2 General Aspects of Kinematic Analysis

Kinematic refers to the motion of bodies without reference to the forces that cause them to move (Goodman, 1989). Kinematic analysis considers the poles of discontinuities along with and the intersection of joints to form a block. Also, in kinematic analysis, the friction of discontinuities could be considered. Kinematic analysis focuses on the feasibility of existing blocks and their falling from a roof or sliding on a one joint face or a two joint conjunction plane. Kinematic analysis could be used to find the potential unstable blocks, the direction which the blocks will slide, and the volume. The assessment is conducted by stereo net plots to find the feasibility of blocks around the opening. As Priest (1980) mentioned, the assumption of kinematic analysis is that the discontinuities will occur in the locations that produce the largest and least stable blocks adjacent to the excavation. Cartney (1977) called this approach Ubiquitous Joint Method. Kinematic analysis is based on the following assumptions:

- 1) The block has a tetrahedral shape formed by three fractures
- 2) Blocks are separated by planar fractures
- 3) Displacement is purely transitional
- 4) The ubiquitous presence of joints

In order to move a given block under gravity, the following three kinematic conditions must be satisfied:

- (1) All pairs of block surface lines must either be parallel or divergent towards the rock face.
- (2) At least one block surface line must be inclined downward from the horizontal towards the excavation.
- (3) All block surface lines must extend from the apex to daylight at the excavation face.

The qualitative kinematic analysis can identify the potential failure mode (sliding or falling). If the kinematic analysis suggests that the investigated fracture configuration can result in a wedge failure, a more detailed analysis is undertaken to determine the factor of safety based on acting forces. As Hencher (1985) mentioned, kinematic analysis could not analyze forces correctly such as water pressure and cohesion of joints, so this analysis should be combined with another type of

analysis which has the ability to estimate the resistance forces and analyze them (such as limit equilibrium or DEM).

3-2-1 Kinematic Analysis Advantages:

This kind of analysis enjoys the simplicity of analysis, which makes it quick to check the potential failure. It also needs little data such as the orientation of structure and fractures. This type of analysis is well coupled with limit equilibrium analysis; however, in principal, other methods can be used to solve the block stability. Kinematic analysis could be combined with statistical methods to find the probable block volume. Another advantage of kinematic analysis is that, in the early stages of project when there isn't enough data in detail, it can quickly find the optimized direction of opening regarding to the rock mass structural orientation.

3-2-2 Disadvantages of Kinematic Analysis

Due to the assumption that displacements are transitional, only sliding and falling failure mode of block failure could be analyzed by this approach (Priest, 1980). This method cannot give any point of view to the designer about the rotation of blocks.

Another disadvantage of this method as mentioned by Priest (1980) is that it is often difficult to visualize the relationship between the information on the projection and the geometry of blocks that are kinematically feasible at a given inclined face.

The ubiquitous presence of joints means that the spatial variability of structure is not considered and this implies that all wedges have equal probability of being present at a particular site. Obviously, this is not necessarily true for most applications (Hadjigeorgiou and Grenon, 2005).

A common limitation to kinematic analysis is the inability to account the fracture location, frequency and size distribution which all have influence on the volume of blocks.

Another disadvantage of kinematic analysis is that the fractures may cross each other and there is not any limitation to the number of crossing fractures in reality, while the kinematic analysis can

only estimate the tetrahedral blocks that are the result of 3 joint conjunctions in addition to the opening face.

Kinematic analysis has the assumption that the joint surface are assumed to extend entirely through the target volume. In other words, no discontinuities will terminate within the region of block (Ohnishi et al., 1985). Therefore, it cannot handle the complex concave blocks.

3-3 Kinematic Analysis with Infinite Joint Length

By having the primary in-data such as joint set and opening orientation, kinematic analysis can estimate the block existence, volume, and possible failure mode: falling or sliding on one (or two) plane(s). Even if this approach is overdesign (Nord, et al. 2007 and Hwang, 2004) it could give the designer the ability to select the best orientation of opening, which produces the lowest block volume.

3-4 Kinematic Analysis with Finite Joint Length

Fracture length is an important key parameter in forming blocks around an opening as mentioned in section 1-5 and by Kim, et al. (2007); Villaescusa and Brown (1991) and ISRM (1978) Fracture length is not unlimited in reality. Block volume predicted by unlimited fracture length can be very conservative. A site investigation gives an idea about the fracture length, but this issue also has some degree of uncertainty. The fracture length could be estimated from a surface geological observation or from a site observation in the pilot tunnel or sections of excavated tunnel. In the latter case, the observed fracture length cannot exceed the opening size. The method to estimate length of discontinuity was described by Pahl (1981). Hwang (2004) proposed an algorithm to consider finite discontinuity persistency in kinematic analysis for both convex and concave blocks.

The kinematic analysis could be performed by considering the fracture length observed from the site in two ways: deterministic and probabilistic. In the deterministic way, fracture length is limited to its maximum observed length. In the other way, Monte Carlo analysis gives us

a probabilistic approach by having the fracture set length distribution, which could be used to limit fracture length. In the following section, the basis for probabilistic approach will be explained.

3-4-1 Deterministic Approach of Kinematic Analysis with Finite Joint Length

The joint length could be limited to either the maximum joint length, (which has been observed) or the mean value. Although the maximum fracture length could happen very rarely for a 3-joint set at the same time, it could determine the worst case. Therefore, it is a conservative design.

3-4-2 Probabilistic Approach of Kinematic Analysis

There is always variation in geological media, and it is very hard to find a representative deterministic value for geometrical parameters. Therefore, the application of statistical methods in geological media is inevitable. The applied probabilistic theory to analyze the geological media considers the variation of geometry properties (orientation and fracture length) of rock mass. The deterministic approach will result in a block volume that cannot identify degree of uncertainty if the input data varies. The limitation to a deterministic value has the disadvantage of a conservative design. Therefore, the probabilistic approach is required to be carried out to avoid the conservative design. The biggest difference between a deterministic approach and a probabilistic one is due to the influence of the variance of input data. The deterministic approach doesn't consider the variance of input data, while variance has great influence both in reality and in the results of probabilistic approach (Park and West, 2001). Kinematic analysis could be performed in the probabilistic way when the input data such as fracture length and orientation were considered to be stochastic values. Monte Carlo simulation could be used for this purpose. Duzgun and Einstein (2004) motioned that the probabilities could be determined either subjectively or objectively. Subjective determination of probabilities requires a well-experienced engineer to look at the ground condition and to tell about the present nature of rock mass and whether the probability of falling blocks has some value, according to his or her experiences. On

the other hand, objective methods of probabilities determination require the application of statistics and probability theories. The objective determination of probabilities could be performed by analyzing the data gathered from case histories or based on performing large number of Monte Carlo analysis in a deterministic process (for example, Duzgun and Einstein, 2004). Monte Carlo simulation in its simplest form is a random number generator that is useful for forecasting, estimation, and risking analysis. A simulation calculates numerous scenarios of a model by repeatedly picking values from a user-predefined probability distribution for the uncertain variables and using those values as in-data for a model. All those scenarios produce related results, The advantage of estimating the probabilities based on Monte Carlo is that the complete probability distribution for factor of safety is obtained if the PDF of input data is precisely assessed and a correlation between the input parameters is estimated (Park and West, 2001). The number of scenarios for a largest block volume from the Monte Carlo-Kinematic analysis could determine the probability of block with the maximum size formed in tunnel. The problem is that how many scenarios is enough.

3-4-2-1 Probabilistic Kinematic Analysis with Varying Joint Orientation and Fracture Length

Fracture orientation is another parameter that is marked highly in the block size, (Dip and Dip direction). Fracture orientation has a distribution that comes from geological survey or borehole exploration. Monte Carlo analysis could be very helpful in conjunction with kinematic analysis. The values for both fracture orientation and length could be randomly selected from the defined distribution. The selected values will be entered to kinematic analysis as data.

3-5 DFN (Discrete Fracture Network)

In Discrete Fracture Network modelling, two major issues are considered: the fracture system geometry and hydro/mechanical properties of every individual fracture. The former is based on stochastic representations of fracture systems, using the probabilistic density functions of fracture parameters (orientation, size, and aperture or transmissivity) formulated according to field mapping results, in addition to the assumption about fracture shape (circular, elliptical or generally polygonal) for three-dimensional problems. Due Fracture mapping can only be conducted at rock exposures of limited areas, boreholes of limited lengths, and with lower and/or upper cut-off limits; therefore the reliability of fracture system characterization depends very much on the quality of mapping and characterization techniques. In addition, the determination of the hydro-mechanical properties of the fractures using in-situ and laboratory tests can only be performed with a limited number of fracture samples. The effect of sample size and location also needs to be evaluated. The fractal concepts have been applied to DFN in order to consider the scale dependent of fracture system geometry for up-scaling. Despite the above difficulty, the DFN model enjoys wide applications for problems of fractured rocks, perhaps due mainly to the fact that, thus far, it is an irreplaceable tool for modelling at the “near-field” scale because the dominance of the fracture geometry at small and intermediate scales can be explicitly approximated in detail. This advantage diminishes for “far-field” problems at large scales when explicit representation of large numbers of fractures makes the computational model less efficient and the continuum model with equivalent properties more attractive. DFN presents more realistic representation of geology and fracture network geometry. Fractures are planar polygons with three or more sides and there is no restriction on locations or orientation. The disadvantage of DFN is that it is highly dependent on the interpretation of in-situ fracture system geometry, which is roughly estimated. Recent developments on the characterization of rock mass fracture system by Schubert and Pötsch (2005) could be very helpful to have better in data to construct and calibrate DFN.

3-6 Problems in DFN Realizations

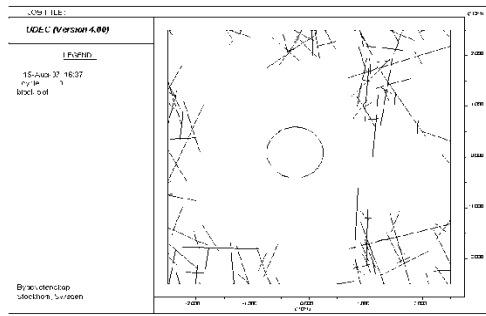
The DFN models are based on stochastic representations of fracture systems using the probabilistic density functions of fracture parameters (orientation, size, and location in 2D modelling) that are formulated according to field mapping results. On the other hand, using the appropriate numbers of DFN realizations for numerical modelling is also very important and still is an issue that is hotly debated among researchers in this field. In order to evaluate the block volume around an excavation by DFN approach, a large number of DFN realizations should be generated. Also, there is no criterion to determine how many realizations are required to analyze the block stability. The following example clarifies this problem:

The TBM tunnel is a tunnel in the south eastern part of Sweden, approximately 300 Km south of Stockholm, in crystalline rock at the depth of 420 m, and was excavated by Tunnel Boring Machine (TBM). Total fracture trace length per sample area is defined as P_{21} by Dershowitz (1984). Table 3-2 shows the statistical parameters of fractures. P_{21} was reported as 0.55 m^{-1} . Studies on the fracture size at Äspö indicate a lognormal distribution with an arithmetic mean of 6 m and a standard deviation of 3 m (Hermanson, 1996)

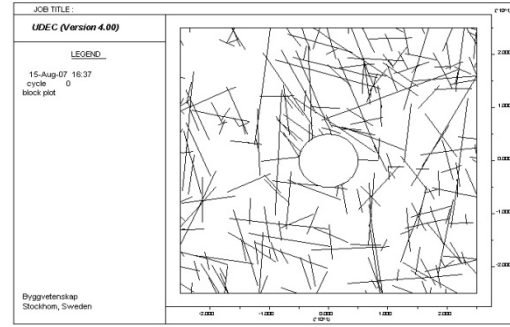
Table 3-2. Statistical Parameters for Fractures Hermanson (1996).

Set	Distribution	Mean Pole (Trend, Plunge)	Dispersion k	Percent of Fractures
1	Fisher	58.7, 11.7	13.37	48.1
2	Fisher	334.2, 5.6	7.82	25.7
3	Fisher	71.7, 85.8	11.92	26.2

Figures 3-2 a and b show two different realizations of DFN. As can be seen from Figure 3-2 a, there is not any block around the tunnel while another realization predicts potential unstable block with different volume. Figure 3-3 shows the potential unstable block volume resulted from 50 DFN realizations.



a



b

Fig. 3-2 Two realizations of DFN for the TBM tunnel

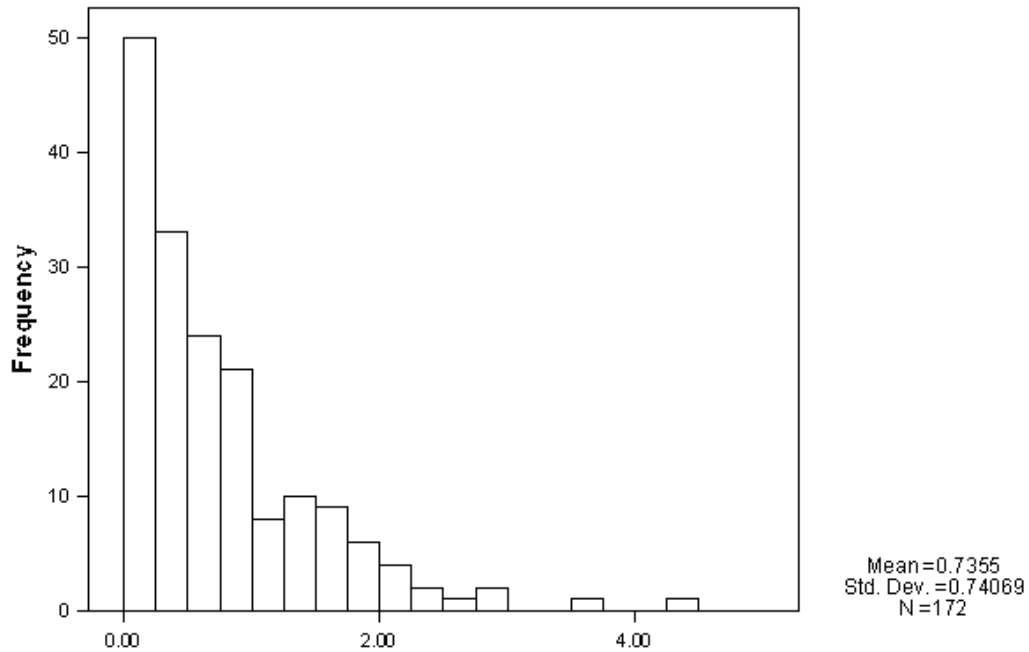


Fig.3-3. Block volume for 1 m length of tunnel (m^3).

As the above example shows, it is understood that different realizations give different volumes of potential failure block, which may vary greatly. The solution to this problem will be explained in Chapter 6.

3-7 Discussions and Conclusions on the Design Tools for Block Existence and Volume

Different design tools have been described to estimate block existence and volume. The advantage and disadvantage of each are also described. Figure 3-4 shows a schematic view of the predicted block volume by different approaches. By infinite fracture length, a large volume of potential unstable blocks is predicted, while by limiting the fracture length to observed maximum fracture length, the volume of potential unstable blocks is reduced. The probabilistic approaches of kinematic analysis (finite joint length and orientation) and DFN are based on stochastic nature of fractures in mass, and will result in a distribution for potential unstable blocks.

The main difference between DFN and kinematic analysis is that the kinematic analysis takes into account blocks that are formed by the conjunction of three joint sets, while in DFN, blocks can be formed by the conjunction of more than three joint sets. In another way, it could be said that, in kinematic analysis, blocks are assumed to have a tetrahedral shape while other polyhedral shape of blocks are possible in DFN approach. Another difference is that kinematic analysis has the purpose of finding the maximum block while DFN does not have this aim.

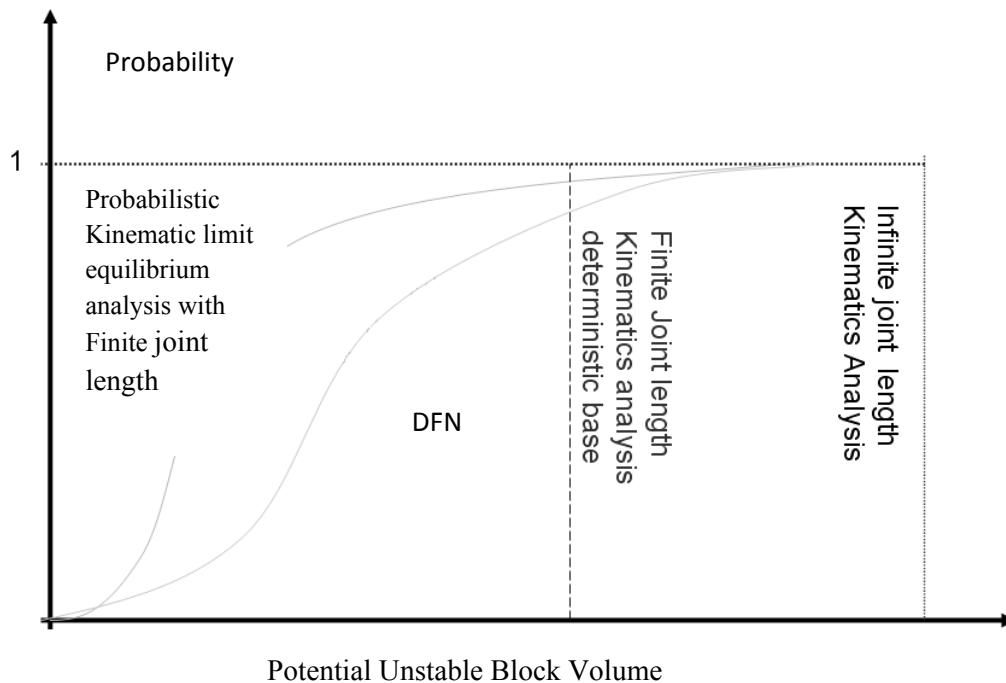


Figure 3-4. Schematic view of different design tool to predict potential unstable block volume

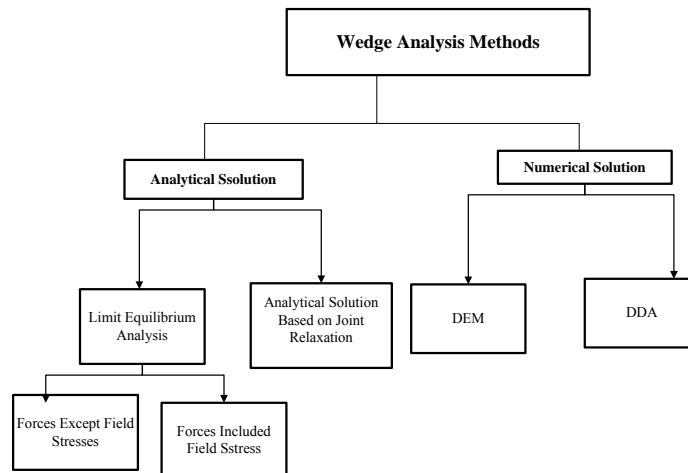
One of the most significant uncertainties in block stability analysis is the block volume estimation. This comes from the fact that the true value for block volume could not be directly measured. As is shown in Figure 3-4, the design tools could be compared to each other. Each of the methods has some assumptions that make that the model predictions differ from reality. However, among them, the calibrated DFN may predict block volume closer to reality.

Chapter 4

Design Tools to Solve Block Stability based on Literature Survey

4-1 Introduction

As mentioned in the previous chapters, the analysis of block stability is divided into two questions: *what is the size of block around opening* and *is the block stable?* To answer the first question, design tools such as kinematic analysis and DFN were explained in Chapter 3. This current chapter focuses on the design tools in order to analyze the stability of block. The design tools to analyze the stability of block as shown in Figure 4-1 could be divided into two main groups: analytical and numerical. Analytical solution could be divided into two groups, analytical solution based on limit equilibrium mechanics and analytical solution based on joint relaxation. Numerical solution, which can solve block stability (Discrete Element Method), could be divided into two numerical techniques: DEM and DDA. Each design tool to analyze the block equilibrium will be explained with their limitations, advantages, and disadvantages.



Fig, 4-1 Different design tools to analyze block stability

4-2 Analytical Solution

Analytical solution is divided in two main groups: The first one is based on the limit equilibrium mechanics; and, the second one is based on the joint relaxation proposed by Bray and Crawford, 1983. These will be explained in detail in the following sections.

4-2-1 Analytical Solution Based on Limit Equilibrium Mechanics

Although many sophisticated numerical methods have been developed, the analytical solution based on Limit equilibrium mechanics is still dominate method used to evaluate block stability of both slope and tunnel; a lot of modern software has been developed based on limit equilibrium for practice in slope stability (such as Slice and Swedge) and block stability in tunnels (such as Unwedge), based on the combination of block theory and limit equilibrium analysis. According to the definition of limit equilibrium mechanics, it is generally used to analyze the condition that would exist at a collapse (Lambe and Whitman, 1969). Limit Equilibrium Mechanics analysis assumes that the block is rigid. This assumption implies that the displacements that take place at discontinuities are much larger than the deformations that occur in the intact rock due to the stresses.

Limit equilibrium technique compares the resisting forces and the driving forces. Driving forces (such as the gravitation force) are compared to the shear resistance forces offered by the contact surfaces to determine whether the block can fall or slide. Since confining stress is difficult to estimate,, the surrounding stress field has been ignored (Hoek et al., 1991). This technique has the disadvantage of ignoring the surrounding stress fields. However, in principal, the forces from confining stresses could be incorporated in limit equilibrium analysis. Therefore, the limit equilibrium technique could be divided into two groups: the first group of analysis considers all forces except forces from field stresses; the second group of analysis considers all forces including forces from stress field (see Fig 4-1). Fig 4-2 shows the limit equilibrium mechanics, which consider the clamping force. The stability condition would be satisfied if $\beta \leq \phi$.

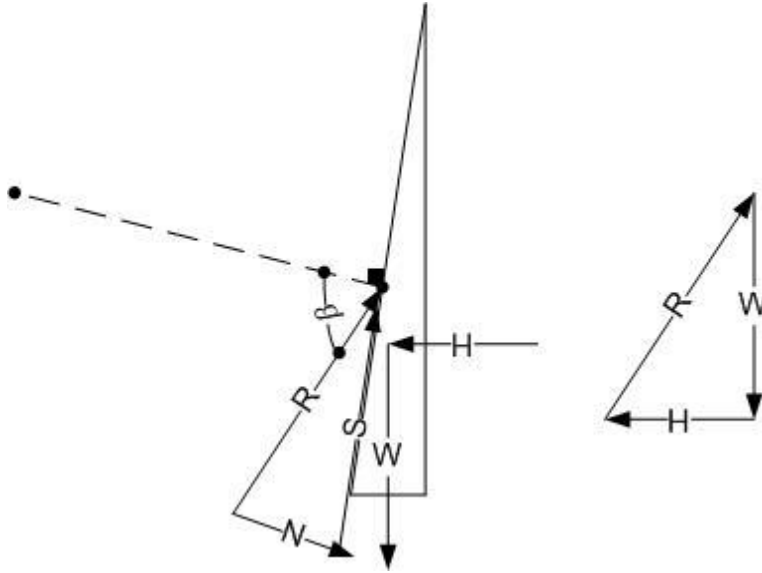


Fig. 4-2 Limit equilibrium analysis by considering the clamping forces

According to Mohr-Columb :

$$S \leq N \tan \varphi \quad 4-1$$

According to Fig 4-2 we can write:

$$\tan(90 - \beta) = \frac{N}{S} \quad 4-2$$

$$\cot an(\beta) = \frac{N}{S} = \frac{1}{\tan \beta} \quad 4-3$$

$$S = N \tan \beta \quad 4-4$$

$$N \tan \varphi \leq N \tan \beta \quad 4-5$$

$$\text{Therefore : } \beta \leq \phi \quad 4-6$$

The main advantage of LE is the simplicity of it and the fact that it could be used with graphical methods or hand calculations; it is quick and understandable.

The analysis that ignores the confining forces is well applicable for near surface excavations in hard rock (Hoek et, al, 1991). The works by Warburton (1981 and 1985) and Goodman and Shi (1985) are samples of application of limit equilibrium analysis in block theory.

Limit Equilibrium Disadvantages

Many block failure problems involve the geometry complexities, material anisotropy, non-linear behaviour, in-situ stress, and coupling process such as hydro mechanical and thermal. Also, the failure involves complex internal deformation and progressive fracturing that could not be considered in rigid block, which is a principal assumption in limit equilibrium method. The limit equilibrium method is relevant to simple block failure along discontinuities. Eberhardt (2002) recommended that in complex cases, limit equilibrium method should be used in conjunction with numerical modelling in order to have a better understanding of failure mechanism. Therefore, the design based on limit equilibrium is inadequate when the failure involved complex mechanisms such as creep, progressive fracturing, brittle fracture, etc. Limit equilibrium can analyze sliding and falling of blocks, and cannot consider rotational failure of blocks.

Chan and Einstein (1981) discussed the limited consideration of driving and resisting forces such as simplified water pressure, seismic force assumptions, and external forces acting through the centre of gravity. They also mentioned that due to the assumption of rigid body deformations and, as a consequence, stresses are not known and the problem is fundamentally indeterminate. Usually, limit equilibrium analysis methods include implicit or explicit assumptions in order to make the problem determinate.

Schubert (2005) mentioned that the shear resistance of joints is assumed to be fully developed at the same instance as the support provides its maximum bearing capacity. Limit equilibrium is purely based on the principal of static equilibrium. That is, the summation of horizontal and vertical forces should satisfy the equilibrium in case of stability. Limit equilibrium says nothing about the strain and displacement compatibility (Krahn, 2003).

4-2-2 Analytical Solution Based on Joint Relaxation

4-2-2-1 Introduction

The importance of in-situ stress on the block stability in the roof of excavations has been noted by Miller (1979). The conservatism is more pronounced in cases with low apical angle of block (Elsworth, 1986 and Diedrichs, 2000). The purpose of analytical solutions is to estimate the stability of finite and removable blocks (according to Goodman and Shi, 1980) that pose one face as the excavation face. The analytical solution based on joint relaxation was developed in order to consider the influences of horizontal stress field and joint stiffness. Crawford and Bray (1983) proposed a two dimensional plain strain analytical solution for stability analysis of blocks in the roof of excavation by considering the horizontal field stresses and discontinuities stiffness. The solution proposed by them covers both symmetric and asymmetric wedges in the roof of opening. They mentioned the model limitations such as the model is two dimensional while in reality the rock blocks are three dimensional. Their work has been the basis for research that has been conducted after them. The detailed history of the works after the Crawford-Bray solution will be presented in the following sections.

Brady and Brown (1985) formulized a safety factor based on joint relaxation. Sofianos (1984) developed a computer program to simulate behaviour of fractured rock based on Goodman's joint element, and compared the results of the different roof wedges subjected to the horizontal stress field to those of the Crawford and Bray solution. Sofianos (1986) divided the solution proposed by Crawford and Bray into the two stages: First, the forces acting on the discontinuities are calculated by elastic analysis. In this stage, it was assumed that the stiffness of discontinuities is very high or in other words, the presence of discontinuities was ignored. In this stage, the rock mass is assumed to be linear elastic, homogenous, and isotropic. In the second stage, the discontinuities' deformation is taken in to account while the rock mass is assumed to be rigid. He also did a parametric study to find the influence of friction angle and the ratio of K_s/K_n on the carrying capacity of block subjected to horizontal stresses. His results show that the friction angle also has great influence on the factor of safety for low values of K_s/K_n . Also he mentioned to that the factor of safety of block doesn't increase monotonically when decreasing the apical angle.

Also the results of his study show, in both numerical and analytical approaches, the carrying capacity of the block is proportional to the horizontal stress field if the stiffnesses are constant during two stages of loading.

Elsworth (1986) mentioned that one limitation of the Crawford and Bray solution is the idealization of homogenous uniaxial stress regime and therefore it is only valid for horizontal roof. Elsworth (1986) amalgamated the solution proposed by Crawford and Bray with analytical solution of stress adjacent a circular opening for hydrostatic stress in-situ condition. His research shows that the effect of stress redistribution consequent to block displacement is shown to markedly affect the ultimate pull-out resistance of blocks. He also mentioned that the developed formula is valid when the ratio of cavity depth to the radius of opening is approximately 25. The simplification of the Elsworth solution is hydrostatic and plain strain condition to calculate the stresses around opening. The assumptions for stress calculation are that the medium is homogeneous, isotropic, and linearly elastic. These limitations come from the limitations of analytical solutions to solve the stresses around a continuum media; this means that the effect of joint presence has not taken into account the stress distribution. The valid range of z/a (depth of excavation/tunnel radius) is suggested to be 25.

Sofianos et al. (1999) used the Kirsch equations (Kirsch, 1898) to estimate tangential stress after excavation around symmetric wedge in non-hydrostatic stress condition. Nomikos et al. (2002) evaluated the tangential stress around a symmetric block in an inclined stress field. Nomikos et al. (2006) formulates the carrying capacity of block for asymmetric block under non-hydrostatic loading. They took into account the effects of horizontal stress in non-hydrostatic loading of in-situ stress on the asymmetric blocks. Nomikos (2008) discussed the progressive failure of symmetric roof wedges.

4-2-2-2 Crawford and Bray Solution

As aforementioned, the proposed solution by Crawford and Bray is the fundamental work to analyze the block stability with consideration of horizontal stress field and joint relaxation. In following, the solution will be explained in detail.

Term Definition in the Crawford-Bray Solution:

σ_h Horizontal stress prior excavation;

c wedge height;

C horizontal force transmitted to across the wedge;

N normal force acting on the joint plane;

S shear force acting on the joint plane;

δ displacement;

α Semi-apical angle of prism; and

K fracture stiffness.

Subscript n and s refer to the normal and shear directions.

Assumptions

1. Blasting does not influence the stability of wedges.
2. There is no vertical load on the wedge except weight of wedge.
3. The criterion is purely friction Mohr-Coulomb criterion without any tensile strength for joints.
4. Rigid body of wedge.
5. Just falling and sliding modes could be considered.
6. A stress field which is not varying with the depth is assumed.

7. Horizontal stresses in the roof of excavation remains constant.
8. The solution is a two-dimensional solution and the analysis is done for unit length of excavation.
9. Linear joint relaxation.

Bray and Crawford (1983) proposed following solution based on the assumptions and force analysis. Figure 4-3-a and b show free-body and force diagram of symmetric triangle wedge generated by two sets of joints in the roof of the tunnel before and after excavation.

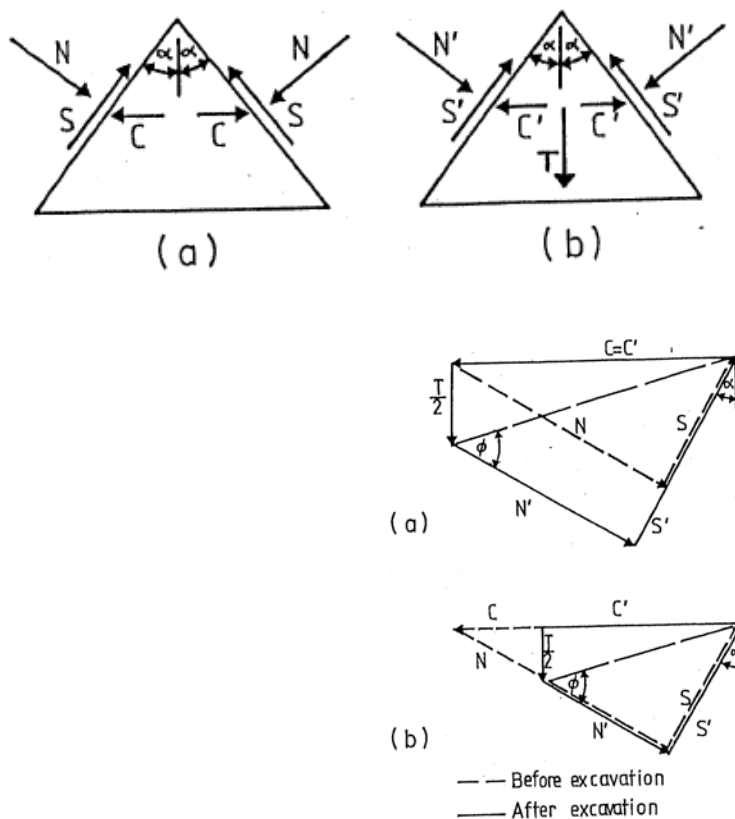


Figure 4-3 Symmetric triangle wedge free-body diagram in the roof of opening: a) before excavation b) after excavation (Crawford and Bray, 1983)

The transmitted force across the wedge(C) can be calculated as the following (before the excavation):

$$C = \sigma_h c$$

4-7

Also N and S could be calculated as the following:

$$N = C \cos \alpha \quad 4-8$$

$$S = C \sin \alpha \quad 4-9$$

The block may be displaced by the amount of δ due to the vertical load on the wedge (wedge weight) after excavation. The amount of displacement in the normal and shear directions of joints could be calculated as the following:

$$\delta_n = -\delta \sin \alpha \quad 4-10$$

$$\delta_s = \delta \cos \alpha \quad 4-11$$

The forces in the joints will be changed due the occurred displacement and could be calculated as the following:

$$\Delta N = -K_n \delta \sin \alpha \quad 4-12$$

$$\Delta S = K_s \delta \cos \alpha \quad 4-13$$

Therefore, the amount of the normal and shear forces after the block displacement could be calculated as the following:

$$N' = N - K_n \delta \sin \alpha \quad 4-14$$

$$S' = S + K_s \delta \cos \alpha \quad 4-15$$

The horizontal force, C, after the block movement, changes and the relationship between C, N' and S' (normal and shear forces after block displacement) is as the following

$$C' = N' \cos \alpha + S' \sin \alpha \quad 4-16$$

The summation of the forces in the vertical direction is as the following:

$$T = 2(S' \cos \alpha - N' \sin \alpha) \quad 4-17$$

According to the Mohr-Coulomb equation, shear and normal forces have the following relations:

$$S' = N' \tan \varphi \quad 4-18$$

The net vertical displacement (δ) and vertical force applied to wedge (T_{yield}) and horizontal forces applied to wedge after movement, C' could be calculated as the following:

$$\delta = \frac{C(\tan \varphi - \tan \alpha)}{(K_s + K_n \tan \varphi \tan \alpha)} \quad 4-19$$

$$T_{\text{yield}} = \frac{2C(K_s \cos^2 \alpha + K_n \sin^2 \alpha)(\tan \varphi - \tan \alpha)}{(K_s + K_n \tan \varphi \tan \alpha)} \quad 4-20$$

$$C' = \frac{C(K_s \cos^2 \alpha + K_n \sin^2 \alpha)(1 + \tan \varphi \tan \alpha)}{(K_s + K_n \tan \varphi \tan \alpha)} \quad 4-21$$

At equilibrium, the vertical force applied to block, T_{yield} could be considered as two components: The first one is the wedge weight; the second one is the required force to cause the block failure. Therefore,

$$T_{\text{yield}} = T' + W \quad 4-22$$

T' represents the marginal safety or in other words, the safety factor defined as

$$FS = \frac{T' + W}{W} \quad 4-23$$

4-2-3 Conclusion of Analytical Solution

The stress field around block provides confining stresses around block and could significantly increase the factor of safety (Goodman and Shi, 1982) and (Curran et al, 2004). Analytical solution which considers the effect of clamping forces consists of the following stages:

1_ Continuum analysis is conducted in order to evaluate the horizontal stress in the roof of opening, therefore regarding to in-situ stress and rock mass strength, elastic or elasto- plastic solution can be used.

2_ Calculation of static equilibrium equation, Equation 4-20, with considering confining stress obtained in stage 1.

The analytical method as stated by Crawford and Bray (1983), takes in to account in-situ horizontal stress ($C = \sigma_h c$) together with effect of reduction of clamping force due to joint relaxation, but it doesn't consider the effects of stress redistribution. The works such as Elsworth (1986) Sofianos (1986 and 1999) and Nomikos (2002 and 2006) tried to cover this point and use the redistributed clamp force.

The analytical solution is a simple solution and considers the clamping effects. Also, the variation of input data could simply be taken into account in a sensitivity analysis.

4-3 Numerical Methods

In numerical approaches, the media is divided into small components. For each component (element), equations for compatibility should be satisfied. For the whole body, the matrices will be assembled and solved. Solving of matrixes could be done by implicit or explicit techniques. The numerical methods are divided into two classes: boundary and domain methods. In the boundary method, only the boundary of excavation is divided into the elements, and the interior of rock mass is represented mathematically as infinite continuum. Domain methods divide the interior of model into simplified elements then the collective behaviour and interactions of elements depict the overall behaviour of structure.

The objective of numerical analysis may take the form of being fully predictable or in cases where the data is limited to establishing and understanding the dominant mechanism that affects the behaviour of the system. Numerical model provides a means to test several hypotheses in order to gain an understanding of the problem. During the modelling, the most appropriate methodology is to start with a simple model and to gradually build up its complexity as the problem dictates (Barbour and Krahn, 2004). The approach followed should incorporate sensitivity analyses on key input parameters. Changing the input parameters of a numerical model leads to a probabilistic approach as the discontinuities' geometry, input strength parameters and boundary condition - and it is as a part of model evaluation.

4-3-1 Discrete Element Method

Rock mass is a discontinuum, anisotropic, and inhomogeneous material. Joints can become open, closed or slipped. These specifications make the designer to use specific design tools. For blocky ground, blocks move into the opening, and the displacement in joints is more than the displacement in the intact rock. The design tools such as FEM, FDM are based on continuum analysis. However, these methods are generally limited to the analysis of relatively small displacements. Although FEM and BEM methods can model discontinuities by joint elements such as the Goodman joint model (1976), there are limitations on the degree of deformation and number of discontinuities. For this discontinuum media, the behaviour of rock mass is governed by discontinuities, and modelling the fractures is also very important. Discrete element methods are specific design tools that could consider the presence of fractures and is broadly used in the underground openings design. These methods can consider a large number of discontinuities in the mass and can handle the displacement along discontinuities and large deformation. Discontinuum analysis permits the sliding along, and opening/closure between, blocks. Several variations of discontinuum analysis exist:

- Distinct element method (DEM)
- Discontinuous deformation analysis(DDA)
- Discrete element of granular material

4-3-1-1 Distinct Element Method (DEM):

The DEM is an explicit discrete element method based on finite difference principles, originated in 1970s by landmark work on the progressive movements of rock masses as two dimensional rigid assemblages (Cundall, 1971). The distinct element method treats the domain as the assemblage of distinct blocks subject to external loading. Because of a high degree of non linearity due to joint existence, the use of explicit solutions is preferred in DEM. Joints are considered as block interfaces and they are treated as the boundary - not as the elements. The basic equation for solving the equilibrium is that the dynamic equation of equilibrium for each block is formulated and repeatedly solved until the boundary condition and laws for contact and

motion are satisfied. The contact displacements at the interfaces of a stressed assembly of blocks are identified and continuously updated throughout the deformation process, and are represented by appropriate constitutive models. The elements interact with one and other through the forces developed at contact points. This methodology is called DEM (Jing and Stephansson, 2007).

The dynamic behaviour is numerically represented by a time stepping algorithm in which the size of the time step is limited by the assumption that velocities and accelerations are constant within the time step. The distinct element method is based on the concept that the time step is so sufficiently small that, during a single step, disturbances cannot propagate between one discrete element and its immediate neighbors. This corresponds to the fact that there is a limited speed at which information can be transmitted in any physical medium. The solution scheme is identical to that used by the explicit finite-difference method for continuum analysis. The time step restriction applies to both contacts and blocks. For rigid blocks, the block mass and interface stiffness between blocks define the time step limitation; for deformable blocks, the zone size is used, and the stiffness of the system includes contributions from both the intact rock modulus and the stiffness at the contacts (Jing and Stephansson, 2007 and Itasca, 2005 and Eberhardt et al. 1997 and Cundal, 1971).

DEM Advantages

Both rigid and deformable solutions are available in DEM approach. The rigid body assumption is expressed in another solution to solve equilibrium of block analytical solution based on limit equilibrium and joint relaxation.

In the rigid body assumption, any deformation is not allowed in intact rock. In analytical solution, it was assumed that the blocks are rigid and the analysis was limited to the translation motion only, while by DEM these two assumptions have been covered and intact rock could be considered as a rigid or a deformable body. However, it can also solve the rotational failure of blocks. The influence of pore pressure and seismic loading could be considered in DEM analysis.

DEM Disadvantages

There is still a lack of knowledge about the contact behaviour and definition of system damping. The three dimensional variation in material properties' geometry and loading condition will have a fundamental effect on the model outcome. Although in principal, three-dimensional DEM (3DEC) is available to solve the problems, for complex fracture geometries the computer time is very long. Another drawback of DEM is that it does not give any direct indication of marginal safety. The end point where the factor of safety is equal to 1 is indirectly known; however, the marginal safety is not known.

The distinct element method requires a prescriptive approach for the subdivision of the mass into complete blocks. The limitation of the approach can be understood where incomplete block formation may lead to increased safety margins or increased resistance.. Furthermore, the method cannot give any understanding of progressive damage, resulting in the formation of either single or multiple fractures (Pine et al., 2007).

The difficulty in the DEM for solving the deformable media is that in order to discretize the media, the non-persistence joints that don't make a block are omitted. Kulatilake et al. (1992) discussed the effects of non-persistence joints on the stress analysis of discontinuum media. They proposed shear and normal joint stiffness of a fictitious joint in order to keep the non-persistence joints in the discontinuum media, and to take them into account. Figure 4-4 shows the joint network of non-persistence joints and fictitious joints in order to make the rock block polygons.

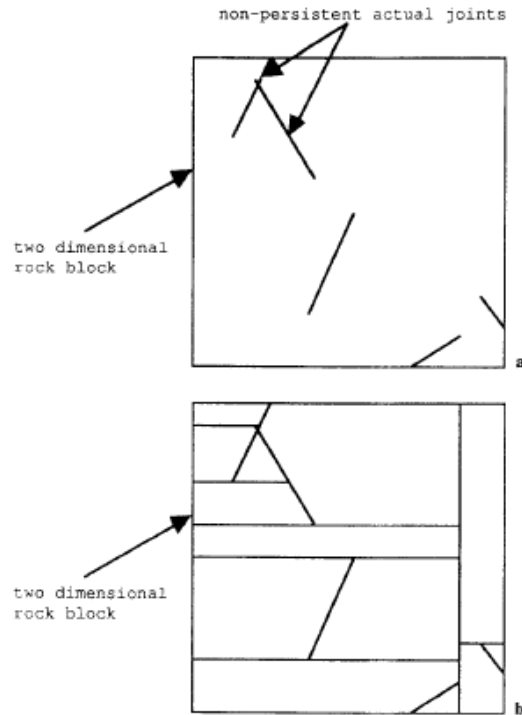


Fig. 4-4 Network of non-persistent joints that does not discretize a 2-D rock block into polygons, b Introduction of fictitious joints to the joint network shown in Fig. a to discretize the rock block into polygons

Note: All the inclined joints are actual joints; all the horizontal and vertical joints are fictitious joints (Kulatilake et al. 19982)

They proposed the properties of a fictitious joint as the following:

- The same strength parameter values should be used for both the intact rock and the fictitious joints.
- A joint shear stiffness (JKS) value for fictitious joints should be chosen to produce a shear modulus/JKS ratio (G/JKS) between 0.008 and 0.012 m.
- A joint normal stiffness/JKS ratio (JKN/JKS) between 2 and 3 should be chosen; the most appropriate value to choose in this range may be the Young's modulus/G value (E/G) for the particular rock.

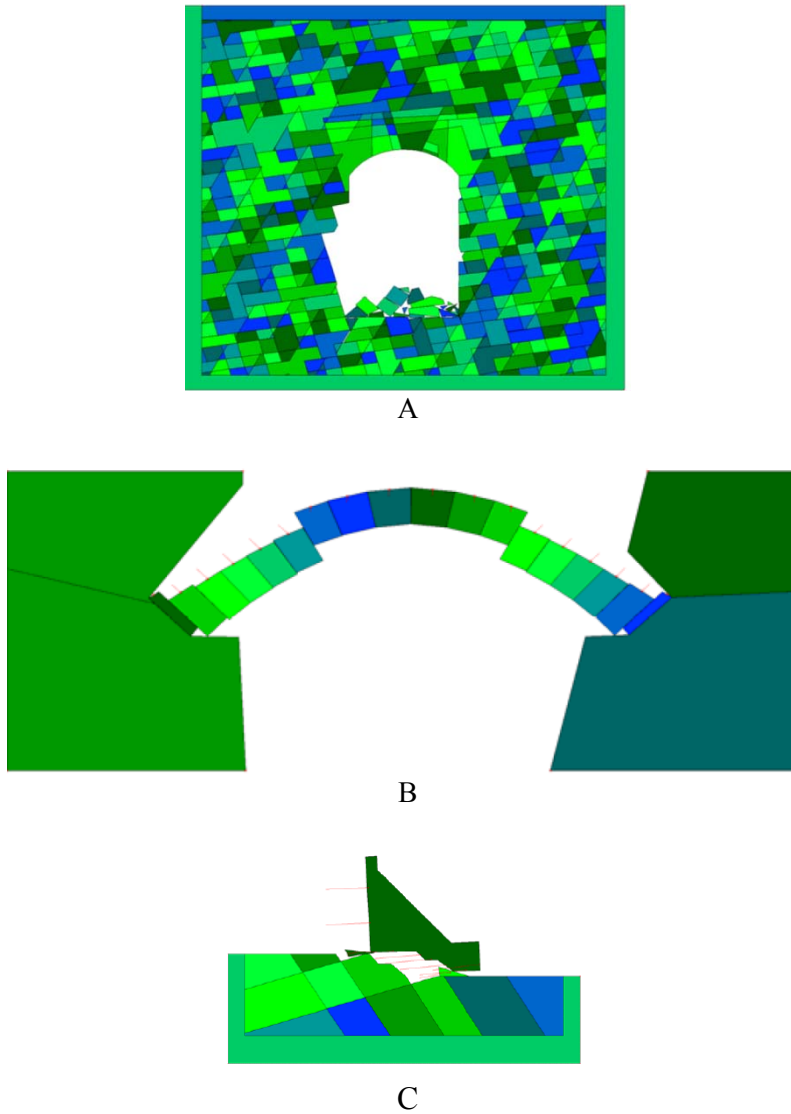
Omitting incomplete fractures imposes some inaccuracy in the stress analysis; also, for complex geometries, still mesh generator is not automatic and takes a lot of workforce.

The assumption of material rigidity is good when most of the deformation in a physical system is accounted for by movement on discontinuities. For example, this condition applies in an unconfined assembly of rock blocks at a low stress level, such as a shallow slope in well-jointed rock. The movements consist mainly of the sliding and rotation of blocks and of opening and interlocking of interfaces (Itasca, 2005).

4-3-1-2 Discontinuous Deformation Analysis (DDA)

DDA is one design tool used to analyze block stability in rock slopes and tunnels; it was first developed for applications in geomechanics for the study of landslides and rock motions (Fig. 4-5a-c) (Shi, 2008). DDA was originally based on back analysis to determine the best fit to the deformed configuration of a block system from measured displacements and deformations (Shi and Goodman, 1985). Coupling between finite element and rigid block system was called DDA by Shi (1988).

The in-data for direct DDA are block geometries, loading forces, deformability constant such as E and ν , and boundary condition. The outputs are movements, deformations, stresses and strains of each block, contact force, and so on.



Fig, 4-5 DDA examples: a) tunnel; b);arch c) foundation (Shi, 2008)

The Unknown block displacements are obtained by minimizing the total potential energy of the system. The formulation is fundamentally discontinuous in the sense of the elements (as DEM). DDA has the ability to analyze blocks with any shapes by considering normal contacts and frictional forces at contact boundaries.

DDA provides a bridge between Finite Element Method (FEM) and limit equilibrium method (Shi, 2008). After some time steps, DDA reaches dynamic or static equilibrium for deformable block system. DDA is similar to DEM method, yet it is implicit while DEM is explicit.

In DDA, the behaviour of any point within a block can be described as using six unknown per block, two translation terms (one in x and another in y direction), one rigid body rotation term, two normal strain terms (one in x and another in y direction) and one shear strain term. Parameters used in DDA are the fracture geometries and mechanical properties such as friction coefficient, rock mass mechanical properties such as density, elastic module, and penalty coefficient, viscosity, velocity energy ratio, time increment, and allowable displacement in a time increment. Determination of some of these parameters with acceptable precision and difficulties has been discussed in Ohnishi et al., 2006.

DDA has the following features (Wu et al. 2004):

- (1) The use of the principle of minimum total potential energy leading to an approximate solution as in the case with FEM. Hence, DDA can be implicitly coupled with FEM.
- (2) Topological identification of the block system.
- (3) Simultaneous consideration of rigid body movement and large deformation.
- (4) The use of the displacement approximation offers easy calculation of the behaviour of blocks with any shape.
- (5) Block kinematic: algebraic inequalities and open close iteration.
- (6) The use of the same formulations to solve both the dynamic analysis and static one. The static analysis can be achieved by applying the dynamic relaxation to the computations. Full dynamic computations can be achieved.
- (7) The modelling of any contact criterion (e.g. Mohr-Coulomb Criteria), boundary condition (e.g. displacement constraint), and load condition (e.g. initial stress, inertia force, volume force, etc.)

DDA computes deformations and displacements of entire body (intact and fractures) based on measured displacements at specified points. Shi and Goodman (1985) showed that monitoring of 3 non-collinear points provides sufficient data to do the analysis. The method can compute the

block displacement, block strain, sliding, and opening of the interface between the blocks based on least square minimization method (Shi and Goodman, 1985). Large displacements are allowed. DDA such as DEM requires the input of all the joints in the rock mass to define the block system. In practice, this is impossible.

Cheng and Zhang (2000) mentioned that the limitation of the original DDA formulation is also related to the linear displacement function used for the blocks. The stress and strain within each block are constant, which are basically only the average values. This is definitely a poor representation for a large block. The use of linear displacement function causes a change in block size; this is called free expansion phenomenon. The changes in the block size cause the misjudgement of contact identification. Wu et al. (2005) improved this problem.

DDA has the following advantages over the DEM (Wu et al., 2004):

- (1) DDA is an implicit analysis method; the time interval used in each time step can be larger than that of DEM without causing numerical instability.
- (2) It is easy to convert an existing FEM code into a DDA code and to include many mature FEM techniques without inheriting the limitations of ordinary FEM, such as small deformation in a continuous material.
- (3) Different from DEM, DDA does not require the existence of artificial damping to obtain the converged answer with correct contact force (see also: Cheng and Zhang, 2000).

In the DDA method, block contact constraints are enforced using the penalty method. This approach leads to inaccuracies. The penalty method also creates block contact overlap, which violates the physical constraints of the problem. Improvement was made by Chihsen et al. (1996) using the augmented lagrangian method instead of the penalty method originated by Shi (1989) that makes certain that the block-to-block contact enforce is more precise, and that block contact forces are determined more precisely. By using the sub-blocking, the DDA method could find the ability to determine the variation of stresses within each large block. Their improvement was made possible so that the blocks break in tension or shear. Sub block fracturing, which they propose, makes the method to investigate crack propagation possible.

4-4 Conclusions of Numerical Methods

Although DEM is a general, flexible, and powerful tool for analyzing discontinuous rock mass, there are drawbacks to its usage. There is difficulty associated with obtaining reliable in-data of geometrical location of joints such as the orientation and the persistence of the discontinuities. There is usually a lack of information on material behaviour at contacts as well as how to define the damping of the system. DEM requires a considerable computation time to solve even simple problems. Although there are some disadvantages of DEM, it can give the idea to the designer about the importance of varying parameters and mechanism of failure. It remains as a qualitative tool and extremely useful in deformation and failure of blocky rock mass and provides insight into failure mechanisms.

From the beginning age of DDA, which Shi (1988), initiated, there were many drawbacks of this method. Still many researchers are working to improve it (Cheng and Zhang, 2000). DDA is currently less powerful than DEM, and it has many limitations.

Besides the limitation of the DDA, it is still not clear how to get the in-data and setting of DDA to solve the block failure. Ohnishi et al. (2006) mentioned the difficulties of determining the required parameters for DDA; they also said that the designer must still be careful about its results.

4-5 Conclusions

Although the use of kinematic-limit equilibrium or key block theory- limit equilibrium are quite simple, a system consisting of an assemblage of blocks cannot be studied. Discrete element methods could consider the system assembly of blocks. On the other hand, it is impossible to have exact joint locations and geometries in practice. Therefore, the use of numerical method is used more to understand the failure mechanism and effect of in-data changes on the results of analysis. The analytical solution based on Limit equilibrium mechanics without consideration of clamping forces is conservative. The analytical solution which takes into account the fracture

stiffness and joint relaxation may lead to a better estimation of failure mechanism and a better prediction of required rock support.

Bray and Crawford proposes the solution of a more detailed analysis that considers the effect of fracture stiffness. For simple cases that follow the plain strain, the failure is sliding or falling or in the cases such as the persistence fractures, the use of analytical solution could be useful if their model uncertainty has become quantified.

There are many parameters that are required to perform the DDA analysis. It is not clear how to obtain these parameters in practice. Still, DDA is underdeveloped and the use of DEM is recommended instead. The progressive failure in combination with fracturing propagation is a phenomenon that cannot solve by the current technology of DEM.

DEM incorporates a careful stress analysis in order to analyze all block failure modes (rotation, falling or sliding). Therefore, DEM analysis is the most accurate analysis by today's knowledge that can be performed by analyzing the block stability for non-progressive failure.

Chapter 5

Model Uncertainty of Kinematic Limit Equilibrium Analysis

5-1 Introduction

Table 1-1 shows different combinations of design tools to estimate block volume and block stability. Chapter 3 discussed the design tools to estimate block volume (Kinematic analysis and DFN). In Chapter 4, design tools to solve block stability such as DEM and analytical solution based on limit equilibrium mechanics has been discussed. In the present chapter, different approaches of Kinematic analysis in combination with limit equilibrium mechanics have been applied to one site in order to estimate unstable block volume. Different approaches of KLE are based on different assumptions in the joint length, field stresses, and joint orientation. The approaches could be both probabilistic and deterministic. Also, a combination of DFN-DEM has been applied to one site in the south eastern part of Sweden, and its outcome was assumed as true value. The model uncertainty of different approaches of KLE could be estimated by comparing the results of them to those of DFN-DEM approach. This chapter covers blocks (A1, B1, C1, B'1, C'1 and D3) of Table 1-1.

Methods to estimate block stability consist of design tools to estimate block size and design tools to estimate stability due to the acting forces. Works by Villaescusa and Brown (1991) and Kim et al. (2007) compared different design tools to estimate block size. Based on the authors' knowledge, no report or research work about the comparison of different block stability methods currently exists. This is the first work in which the uncertainties of different approaches of Kinematic Limit Equilibrium (KLE) is identified. Figure 6-1 shows a view of different approaches of KLE and DFN-DEM in this chapter.

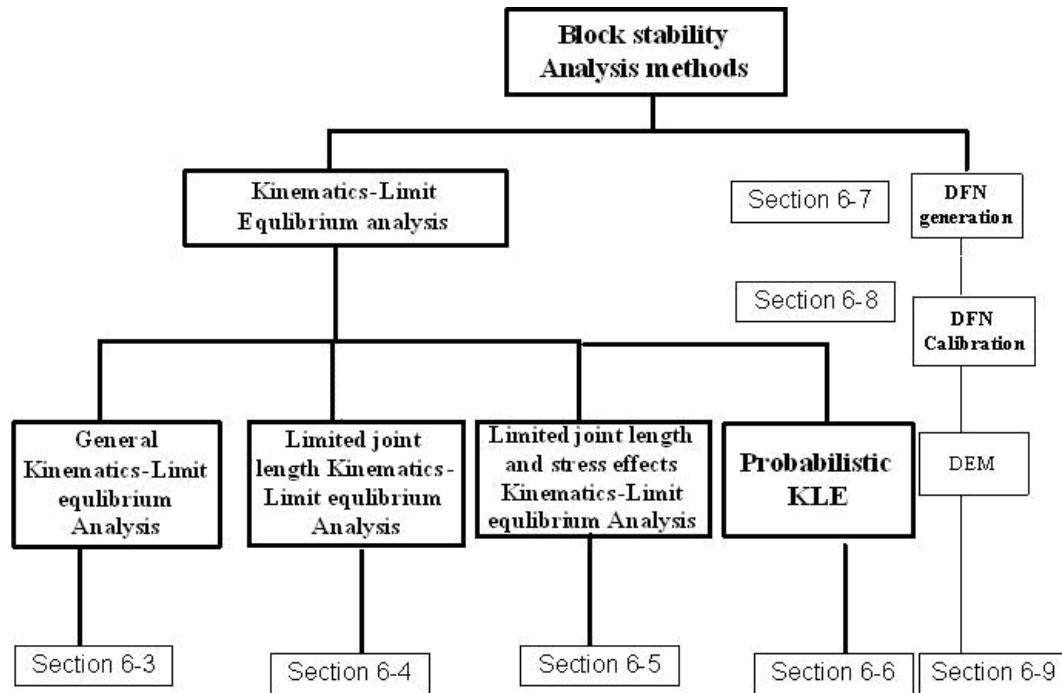


Fig. 5-1 Different approaches of KLE and DFN-DEM

In the following sections, a review of Clab2 site will be given first. In section 5-3, conventional kinematic limit equilibrium has been applied to the Clab2. The KLE has been applied to the site with considering the fracture persistency (Section 5-4). In section 5-5, both the joint persistency and stress field have been taken into account in KLE analysis. In section 6-6, the probabilistic approach of KLE (PKLE) has been applied to the site. In this study, a model uncertainty of KLE for is estimated and compared with the results of a hybrid DFN-DEM analysis, which provides a closer representation of reality.

Section 5-7 discusses the application of DFN to the site. Based on statistical measurements from the site, different DFN realizations have been generated. DFN realizations have been compared and calibrated with the fracture mapping based on significant statistic test (section 5-8). The calibrated realizations of DFN have been imported to UDEC, which is based on DEM in order to solve the equilibrium. Section 5-9 shows the result from DFN-DEM approach. Finally, a discussion and conclusion of this chapter will be given in 5-10.

5-2 Clab 2 Cavern and Rock Mass Description

Clab2 Cavern is intended to serve as an interim storage facility for spent nuclear fuel. It has the following dimensions: 115m length, 21m width, and 27m height in direction of N12E (Starzec and Anderson, 2002). Rock mass parameters are listed in Table 5-1 (Stille and Fredriksson, 1996).

Table 5-1. Rock mass parameters (Stille and Fredriksson, 1996).

Parameter	Value	Unit
Elastic	40	GPa
Poisson	0.2	
Volumetric	2.6	ton/ m^3
Tensile	5	MPa
Cohesion	1.3	MPa
Friction	35	degree
Dilation	10	degree
Residual	1.3	MPa

Figure 5-2 presents mapped fractures and weak zones from the floor of cavern (Starzec and Andersson, 2002). Figure 5-3 shows the hemisphere projected joints from the mapped joints in the cavern floor (Starzec and Anderson, 2002). Starzec and Anderson divided the mapped fractures into 2 joint sets, while Stille and Fredriksson (1996) divided the same stereo projection into 6 joint sets (Figure 5-4). From the author's point of view, both show same fracture mapping. The equivalency of 6 joint sets to that of two joint sets has been shown in Figure 5-5. From Figure 5-5 it can be observed that 6 joint sets cover the dispersion of shown two joint sets.

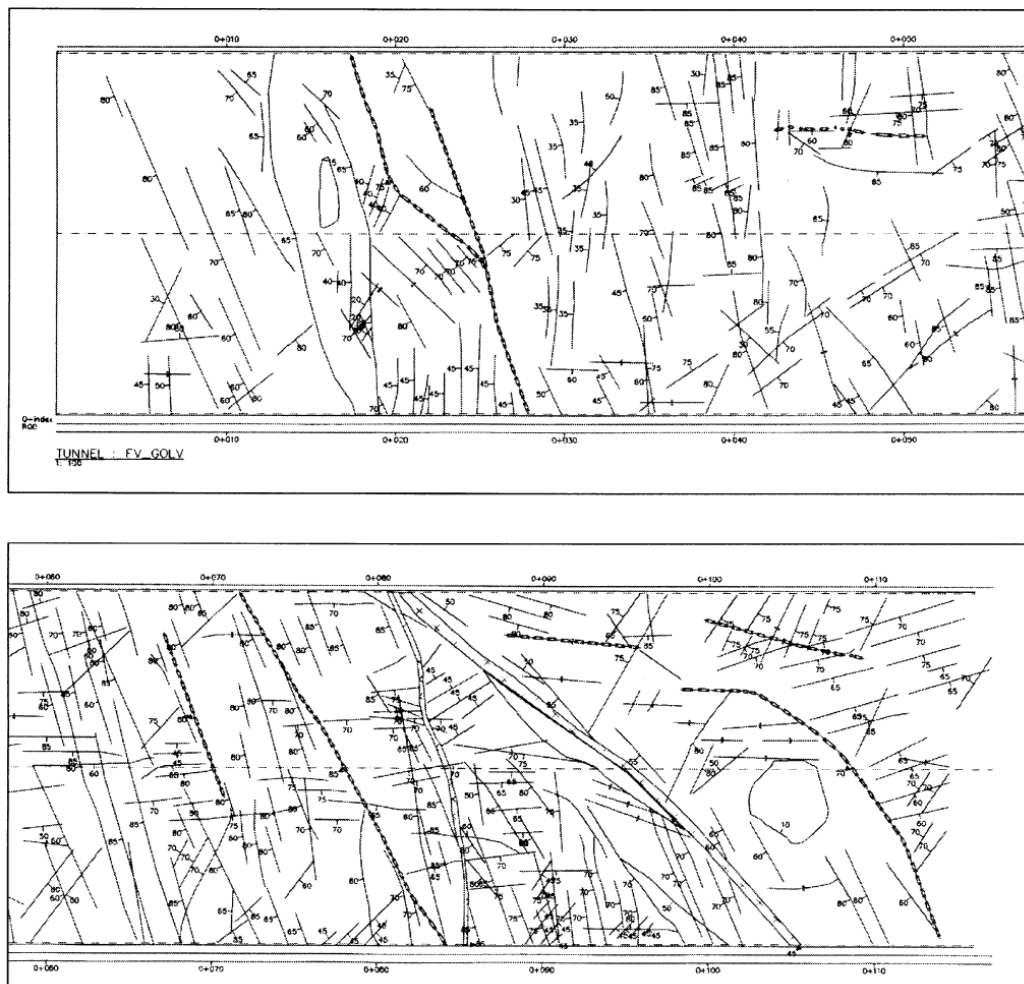


Fig. 5-2 Mapped fractures trace length and weakness zones from cavern floor

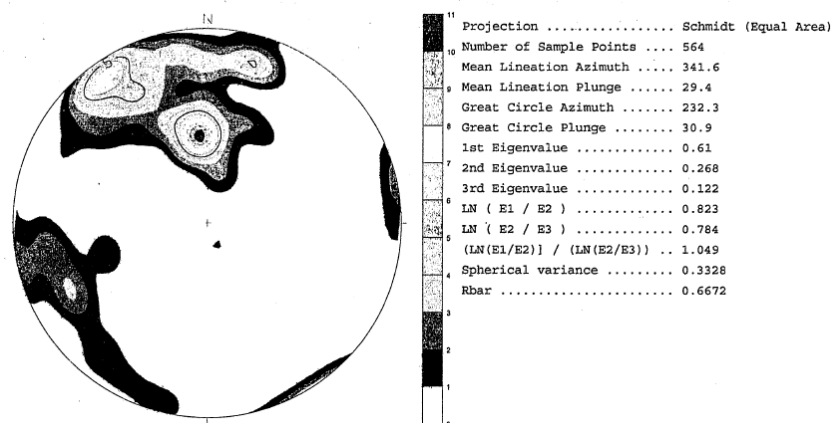


Fig 5-3. Hemisphere projection from the mapped fracture in floor of cavern (Starzec and Andersson,2002)

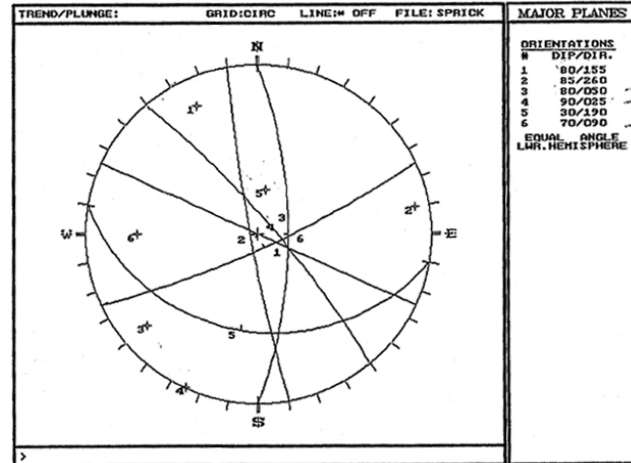


Figure 5-4. Hemisphere projection of joints (Stille and Fredriksson, 1996)

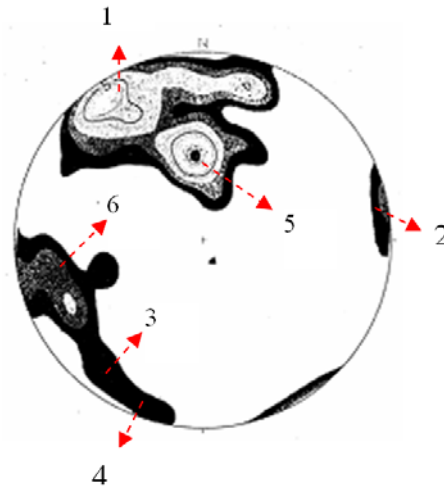


Fig 5-5 Hemisphere projection from the mapped fracture in floor of cavern (Starzec and Andersson, 2002) and their equivalency to 6 joint sets.

Joint mechanical parameters are listed in Table 5-2 (Stille and Fredriksson, 1996) and (Delin and Stille, 1993). Maximum principal stress has been reported horizontal and oriented E-W with magnitude of 6 MPa. Intermediate stress has been reported 4 MPa in N-S in horizontal plane. Minimum principal stress is vertical varying by value of overburden (Röshoff et al., 1983)

Table 5-2. Mechanical parameters of joints (Stille and Fredriksson, 1996) and (Delin and Stille, 1993).

Joint	Friction	Joint	Kn(GPa/m)	Ks(GPa/m)
30		0	58.3	10.3

At least three joint sets are required in order to perform kinematic-limit equilibrium analysis. Therefore 6 joint sets, as proposed by Stille and Frederiksson (1996), have been used for kinematic-limit equilibrium analysis. Joint sets could combine to form largest wedges, which have the potential for failure. There are 20 different combinations of block configuration from the 6 different joint sets.

Four kinds of analyses based on kinematic-limit equilibrium were applied to Clab2: conventional KLE analysis (unlimited joint length without application of field stresses), KLE with limited joint length, and KLE with considering both field stresses and limited joint length and finally probabilistic KLE.

The results of KLE were compared to those of DFN-DEM. The statistical distributions with their properties are required in order to make DFN generations. In this study, the geometric parameters for generating fracture network are based on the floor mapping results of a site characterization at the CLAB 2 as described in (Starzec and Andersson, 2002). Two major fracture sets have been detected and the orientations of fracture sets follow the Fisher distribution. Table 5-3 shows the summary of orientation of set identification in CLAB 2.

Table 5-3. Orientation of identified joint sets in CLAB 2 (Starzec and Andersson, 2002).

Orientation set	Mean DipDirection (degree)	Mean (degree)	Dip Concentration coefficient, <i>K</i>	Fracture percentage of the observed data (%)
Set 1	156.6	60.1	7.63	66.1
Set 2	67.6	75.5	9.81	33.9

The fracture length varies between 1.1 to 25 meters and follows to the lognormal distribution according to provided data in Table 5-4 (Starzec and Andersson, 2002).

Table 5-4. Fracture radius (length) distribution parameters in CLAB 2 (Starzec and Andersson, 2002)

Orientation set	Arithmetic (m) μ_m	mean	Arithmetic dev.(m), S	std. \tilde{l}_{log}	First moment,	Second moment, b
Set 1	4.8		1.7		1.268	0.778
Set 2	4.5		1.4		1.233	0.738

The observed two-dimensional fracture intensity (P_{21}) in CLAB 2 was found to be 1.32 m/m^2 . By definition, $P_{21} = \text{Total fracture lengths/Unit area} = \text{Mean of fracture length} \times (\text{Total number of fractures/Unit area}) = \mu_m \times P_{20}$.

Therefore, in this particular study, considering the fracture percentage of the observed data, then $P_{21}=1.32 = (4.8 \times 66.1\% + 4.5 \times 33.9\%) \times P_{20}$, and finally $P_{20}=0.28$.

P_{20}^1 =Fracture density for fracture set number 1= $0.28 \times 66.1\%=0.186$ and likewise,

P_{20}^2 =Fracture density for fracture set number 2= $0.28 \times 33.9\%=0.095$.

5-3 Conventional Kinematic Limit Equilibrium Analysis

The stereographical plot can be used to quickly check the risk for the block instability. The strike lines can be accommodated within the tunnel shape after finding the block volume and its weight. Stereo plot gives an indication to which block kinematically has potential to fail and should be analyzed in depth (Cartney, 1977). In the case of failure, equilibrium analysis could be used for detail analysis. Limit equilibrium considers wedge weight. UNWEDGE software, which is based on KLE, has been used to analyze the wedge stability. The software is based on ubiquitous joint analysis, which means that joints are presented everywhere in the model (Cartney, 1977). As aforementioned, six joint sets, as proposed by Stille and Fredriksson (1996), have been used for kinematic-limit equilibrium analysis. Joint sets could combine to form largest wedges, which have the potential for failure. There are $\binom{6}{3} = 20$ different combinations of block configuration.

Figure 5-6 shows a schematic spatial location of wedges around opening.

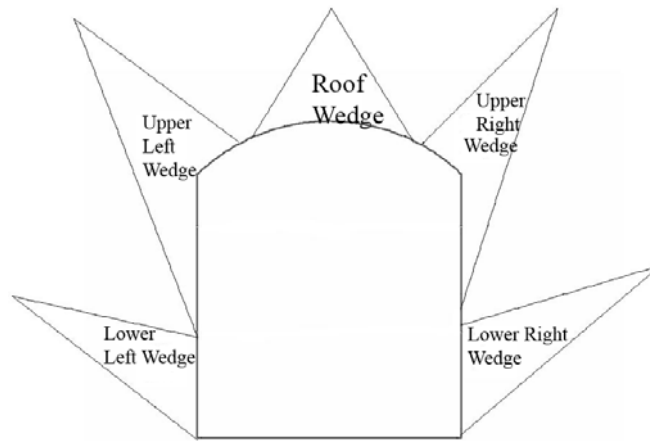


Figure 5-6. Spatial locations of wedges around opening

The joint length is unlimited and the stress field is not considered in conventional analysis. Table 5-5 shows the unstable block volume for 20 combinations that have the safety factor lower than 1 from conventional analysis (unlimited joint length and without field stresses).

Table 5-5. Unstable block volume (m^3) by conventional KLE

Combination	Lower right wedge wall	Lower left wedge wall	Upper left wedge	Upper right wedge	Roof wedge
1,2,3	0.1	0.1			1661
1,2,4	0.1	0.1			2721
1,2,5	0.1	0.1	0.15		103.78
1,2,6	0.1	0.1			1518.8
1,3,4					5542
1,3,5		199.2			14.6
1,3,6					37889
1,4,5	89			1	2.2
1,4,6					13616
1,5,6		600.4			104.8
2,3,4	18.7				675
2,3,5	131.2				120.4
2,3,6	110.6	109.4			719.4
2,4,5	36			0.75	30.2
2,4,6	33.4	32.15			1080
2,5,6					
3,4,5			378		
3,4,6					124117
3,5,6			2652		
4,5,6			1439	0.6	

From the Table 5-5, it was understood that combination between joints 3,4 and 6 gives the largest block around the cavern. The volume of block was calculated as $124117 m^3$. The required tunnel length to form the block is 21.5 m; therefore, the maximum block volume per 1 meter of tunnel length is calculated as $5778 m^3$. Block apex height was calculated as 1848m. However, the overburden is 30 m and the block apex is higher than the overburden. This type of analysis is an oversimplification of reality. Figure 5-7 shows the block in the roof of tunnel.



Fig. 5-7 Joint combination f 3,4,6 conventional KLE

5-4 Kinematic Analysis Considering Joint Length

In this type of analysis, joint length is limited to 25 m according to the maximum observed joint trace length (Starzec, 2002). The analysis doesn't consider field stresses. Table 5-6 shows the unstable block volume, when the joints are limited to the observed length.

Table 5-6. Unstable block volume (m^3) from KLE with considering the joint length.

Combination	Lower right wedge wall	Lower left wedge wall	Upper left wedge	Upper right wedge	Roof wedge
1,2,3	0.1	0.1			300.6
1,2,4	0.1	0.1			122.7
1,2,5	0.1	0.1	0.15		103.8
1,2,6	0.1	0.1			53.8
1,3,4		12			
1,3,5		195			14.6
1,3,6		15			
1,4,5		87		1	2.2
1,4,6		19.3			
1,5,6		473.2			104.8
2,3,4	18.7	17.97			227.4
2,3,5	131.2	127.2			120.4
2,3,6	110.6	109.4			114.3
2,4,5	36			0.75	30.2
2,4,6	33.4	32.15			55.82
2,5,6					
3,4,5			153.62		
3,4,6			0.29		
3,5,6			450.8		
4,5,6			554	0.6	

As it can be seen from table 5-6, combination between joints 4,5 and 6 gives the largest block. The largest block has been form in 18.2 m of tunnel length. A volume of $30.4 m^3$ per 1 m of tunnel length resulted from analyses. Fig 5-8 shows the block resulted from combination between joints 3,4 and 6.

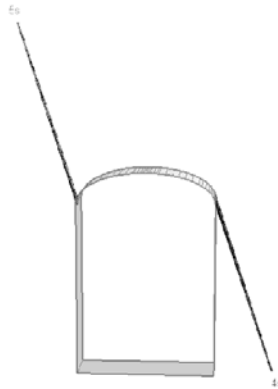


Fig 5-8 Combination 3,4,6 with considering joint persistency

By comparing Figures 5-7 and 5-8, it is understood that, by considering the joint trace length, forming of that large block (124117 m^3) is impossible. By considering the joint trace length instead of that large block, two small blocks form, and the volume of unstable block from 124117 is reduced to 0.29 m^3 .

5-5 Kinematic Analysis Considering Joint Length and Stress Field

In this type of analysis, both joint length and stress field have applied. The results have been shown in Table 5-7. As it can be seen from the table, the largest block has the volume of 473 m^3 from the combination 1,5,6. The block is formed in the tunnel length of 21.6 m. The formed largest block volume per 1 meter of tunnel length could be calculated as 21.8 m^3 . A comparison between Table 5-6 and 5-7 shows that, by considering the stress field, most of the roof blocks became stable. Figure 5-9 shows the combination 1,4,6 by considering both stress field and joint length; and Fig. 5-10 shows the same joint combination for conventional analysis. By looking at the tables 5-7 and 5-5 respectively, it is understood that by considering the stress field and joint length, the unstable block volume is zero while for conventional analysis, it is 13616 m^3 . The design based on conventional analysis is overdesign and it imposes expenditure to a project.

Table 5-7. Unstable block volume (m^3) from the KLE analysis by considering joint length and field stresses.

Combination	Lower right wedge wall	Lower left wedge wall	Upper left wedge	Upper right wedge	Roof wedge
1,2,3	0.1	0.1			
1,2,4	0.1	0.1			
1,2,5	0.1	0.1	0.15		
1,2,6	0.1	0.1			
1,3,4					
1,3,5		195			14.6
1,3,6					
1,4,5				1	2.2
1,4,6					
1,5,6		473.2			
2,3,4					
2,3,5					
2,3,6					
2,4,5	36			0.75	
2,4,6	33.4	32.15			
2,5,6					
3,4,5					
3,4,6					
3,5,6					
4,5,6				0.6	

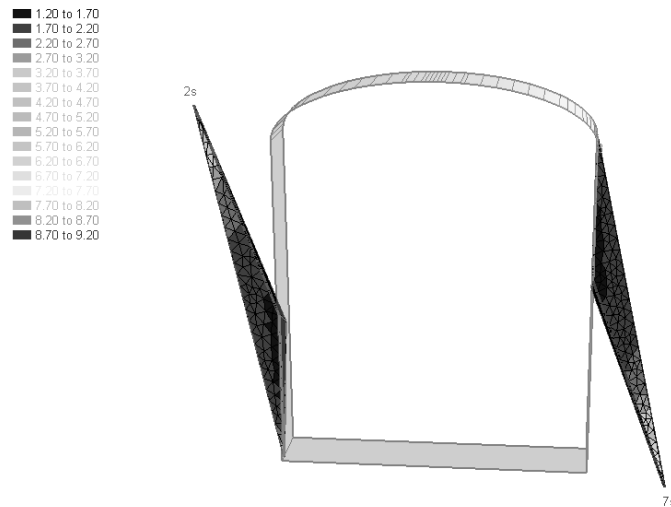


Fig 5-9. 1,4,6 Combination with applied stress and joint persistency

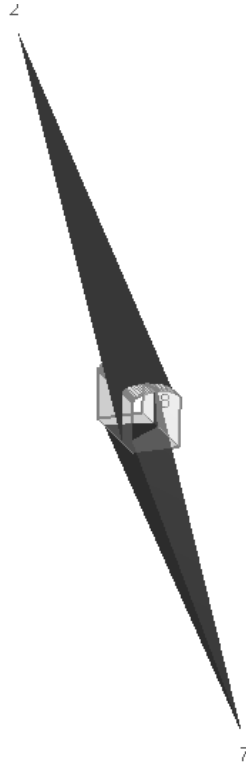


Fig. 5-10. 1,4,6 Combination unlimited joint length (conventional analysis)

5-6 Probabilistic Kinematic Analysis

As it can be seen from the Table 5-5, the conventional KLE with infinite assumption of joint persistency is an oversimplification of reality and leads to an overestimation of unstable block volume around an opening. An estimation of the appropriate fracture length may result in a more economical design of an opening. The effects of fracture persistency on the block volume estimation have been discussed in (Villaescusa and Brown, 1991 and Kim et al., 2007). There is always a variation in the fracture geometric data, and it is very hard to find a representative value for them. The deterministic approach will result in a block volume that cannot show the influences of in-data variation. Therefore, the application of probabilistic methods in fracture

geometric analysis is inevitable. The probabilistic theory applied to estimate block volume considers the variation of fracture geometries in rock mass.

Kinematic analysis could be performed in the probabilistic approach if input data such as fracture length and orientation were considered as stochastic values. A Monte Carlo simulation could be used for this purpose. A code based on Fortran has been developed to pick the values for joint persistency. Moreover, the code has been modified in order to pick the values for joint orientation, which will be explained in section 5-7-2. Figure 5-11a shows the contour plots of pole of fracture planes that are generated and used in our probabilistic KLE analysis as well as the contour plot of poles of mapped fracture during the excavation of the cavern (Fig. 5-11b). As can be seen, the fracture orientations generated using the Monte Carlo method (Fig. 5-11a) fit well with the real mapped fracture orientation shown in Fig. 5-11b. This confirms that random selection of joint orientation accommodate with those observed in the floor of the cavern.

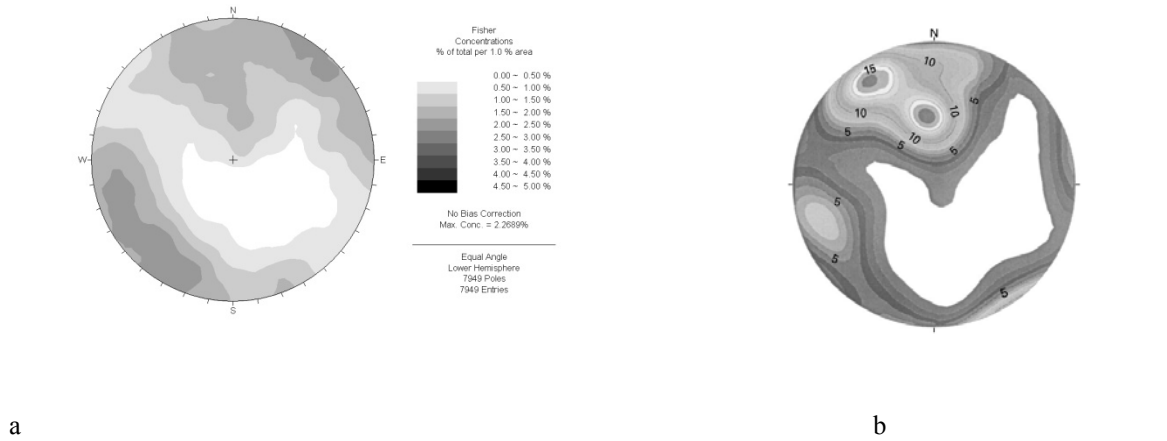


Fig. 5-11. (a) Fracture orientation resulting from Monte Carlo simulation (b) and fracture orientation resulting from fracture field mapping (Starzec and Anderson, 2002)

In this approach, the in-data for estimating block volume (including joint orientation and joint length) have been calculated based on probabilistic approach and the field stresses has been applied. The volume of unstable blocks was estimated for 1m of tunnel length based on the probabilistic KLE. Figure 5-12 shows the estimated block volume per 1m of tunnel length, which is the result of the KLE approach. The calculated mean value of block volumes is 0.05m^3 per meter of tunnel length.

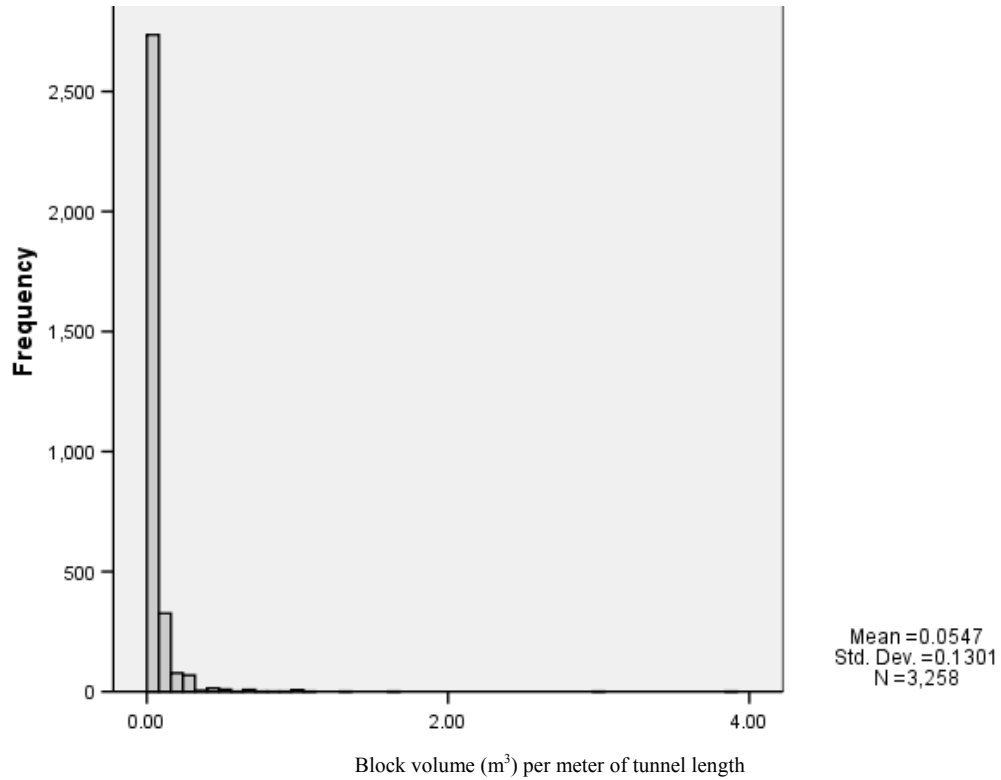


Fig. 5-12. Key block distribution resulting from probabilistic KLE

5-7 DFN Generations

The geometric parameters for generating fracture network were described in table 5-4. Table 5-3 shows the summary of orientation of set identification in CLAB 2 (Starzec and Andersson 2002).

5-7-1- Fracture Trace Lengths

The fracture length varies between 1.1 to 25 meters and follows the lognormal distribution, according to the following equation and using provided data in Table 5-4 in (Starzec and Andersson 2002):

$$l = \exp(\sqrt{2} \text{berfinv}\{F[g(l_{\max}) - g(l_{\min})] + g(l_{\min})\} + \bar{l}_{\log}). \quad 5-1$$

In this equation $g(l) = erf[(\ln l - \bar{l}_{\log}) / \sqrt{2b}]$, $erf()$ is error function of variable $()$, F is a number randomly generated using the uniform distribution in the range of $0 \leq F \leq 1$, l_{\min} and l_{\max} are the minimum and maximum fracture lengths, \bar{l}_{\log} and b are first and second moments of lognormal distribution.

5-7-2- Orientations of Fractures

The orientations of fracture sets follow to Fisher distribution. If θ is the angle of deviation from the mean orientation angle:

$$\theta = \cos^{-1} \left\{ \frac{\ln[e^k - F(e^k - e^{-k})]}{K} \right\}, \quad 5-2$$

Where K is the Fisher constant, which is assigned for each joint set according to Table -3. The Monte Carlo Method is then used to generate the trace lengths and the orientations of fractures based on equations (5-1) and (5-2).

5-7-3- Location of the Fractures

In this study, location of fractures follows a Poisson process. The locations of fracture centres are generated by generating random numbers based on a recursive algorithm that adopts the decimal part of calculated numbers with the following recursive equation

$$R_{i+1} = 27.0R_i - \text{int}(27.0R_i), \quad 5-3$$

where R_i is a random number in the range $0 \leq R_i \leq 1$, $\text{int}(x)$ is the integer part of the number x , and an initial value of R_0 is generated from the multiplicative congruencies algorithm (Priest 1993). If the generation space is defined in terms of two coordinate ranges $x_{g1} < x_{g2}$ and $y_{g1} < y_{g2}$ along a

local set of Cartesian axes, mid-point coordinates (x_i and y_i) of every fracture can be generated through the following equations (Priest 1993)

$$x_i = x_{g1} + R_i(x_{g2} - x_{g1}), \quad 5-4$$

$$y_i = y_{g1} + R_{i+1}(y_{g2} - y_{g1}). \quad 5-5$$

This algorithm was applied to generate the coordinates of the centres of the fractures in large-scale DFN models.

The observed two-dimensional fracture intensity (P_{21}) in CLAB 2 floor was found to be 1.32 m/m². By definition, P_{21} = Total fracture lengths/Unit area = Mean of fracture length \times (Total number of fractures/Unit area) = $\mu_m \times P_{20}$.

Therefore, in this particular study, considering the fracture percentage of the observed data, then: $P_{21} = 1.32 = (4.8 \times 66.1\% + 4.5 \times 33.9\%) \times P_{20}$, and finally $P_{20} = 0.28$.

P_{20}^1 = Fracture density for fracture set number 1 = $0.28 \times 66.1\% = 0.186$ and likewise,

P_{20}^2 = Fracture density for fracture set number 2 = $0.28 \times 33.9\% = 0.095$.

Fig. 5-13 shows the distribution of mid-point location of fractures in 105m \times 105m model.

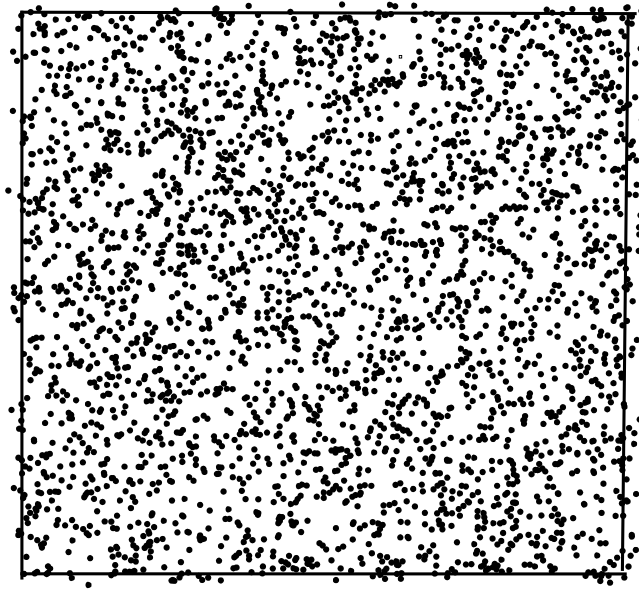


Fig. 5-13 Mid-point location of fractures in 105m \times 105m model

Despite the fact that the fracture transmissivity, which is related to the hydraulic aperture through the cubic law, is found to follow either lognormal or power law distributions and could be correlated with fracture trace length (Baghbanan and Jing, 2007), and also the fracture deformability could be a function of fracture aperture (Baghbanan and Jing, 2008), in this study in the spirit of simplicity, it is considered constant fracture aperture and normal stiffness for all of the fractures in the DFN model.

5-7-4- Fracture Generation Using Monte-Carlo Simulation

Fracture generation was performed based on the information of fracture location, orientation, size (trace length in 2D), aperture and P_{20} (Fracture density). Fracture density is used according to the calculated fracture density for each fracture sets and a Monte Carlo Method is facilitated using their corresponding Cumulative Distribution Function to simulate another parameters. A FORTRAN program, which was originally developed and used in (Min et al., 2004 and Baghbanan and Jing, 2007) is modified and used for generation DFN models in this study. To avoid a boundary effect, sufficiently large parent fracture networks were generated first to produce all possible candidate fractures and, of these candidates, the fractures that within the analysis area are selected. The size of the parent network was chosen to be 300 m \times 300 m. Then, small-scale DFN models are extracted from large-scale models. Fig. 5-14 shows an example of generation sequential DFN models from a parent model.

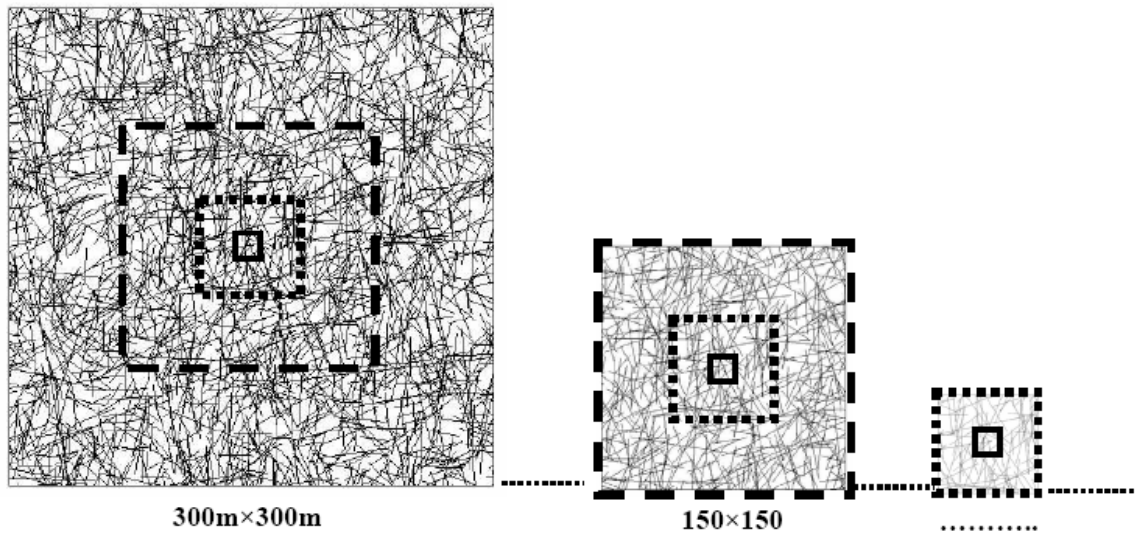


Fig. 5-14 Schematic view of generations of fracture networks

5-8 Calibration of DFN

In order to evaluate the rock block volume around an excavation using the stochastic DFN approach, a large number of DFN realizations should be generated. Furthermore, there is no criterion to determine how many realizations are required to analyze the block stability. This is still a subject of debate among researchers in this field of study.

In this study, the William-Watson's (W-W) statistical test was used to find the most similar DFN realizations with a mapped fracture pattern from the field. The W-W test is a statistical test of means for spherical data, which is conducted on the composite data set to determine the equivalency on the mean fracture orientations from two sets of observations. In this method, the orientation of fracture measurements is converted to polar coordinates for the calculation of a resultant vector. The resultant length of the vector is a measure of the concentration around a mean direction, if one exists. The calculated resultant lengths are used in a statistical F-approximation to test whether or not the mean fracture orientations of the two data sets are statistically different. The null hypothesis for the F-test states that the mean directions from two samples are not significantly different. This hypothesis is rejected when the calculated F statistic is greater than the critical value for a desired level of significance (Mardia, 1972 and Batschelet, 1981). The fractures in the roof and walls of the cavern and a cross cut perpendicular

to it were mapped (see Fig. 5-15) (Berglund, 2001). The W-W test was applied to both mapped tunnel surfaces (cross-cut of cavern and main cavern).

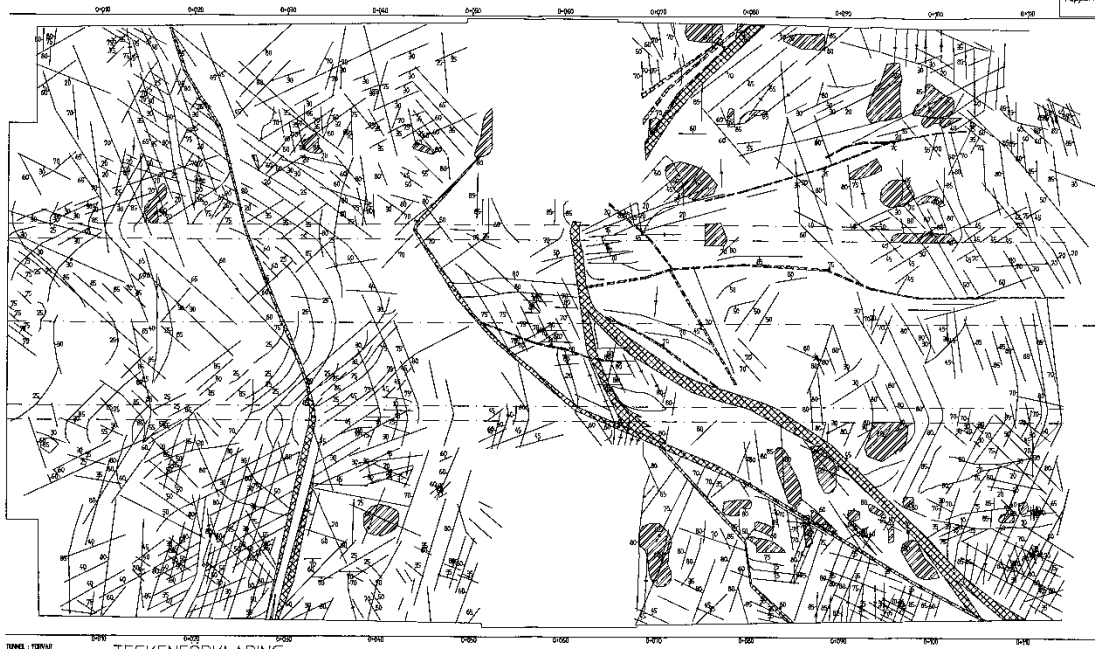


Fig. 5-15 Fracture mapping of roof and walls in the cavern

100 DFN realizations were first generated. A code in FORTRAN was developed based on the W-W test to check the compatibility of DFN realizations with the results of fracture mapping. Out of 100 DFN realizations, 9 were good matches with both (main cavern and cross-cut tunnel) fracture-mapping surfaces in the field.

5-9 DFN-DEM

The block assemblages which confirmed by W-W statistical test were analyzed by DEM. Figure 5-16 shows a pattern of the potential failed blocks from a DFN-DEM analysis. The red vectors show the displacements, and the assemblage of blocks is represented in

green. The estimated failed blocks in this analysis include both secondary blocks and other blocks located in the perimeter of cavern. Secondary blocks are the blocks which don't share a cavern boundary.

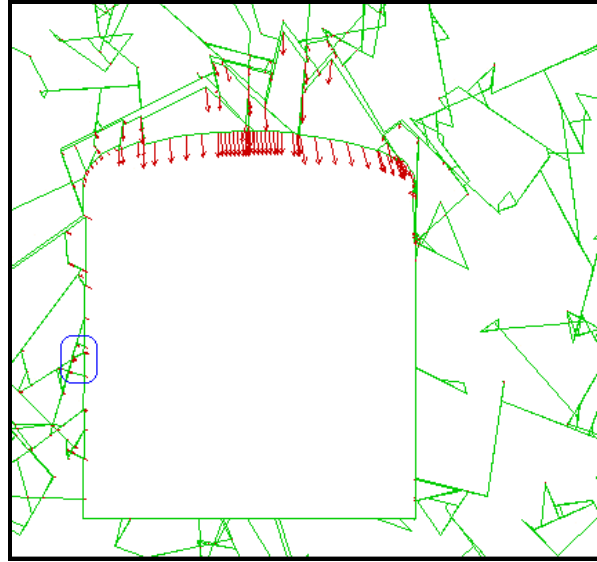


Fig. 5-16. Failed block around the cavern

Figure 5-17 show different types of block in the perimeter of the opening (see section 1-3).

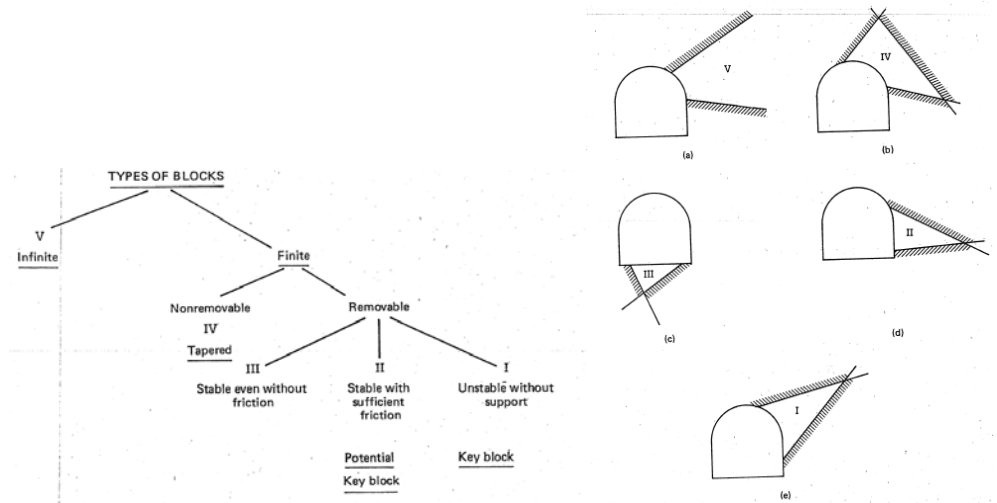


Fig. 5-17 Block types around tunnel (Goodman and Shi, 1985)

The purpose is to find the failed key blocks from the other types of failed block in this figure. Only potential failed blocks that share a cavern boundary (wall or roof) are compared with the block types shown in Figure 5-17. They are then classified into removable and non-removable groups. Class III consists of the blocks located in the floor of cavern, which were not taken into consideration. Other failure categories defined by Goodman and Shi are categories I and II in Figure 5-17 (Goodman and Shi, 1985). According to Goodman and Shi (1985), these types of blocks (types I and II) are the blocks that are dangerous and whose safety must be secured. Figure 5-18 shows an enlarged section marked by a blue line inside Figure 5-16. As can be seen in Figure 5-18, block number 1 can definitely be categorized as a tapered block and block number 2 as a key block. The third dimension of the block was calculated as the square root of the block area. Based on the third dimension of the block, it is possible to calculate the block volume for 1m of tunnel length. The number of blocks per 1m of tunnel length can also be obtained by determining the third dimension. For instance, when the block area is 0.25, the third dimension of the block is $l = \sqrt{0.25} = 0.5$, so the block volume is $V = 0.5 \times 0.25 = 0.125$. Therefore, in each unit length of tunnel, two blocks with this volume might appear. This procedure was applied for both block failure modes I and II in our analysis. Figure 5-19 shows the unstable key block volume distribution, which resulted from the DFN-DEM approach for each unit length of tunnel. The calculated mean value for the potential block volume is 0.34.

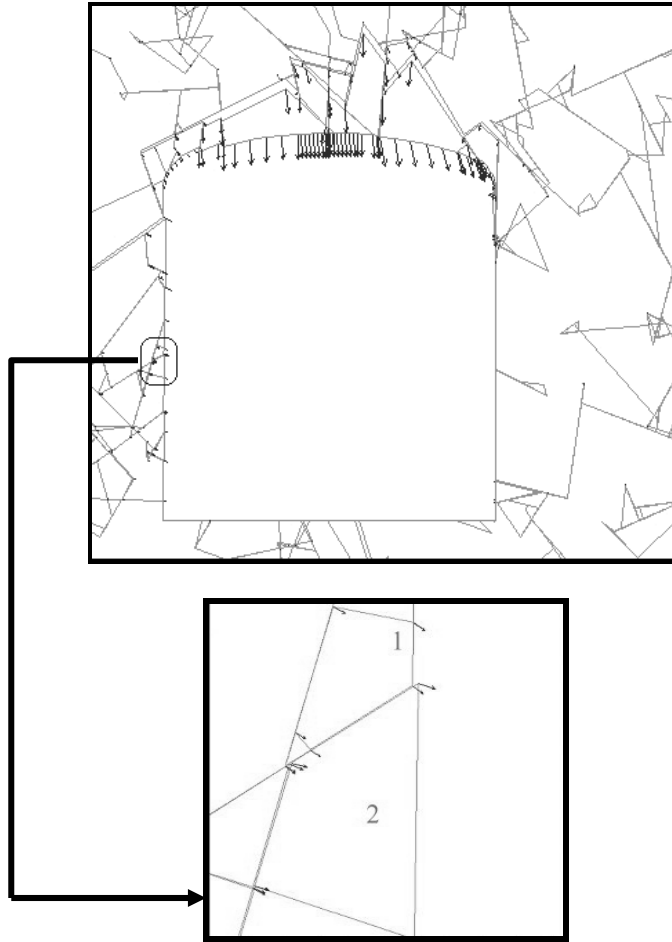


Fig. 5-18. Key block and tapered block around the cavern

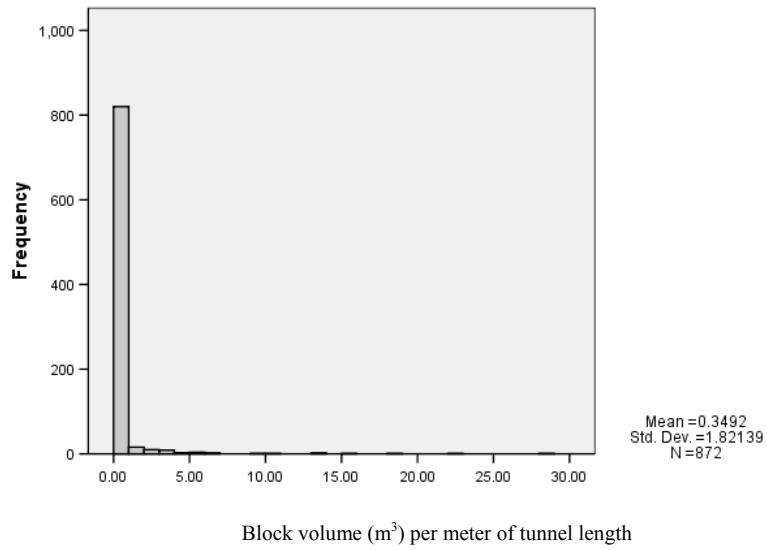


Fig. 5-19. Distribution of key block volume resulting from DFN-DEM

5-10 Discussion

The calculated volumes of possible failed blocks using the KLE method based on a Monte Carlo simulation yields results that are almost six times smaller than those from a DFN-DEM analysis (compare Figures 5-12 and 5-19).

The reason for this significant difference is that, in a DFN-DEM analysis, fracture termination is taken into consideration while in a KLE analysis it is not taken into account. The fracture termination ratio is defined in (ISRM, 1978) as the following formula:

$$T_i = \frac{100N_i}{N_i + N_a + N_o} \quad 5-6$$

Where N_i , N_a , and N_o are respectively the total number of discontinuities whose semi-trace terminations are in intact rock, at other discontinuities or are obscured, these have been calculated for a complete scanline sample or for a specific discontinuity set. A larger value for the fracture termination ratio indicates that a large portion of discontinuities terminates in the intact rock. Therefore, in a rock mass such as this, a large number of rock bridges are created compared with the expected discrete blocks, which means that the size of the blocks generated is much larger than when the fracture termination ratio is small. Starzec and Anderson (2002) reported this ratio around 13% of the fractures terminate in intact rock in this specific site investigation; while in the KLE analysis, this ratio is negligible (0%).

Figure 5-20 shows the fracture system before eliminating the incomplete fractures in UDEC. In this program, dead-end fractures (terminated fractures in intact rock) are eliminated, as shown in Figure 5-17. Elimination of incomplete fractures decreases fracture intensity; consequently, estimated block volumes are increased.

The two design tools used for the block stability analysis in this study are facilitated by different processes. The discontinuum formulation for rigid blocks and the explicit time-marching solution of the full equations of motion (including inertial terms) in DEM modelling allow the analysis of progressive, large-scale movements of blocks in blocky rock media; whereas, analytical solutions used in KLE compute the static force

equilibrium of the bodies and do not address the changes in force distribution that accompany displacements of the bodies. The solution using DEM was assumed to be the real solution; therefore, the difference between limit equilibrium and DEM could be counted as model uncertainty.

Figure 5-21 shows the exposed area of the block in the roof of the cavern in question in the KLE analysis using the Unwedge program. The exposed area of blocks was also calculated based on fracture mapping performed at the site. Figure 5-22 shows the distribution for the exposed area from fracture mapping. The mean value for the figure calculated is 2.69 m^2 . For the repeated Monte Carlo simulations in the KLE analysis, the exposed area was calculated. Figure 5-23 shows the distribution for the exposed area based on the probabilistic kinematic analysis. The calculated mean value is 0.97 m^2 . For the DFN approach, the mean value for the exposed area was calculated as 2.7 m^2 .

The ubiquitous presence of joints in a kinematic analysis means that the spatial variability of structure was not considered. This implies that all block wedges have the same possibility of being present in a particular situation. Obviously, this is not necessarily true for most applications (Hadjigeorgiou and Grenon, 2005).

In real conditions, all fractures may cross each other and there is not a limitation on the number of crossing fractures; however, the kinematic analysis can only estimate the tetrahedral blocks, which are the result of three-joint plane conjunctions in addition to the opening face.

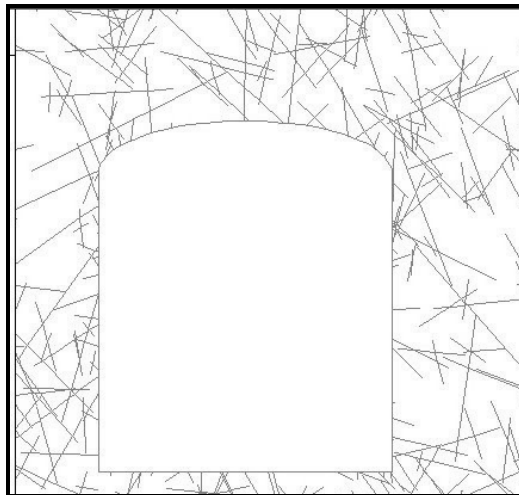


Fig. 5-20. Fracture network before eliminating incomplete fractures

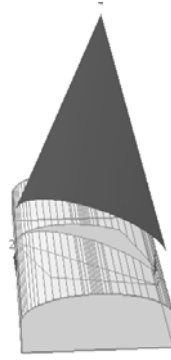


Fig. 5-21. Exposed area of a block in the roof of the opening

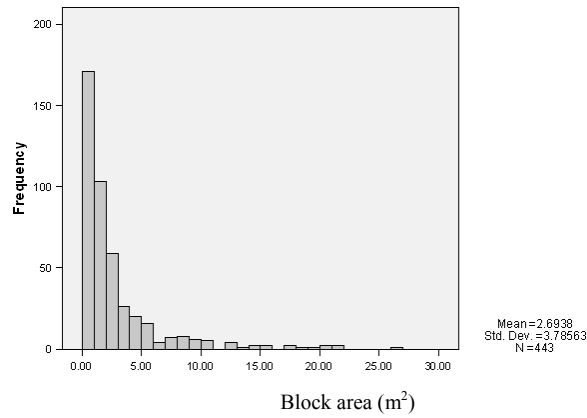


Fig 5-22. Distribution of the exposed area of block resulting from fracture mapping

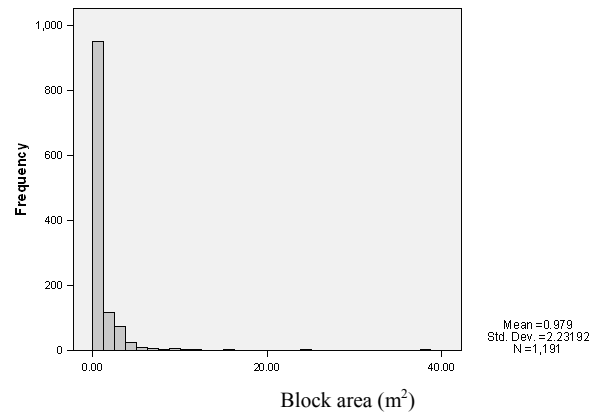


Fig 5-23. Distribution of the exposed area of block resulting from repeated Kinematic Limit Equilibrium analyses performed based on Monte Carlo simulations for length and orientation of fractures

Table 5-8 shows the outcome of different approaches to predict the unstable block volume for 1 m of tunnel length

Table 5-8. Unstable block volume predicted by different approaches for 1 m of tunnel length

Kinematic-Limit Equilibrium Analysis(m ³)				DFN-DEM
Conventional	Limited Joint Length	Limited Joint Length ad Stress Field	Probabilistic	
5778	30.4	21.8	0.05	0.34

5-11 Conclusions

Results of DFN-DEM analysis, which have been confirmed by a William-Watson test, were considered to be real. The conventional KLE which doesn't consider the fracture length and field stresses is on safe side and leads to a conservative design. By considering the fracture length in KLE, the estimated unstable block volume is reduced. But still this approach is on safe side and it is overdesign. Considering of stress field together with fracture length will reduce the unstable block volume further. But still this approach is on safe side and it is overdesign. It can also be concluded that a kinematic analysis based on a Monte Carlo simulation estimates block volume smaller than reality. The results of probabilistic approach analyses (both PKLE and DFN-DEM) could be shown in a distribution for the potential unstable block volume. This will show the designer the probability for forming block with a specific volume. The designer could decide about the acceptable unstable block volume related to its probability.

The results show that even considering limited joint length in kinematic analysis and the clamping forces in the limit equilibrium analysis, there is a great model uncertainty of our standard design tools for block stability analysis.

The analyses show that the results of probabilistic kinematic analysis are interesting and commercial software ought to develop to facilitate the calculation.

Chapter 6

Model Uncertainty of Bray-Crawford Solution

6-1. Introduction

As described in Chapter 4, the analytical solution proposed by Bray and Crawford (1983) is one design tool used to estimate safety and required rock support for blocks around tunnels. In order to perform the reliability analysis, it is necessary to consider the model of uncertainty. The purpose of this chapter is to measure the model uncertainty of the analytical solution based on the theory of model uncertainty (described in Chapter 2).

6-2. Methodology Used to Assess Model Uncertainty

Model uncertainty can only be quantified either by comparison with other more involved models that exhibit a closer representation of the nature or by comparison with collected data from the field or the laboratory (Ditlevsen, 1982). The author has not found any recorded case in which failed block geometry, volume, resistance parameters, and stresses, were measured. Therefore, the results of Crawford-Bray model have been compared to those results of Distinct Element Method (DEM) which have closer representation of reality. Figure 6-1 shows the methodology employed to quantify the model uncertainty of Bray-Crawford solution. The methodology that has been used here to assess the model uncertainty is to calculate the vertical force at failure based on analytical solution (T_{analytic} Eq. 4-20), and compare it with the vertical force required to fail the block calculated by DEM (T_{numeric}). In other word, model uncertainty factor (I) could be calculated as
$$I = \frac{T_{\text{numeric}}}{T_{\text{analytic}}}$$

UDEC, which is based on DEM, has been used to solve the same block geometries with the same properties used in analytical solution. In numeric model, in order to assess the vertical force at failure, the block density was increased or decreased until it reaches to the limit equilibrium. The corresponding block weight at limit equilibrium represents the vertical force at failure (T_{numeric}).

The T_y values higher than the natural weight of block (W) means that the block is stable. On the other hand, T_y lower than the natural weight of block means that the block is unstable. In other word $T_y - W > 0$ means that the block is stable, while $T_y - W < 0$ means that the block is unstable.

Two groups of studies have been done. First a primary study has been done to study the influence of vertical in-situ stress on the model uncertainty of analytical solution. In this study, Monte Carlo has been used to select friction angle and joint shear and normal stiffness. Thereafter a more detail study was carried out in order to describe how model uncertainty depends on variation of key parameters. In the last study, the selection of joint friction angle, shear and normal stiffness are not based on Monte Carlo. In this study the values of joint shear and normal stiffness are calculated based on in-situ stress, apical angle and friction angle. The following sections describe the Monte Carlo.

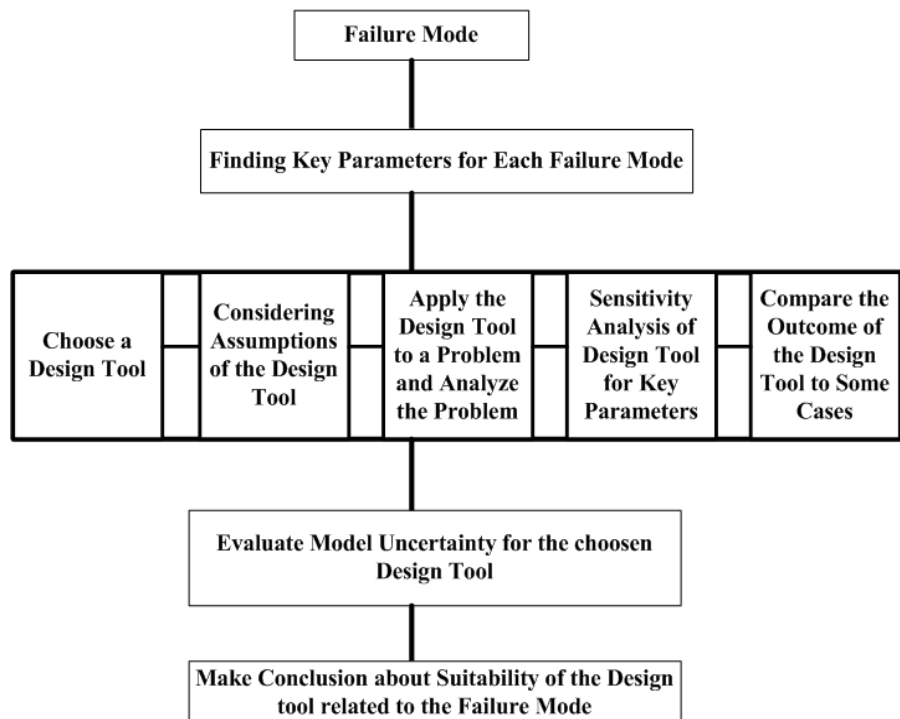


Fig.6-1. Methodology to assess model uncertainty

6-2-1. Monte Carlo Simulation

The Monte Carlo simulation in its simplest form is a random number generator that is useful for forecasting, estimating, and risking analysis. A simulation calculates numerous scenarios for a model by repeatedly picking values from a probability distribution for the uncertain variables and using those random values for in-data in the model. All those scenarios produce related results in a model.. Series of Monte Carlo simulations ran to select values for K_n , K_s and ϕ selected from a typical rock condition. The statistical parameters for K_n , K_s and ϕ are listed in Table 6-1 (Lanaro and Fredriksson, 2005). A code based on Fortran has been developed in order to select the input data based on Monte Carlo simulation. Note that the values of joint normal and shear stiffness (K_n and K_s) in analytical solution are related to those of the numerical solution by the length L of the discontinuity bounding the wedge (Crawford, 1982).

Table 6-1. Statistical parameters for K_n , K_s and ϕ (Lanaro and Fredriksson, 2005)

Parameter	Distribution	Minimum value	Mean value	Maximum value	Standard deviation
K_n (GPa/m)	Normal truncated	49.2	100.2	179.3	31.9
K_s (GPa/m)	Normal truncated	10.3	29.3	48.7	10.6
ϕ degree	Normal	24	32	40	4

6-3 Primary Study

Figure 6-2 shows a two-dimensional geometry of the model that has been employed in order to assess the true value. The geometry consists of a $5 \times 5m$ square shape tunnel with a single triangular block with 30 degree of semi-apical angle and a base dimension of 3 m in the roof of tunnel. The horizontal stress was set to 6.6 MPa, which has been measured in a CLAB2 cavern and has an overburden of 30 m (Fredriksson et al., 2001).

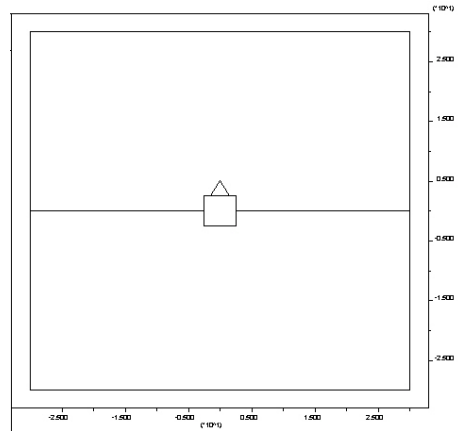


Fig.6-2. Employed geometry for both analytical and numerical method

Two groups of modelling have been done. The groups are different according to vertical in-situ stress. The first group considered no value of vertical in-situ stress. The other group considered some value of vertical in-situ stress (5 and 10 MPa). The rigid mode of analysis has been chosen for the numeric model as the analytical model has a rigid body assumption.

According to Barton and Choubey (1977) and Barton (1971), as a rule of thumb, displacement equal to 1% of joint length is the displacement at failure. This criterion has been adopted in a Fish function in UDEC to check the stability condition. In addition to this criterion, the unbalance force has been recorded and checked to ensure whether or not the block is stable.

The following sections show the model uncertainty for different values of vertical stress (0, 5 and 10 MPa).

6-4. Results Model Uncertainty in the Absence of In-Situ Vertical Stress

The calculation based on the horizontal stress of 6.6 MPa has been conducted for many random selection of joint properties (K_n , K_s and ϕ) based on Monte Carlo. The ratio values for $T_{y_{\text{numeric}}} / T_{y_{\text{analytical}}}$ has been shown in Figure 6-3. In this figure, the horizontal axis is the coefficient of model uncertainty. The mean value and standard deviation for the coefficient I were calculated as 1.013 and 0.26%, respectively.

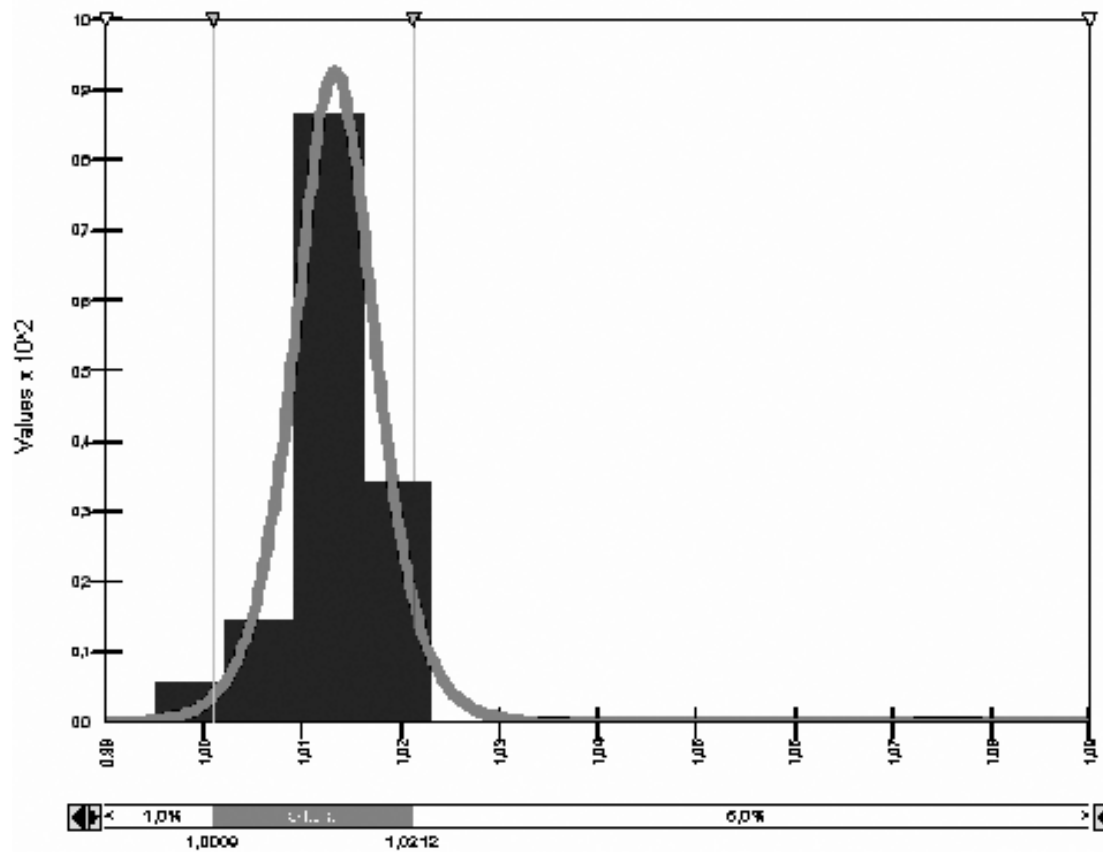


Fig. 6-3. Model uncertainty for $\sigma_x=6.6$, $\sigma_y=0$ MPa

As it is obvious from the Figure 6-3, in the absence of in-situ vertical stress and high value of horizontal stress, the analytical solution could estimate the block stability properly.

6-5. Results Model Uncertainty in the Presence of In-Situ Vertical Stress

The model uncertainty for Bray-Crawford solution has been estimated for cases with $\sigma_{xx}=6.6$ MPa, $\sigma_{yy}=5$ MPa and $\sigma_{xx}=6.6$ MPa, $\sigma_{yy}=10$ MPa,. Figures 6-4 and 6-5 show the model uncertainty of Bray and Crawford solution in the presence of vertical in-situ stresses by 5 and 10 MPa, respectively. In those figures, the horizontal axis is the model uncertainty.

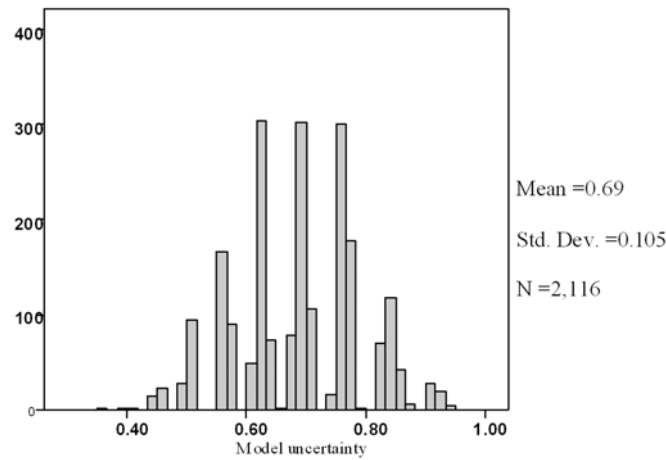


Fig. 6-4 Bray model uncertainty in the presence of 5 MPa vertical in-situ stress

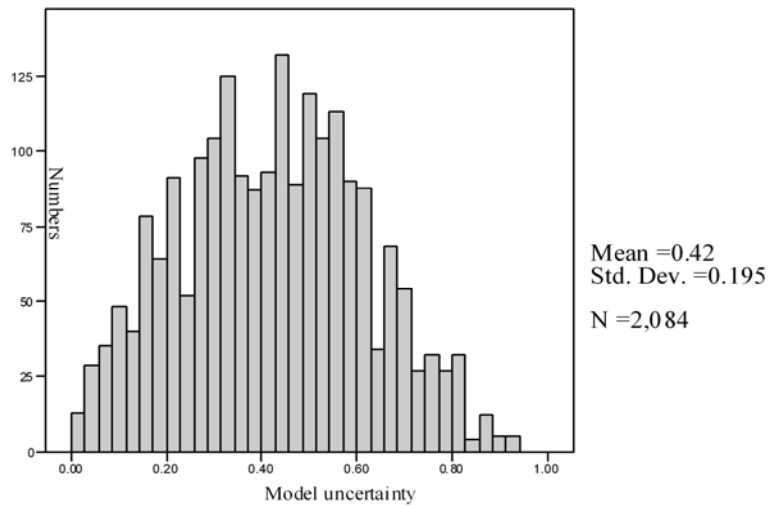


Fig. 6-5 Bray model uncertainty in the presence of 10 MPa vertical in-situ stress

It is understandable that uncertainty in the model is increased by increasing of vertical stress. The comparison between figures 6-4 and 6-5 shows that the mean value of model uncertainty factor is decreased by increasing of vertical stress in other word, the uncertainty in the model is increased by increasing of vertical in-situ stresses. The standard deviation of model uncertainty is increased by increasing of vertical in-situ stresses.

Table 6-2 shows the model uncertainty of analytical solution for one realization of Monte Carlo in different in-situ vertical stress. The horizontal in-situ stress was assumed to be 6.6 in all cases.

Table 6-2. Results of one realization with different vertical in-situ stress

σ_y	T_y (Analytical) MN	T_y (Numeric) MN	Ratio $T_y \text{ Numeric} / T_y \text{ Analytic}$
0	3.692	3.74	1.013
0.86	3.692	3.45	0.93
1.5	3.692	3.23	0.87
2.5	3.692	2.9	0.78
4	3.692	2.39	0.64
6	3.692	1.754	0.47
8	3.692	1.43	0.39
10	3.692	1.14	0.31

It is obvious from Table 6-2 that by increasing the vertical stress, the uncertainty in model increases (model uncertainty factor is decreased) and the value of model uncertainty depends on the value of in-situ vertical stress.

In this section, the model uncertainty has been assessed for various values of vertical in-situ stress while the horizontal stress is considered constant (6.6 MPa) for all cases. In the following section therefore it was tried to assess the model uncertainty in detail including more stress situations and more variation of joint resistance parameter ratio for different apical angle.

6-6. *Detail Study of Model Uncertainty of Analytical Solution*

According to sections 6-3 to 6-5, it was discovered that the uncertainty of analytical solution depends on the in-situ stress condition. In principal, model uncertainty depends on model assumptions, simplification and in-data; therefore the model uncertainty of analytical solution was estimated for different stresses, resistance properties, and block geometries (apical angles).

The tunnel depth was considered as 20, 100, and 400 m. For each depth, the K_0 (ratio of horizontal stress to vertical stress) was considered to be 0.5, 1, and 2. Therefore, from the stress state, there are $3 \times 3 = 9$ states for stresses. Other important parameters are the block semi-apical angle and joint friction angle. The block semi-apical angle was considered to be 10, 20, 30, and 40 degrees. The friction angle was considered 30, 40, and 50 degrees. The cases in which the semi-apical angle is equal or greater than friction angle are neglected.

Other important key parameters are joint shear and normal stiffness. The values of joint shear stiffness have could be calculated based on Eq. 6-1 (Barton and Chouby, 1977).

$$K_s = \frac{100}{L} \sigma_n \tan \left[JRC \log_{10} \left(\frac{JCS}{\sigma_n} \right) + \phi_r \right] \quad 6-1$$

The in-data in equation 6-1 are normal stress on the joint plane, σ_n , total joint friction ($\phi_r + i$), and joint length (L). By knowing the values of vertical and horizontal stresses, the value of σ_n could be calculated from a continuum analysis, such as BEM, in the joint plane. The EXAMINE 2D (Curran, et al, 1995) based on BEM has been employed to calculate σ_n in different in-situ stress condition (vertical and horizontal) and different apical angles. Table 6-3 shows the calculated values for σ_n . Joint length has been calculated for a geometry in which the block has the specific semi-apical angle, and a base of 3 m. The value of total friction angle has been used instead

of
$$\left[JRC \log_{10} \left(\frac{JCS}{\sigma_n} \right) + \phi_r \right].$$

Table 6-3. Calculated values of σ_n based on BEM for different depth and stress state

Depth(m)	α	σ_v (MPa)	σ_h (MPa)	σ_n (MPa)
20	10	0.5	0.25	0.275
	20	0.5	0.25	0.238
	30	0.5	0.25	0.17
	40	0.5	0.25	0.11
	10	0.5	0.5	0.574
	20	0.5	0.5	0.544
	30	0.5	0.5	0.45
	40	0.5	0.5	0.339
	10	0.5	1	1.17
	20	0.5	1	1.15
	30	0.5	1	1.01
	40	0.5	1	0.789
100	10	2.5	1.25	1.375
	20	2.5	1.25	1.19
	30	2.5	1.25	0.86
	40	2.5	1.25	0.57
	10	2.5	2.5	2.87
	20	2.5	2.5	2.72
	30	2.5	2.5	2.26
	40	2.5	2.5	1.69
	10	2.5	5	5.86
	20	2.5	5	5.79
	30	2.5	5	5.05
	40	2.5	5	3.94
400	10	10	5	5.5
	20	10	5	4.76
	30	10	5	3.5
	40	10	5	2.28
	10	10	10	11.49
	20	10	10	10.89
	30	10	10	9.04
	40	10	10	6.78
	10	10	20	23.47
	20	10	20	23.17
	30	10	20	20.21
	40	10	20	15.78

The joint normal stiffness could be calculated regarding to the values of joint shear stiffness and the ratio of K_n/K_s . The ratio of K_n/K_s depends strongly on the normal stress (Bandis, et al, 1981, Oda, et al. 1993). An extremely high ratio (let us say 130) appears on stress levels less than 0.5MPa. Beyond 0.5MPa, the ratio decreases with increasing σ_n toward an asymptotic value of approximately 10. It seems reasonable, however, to assume that the ratio is within the range of 1 to 10 if the normal stress σ_n , is larger than, at least, 0.5 MPa.

As can be seen from Fig 6-6, there are different ratios of normal to shear stiffness depending on the normal stress (for example, for the $\sigma_n = 0.2$, the possible range could be between 10 and 40). The selected ratio could be 10, 30, and 40. Total 243 models have been built in different apical, friction angle, horizontal and vertical stresses and different stiffness ratio.

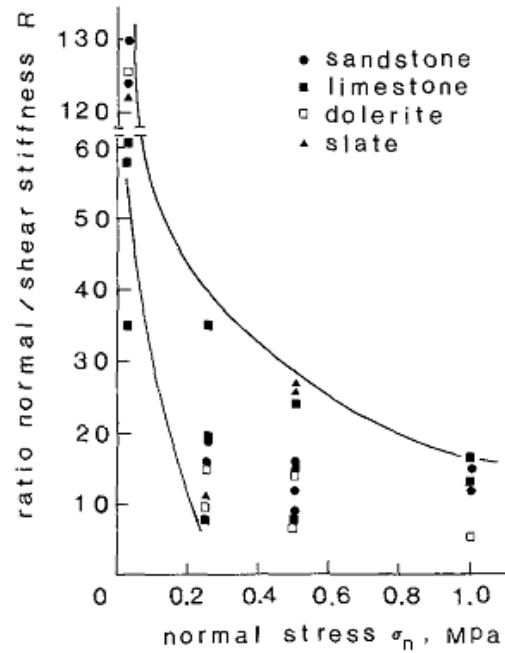


Fig. 6-6 Dependence of stiffness ratio (R) on normal stress (Bandis et al., 1981)

Tables 6-4 through to 6-7 show the calculated values of K_n and K_s in different stress conditions, stiffness ratio, friction angle, and block apical angle. These values have the unit of MPa/m.

Table 6-4. Calculated K_n and K_s values for a block with semi-apical angle of 10 degrees

σ_v	σ_h	Φ			Φ			Φ		
		30			40			50		
		K_n/K_s			K_n/K_s			K_n/K_s		
0.5	0.25	10	30	40	10	30	40	10	30	40
K_n		18.3	54.9	73.2	26.7	80.1	106.8	37.9	113.7	151.6
K_s		1.83	1.83	1.83	2.67	2.67	2.67	3.79	3.79	3.79
		K_n/K_s			K_n/K_s			K_n/K_s		
0.5	0.5	10	20	30	10	20	30	10	20	30
K_n		38.4	76.8	115.2	55.8	111.6	167.4	79.2	158.4	237.6
K_s		3.84	3.84	3.84	5.58	5.58	5.58	7.92	7.92	7.92
		K_n/K_s			K_n/K_s			K_n/K_s		
0.5	1	1	5	10	1	5	10	1	5	10
K_n		7.82	39.1	78.2	11.37	56.85	113.7	16.15	80.75	161.5
K_s		7.82	7.82	7.82	11.37	11.37	11.37	16.15	16.15	16.15
		K_n/K_s			K_n/K_s			K_n/K_s		
2.5	1.25	1	5	10	1	5	10	1	5	10
K_n		9.19	45.95	91.9	13.36	66.8	133.6	18.98	94.9	189.8
K_s		9.19	9.19	9.19	13.36	13.36	13.36	18.98	18.98	18.98
		K_n/K_s			K_n/K_s			K_n/K_s		
2.5	2.5	1	5	10	1	5	10	1	5	10
K_n		19.2	96	192	27.9	139.5	279	39.6	198	396
K_s		19.2	19.2	19.2	27.9	27.9	27.9	39.6	39.6	39.6
		K_n/K_s			K_n/K_s			K_n/K_s		
2.5	5	1	5	10	1	5	10	1	5	10
K_n		39.2	196	392	56.97	284.85	569.7	80.92	404.6	809.2
K_s		39.2	39.2	39.2	56.97	56.97	56.97	80.92	80.92	80.92
		K_n/K_s			K_n/K_s			K_n/K_s		
10	5	1	5	10	1	5	10	1	5	10
K_n		36.79	183.95	367.9	53.47	267.35	534.7	75.95	379.75	759.5
K_s		36.79	36.79	36.79	53.47	53.47	53.47	75.95	75.95	75.95
		K_n/K_s			K_n/K_s			K_n/K_s		
10	10	1	5	10	1	5	10	1	5	10
K_n		76.86	384.3	768.6	111.71	558.55	1117.1	158.67	793.35	1586.7
K_s		76.86	76.86	76.86	111.71	111.71	111.71	158.67	158.67	158.67
		K_n/K_s			K_n/K_s			K_n/K_s		
10	20	1	5	10	1	5	10	1	5	10
K_n		157.01	785.05	1570.1	228.2	1141	2282	324.1	1620.5	3241
K_s		157.01	157.01	157.01	228.2	228.2	228.2	324.1	324.1	324.1

Table 6-5. Calculated K_n and K_s values for a block with semi-apical angle of 20 degrees

		Φ			Φ			Φ		
		30			40			50		
		K_n/K_s			K_n/K_s			K_n/K_s		
0.5	0.25	10	30	40	10	30	40	10	30	40
K_n		31.5	94.5	126	45.9	137.7	183.6	65.2	195.6	260.8
K_s		3.15	3.15	3.15	4.59	4.59	4.59	6.52	6.52	6.52
		K_n/K_s			K_n/K_s			K_n/K_s		
0.5	0.5	10	20	30	10	20	30	10	20	30
K_n		72.2	144.4	216.6	104.9	209.8	314.7	149	298	447
K_s		7.22	7.22	7.22	10.49	10.49	10.49	14.9	14.9	14.9
		K_n/K_s			K_n/K_s			K_n/K_s		
0.5	1	1	5	10	1	5	10	1	5	10
K_n		15.26	76.3	152.6	22.18	110.9	221.8	31.15	155.75	311.5
K_s		15.26	15.26	15.26	22.18	22.18	22.18	31.15	31.15	31.15
		K_n/K_s			K_n/K_s			K_n/K_s		
2.5	1.25	1	5	10	1	5	10	1	5	10
K_n		15.79	78.95	157.9	22.95	114.75	229.5	32.6	163	326
K_s		15.79	15.79	15.79	22.95	22.95	22.95	32.6	32.6	32.6
		K_n/K_s			K_n/K_s			K_n/K_s		
2.5	2.5	1	5	10	1	5	10	1	5	10
K_n		36.1	180.5	361	52.46	262.3	524.6	74.51	372.55	745.1
K_s		36.1	36.1	36.1	52.46	52.46	52.46	74.51	74.51	74.51
		K_n/K_s			K_n/K_s			K_n/K_s		
2.5	5	1	5	10	1	5	10	1	5	10
K_n		76.84	384.2	768.4	111.68	558.4	1116.8	158.62	793.1	1586.2
K_s		76.84	76.84	76.84	111.68	111.68	111.68	158.62	158.62	158.62
		K_n/K_s			K_n/K_s			K_n/K_s		
10	5	1	5	10	1	5	10	1	5	10
K_n		63.17	315.85	631.7	91.81	459.05	918.1	130.408	652.04	1304.08
K_s		63.17	63.17	63.17	91.81	91.81	91.81	130.408	130.408	130.408
		K_n/K_s			K_n/K_s			K_n/K_s		
10	10	1	5	10	1	5	10	1	5	10
K_n		144.5	722.5	1445	210.06	1050.3	2100.6	298.34	1491.7	2983.4
K_s		144.5	144.5	144.5	210.06	210.06	210.06	298.34	298.34	298.34
		K_n/K_s			K_n/K_s			K_n/K_s		
10	20	1	5	10	1	5	10	1	5	10
K_n		307.52	1537.6	3075.2	446.9	2234.5	4469	634.78	3173.9	6347.8
K_s		307.52	307.52	307.52	446.9	446.9	446.9	634.78	634.78	634.78

Table 6-6. Calculated K_n and K_s values for a block with semi-apical angle of 30 degrees

		Φ			Φ		
		40			50		
		K_n/K_s			K_n/K_s		
0.5	0.25	10	25	50	10	25	50
K_n		47.54898	118.8724	237.7449	67.5327	168.8318	337.6635
K_s		4.754898	4.754898	4.754898	6.75327	6.75327	6.75327
		K_n/K_s			K_n/K_s		
0.5	0.5	10	20	30	10	20	30
K_n		126.4243	252.8487	379.273	179.5575	359.1151	538.6726
K_s		12.64243	12.64243	12.64243	17.95575	17.95575	17.95575
		K_n/K_s			K_n/K_s		
0.5	1	1	5	10	1	5	10
K_n		28.24969	141.2484	282.4969	40.12237	200.6119	401.2237
K_s		28.24969	28.24969	28.24969	40.12237	40.12237	40.12237
		K_n/K_s			K_n/K_s		
2.5	1.25	1	5	10	1	5	10
K_n		24.05419	120.2709	240.5419	34.1636	170.818	341.636
K_s		24.05419	24.05419	24.05419	34.1636	34.1636	34.1636
		K_n/K_s			K_n/K_s		
2.5	2.5	1	5	10	1	5	10
K_n		63.21217	316.0609	632.1217	89.77877	448.8939	897.7877
K_s		63.21217	63.21217	63.21217	89.77877	89.77877	89.77877
		K_n/K_s			K_n/K_s		
2.5	5	1	5	10	1	5	10
K_n		141.2484	706.2422	1412.484	200.6119	1003.059	2006.119
K_s		141.2484	141.2484	141.2484	200.6119	200.6119	200.6119
		K_n/K_s			K_n/K_s		
10	5	1	5	10	1	5	10
K_n		97.61526	488.0763	976.1526	138.6407	693.2033	1386.407
K_s		97.61526	97.61526	97.61526	138.6407	138.6407	138.6407
		K_n/K_s			K_n/K_s		
10	10	1	5	10	1	5	10
K_n		252.8487	1264.243	2528.487	359.1151	1795.575	3591.151
K_s		252.8487	252.8487	252.8487	359.1151	359.1151	359.1151
		K_n/K_s			K_n/K_s		
10	20	1	5	10	1	5	10
K_n		565.2735	2826.367	5652.735	802.8447	4014.223	8028.447
K_s		565.2735	565.2735	565.2735	802.8447	802.8447	802.8447

Table 6-7. Calculated K_n and K_s values for a block with semi-apical angle of 40 degrees

		Φ		
		50		
		K_n/K_s		
0.5	0.25	10	25	50
K_n		56	140	280
K_s		5.6	5.6	5.6
		K_n/K_s		
0.5	0.5	10	20	35
K_n		173.3	346.6	606.55
K_s		17.33	17.33	17.33
		K_n/K_s		
0.5	1	1	5	10
K_n		40.35	201.75	403.5
K_s		40.35	40.35	40.35
		K_n/K_s		
2.5	1.25	1	5	10
K_n		29.15	145.75	291.5
K_s		29.15	29.15	29.15
		K_n/K_s		
2.5	2.5	1	5	10
K_n		86.44	432.2	864.4
K_s		86.44	86.44	86.44
		K_n/K_s		
2.5	5	1	5	10
K_n		201.5	1007.5	2015
K_s		201.5	201.5	201.5
		K_n/K_s		
10	5	1	5	10
K_n		116.6	583	1166
K_s		116.6	116.6	116.6
		K_n/K_s		
10	10	1	5	10
K_n		346.78	1733.9	3467.8
K_s		346.78	346.78	346.78
		K_n/K_s		
10	20	1	5	10
K_n		807.11	4035.55	8071.1
K_s		807.11	807.11	807.11

Bray and Crawford suggested that the value for clamping force in Eq. 4-20 could be calculated as the $C = h \times \sigma_h$ in which h is the height of block and σ_h is the horizontal in-situ stress. Examine 2D could be used to analyze stresses for openings with square shapes and the results are corresponding to those of Kirsch solution which has been implemented for block stability analysis for circular opening by Elsworth (1986). The use of EXAMINE 2D to determine the stresses around underground excavation and application of that to the relaxation process is reported (Mauldon and Zhao, 1995). As it can be seen from table 6-8, in most of the cases, the calculated clamping force by EXAMINE 2D is higher than that suggested by Bray-

Crawford($C = \sigma_h c$). Also, as expected, the values of clamping force decreases by increasing the semi-apical angle. Furthermore, by increasing the horizontal in-situ stress, the value of clamping force increases. The model uncertainty of analytical solution was determined based on the BEM calculations of clamping forces.

The models have been built based on the geometry consists of a $5 \times 5m$ square shape tunnel with a single triangular block with different degree of semi-apical angle and base dimension of 3 m in the roof of tunnel. The deformable body of blocks has been chosen to analyze in UDEC.

Table 6-8. Calculated clamping force in different stress condition

Depth(m)	α	σ_v (MPa)	σ_h (MPa)	C(MN) BEM	C(MN) Bray
20	10	0.5	0.25	2.4	2.12
	20	0.5	0.25	1.1	1.03
	30	0.5	0.25	0.6	0.64
	40	0.5	0.25	0.3	0.44
	10	0.5	0.5	5	4.25
	20	0.5	0.5	2.5	2.06
	30	0.5	0.5	1.5	1.295
	40	0.5	0.5	1	0.89
	10	0.5	1	10.25	8.5
	20	0.5	1	5.4	4.12
	30	0.5	1	3.5	2.59
	40	0.5	1	2.4	1.78
100	10	2.5	1.25	11.9	10.625
	20	2.5	1.25	5.5	5.15
	30	2.5	1.25	2.9	3.2375
	40	2.5	1.25	1.6	2.225
	10	2.5	2.5	25	21.25
	20	2.5	2.5	12.6	10.3
	30	2.5	2.5	7.8	6.475
	40	2.5	2.5	5	4.45
	10	2.5	5	51.3	42.5
	20	2.5	5	27	20.6
	30	2.5	5	17.4	12.95
	40	2.5	5	12	8.9
400	10	10	5	47.7	42.5
	20	10	5	21.8	20.6
	30	10	5	11.8	12.95
	40	10	5	6.4	8.9
	10	10	10	100.2	85
	20	10	10	50.5	41.2
	30	10	10	31.1	25.9
	40	10	10	20.3	17.8
	10	10	20	205.3	170
	20	10	20	107.9	82.4
	30	10	20	69.8	51.8
	40	10	20	48	35.6

6-7. *Results of Simulations*

Fig 6-7 shows the results of all simulations. As it can be seen in this figure, if there is not any information about the depth, stress ratio, stiffness ratio, apical, and friction angle, then the model uncertainty varies substantially. The range is between -1 and 1. The mean value for the model uncertainty factor is 0.42. In this figures, the negative sign has the meaning that the analytical solution predicts the block is stable while DEM predicts the block is falling. The model uncertainty varies based on the in-situ stress situation, joint stiffnesses, apical and friction angle. In the following section first the reason for the difference between the outcome of analytical and DEM will be described and thereafter the variation of model uncertainty and its dependent with the mentioned parameters will be discussed.

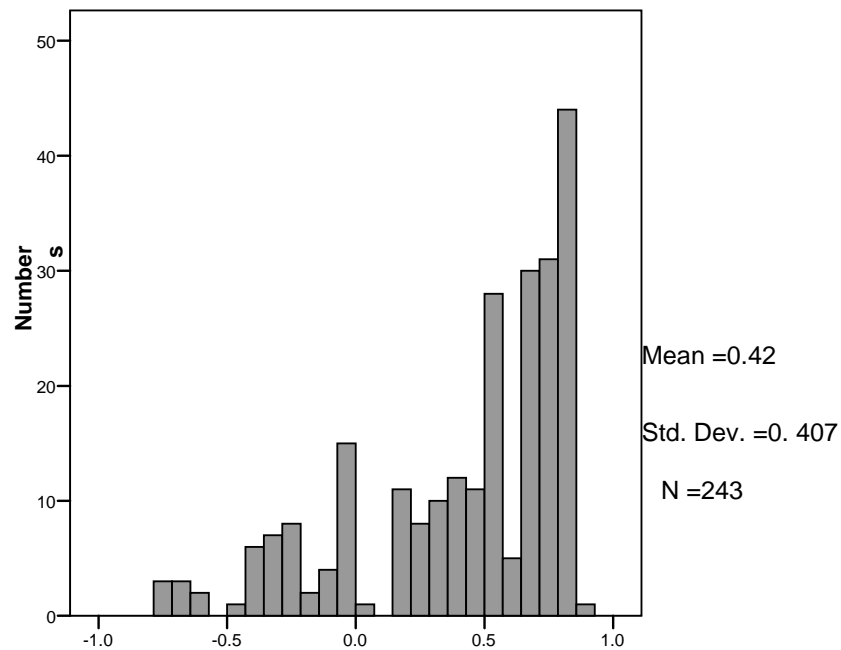


Fig. 6-7 Model uncertainty for all models

6-8. **Discussion**

The analyses show a difference between the results of DEM and analytical solution (see Fig 6-7). Some cases have been selected in order to discuss in detail. The selected cases are for depth of 100 m and $K_0=0.5$ with different stiffness ratio (1, 5, 10). The unit weight was considered as 2700 KN/m^3 . In-data are described in table 6-9.

Table 6-9. In-data for analyzed block

Parameter	Value
Semi-apical angle (degrees)	10
Friction angle (degrees)	30
Joint shear stiffness (MPa/m)	9.19
Vertical stress (MPa)	2.5
Horizontal Stress(MPa)	1.25

Figure 6-8 shows the applied geometry for the block in the roof of tunnel. According to the shown geometry, the joint length could be calculated as 8.63 m and the calculated clamping force by EXAMINE 2D is 11.9 MN. The in-situ condition is that the in-situ vertical and horizontal stresses are principal stresses.

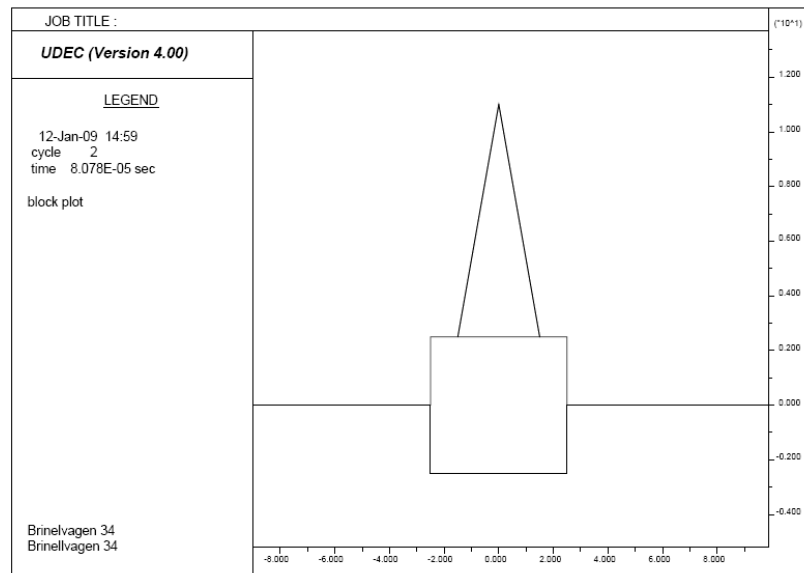


Fig. 6-8. Geometry of block

Eq. 4-19 which could be use to estimate block displacement is based on full mobilization of friction angle. This is not the case for all blocks with a natural density. In order to compare displacements from analytical and numerical solution, Eq. 4-19 must be revised in the way that the mobilization of friction angle is corresponding to the weight of the block. The displacement could be calculated from the Eq. 2-6, which is obtained from putting the block weight equal to T in Eq. 11-4, and is also by putting Eq. 8-4 and 9-4 into Eq. 11-4 and solving for δ .

$$\delta = \frac{W/2}{(K_s \cos^2 \alpha + K_n \sin^2 \alpha)} \quad 6-2$$

Table 6-10 shows the analytical and numerical calculations for shear, normal forces, and displacement. It is obvious that there is substantial difference between the outcome of DEM and analytical solutions (Table 6-10).

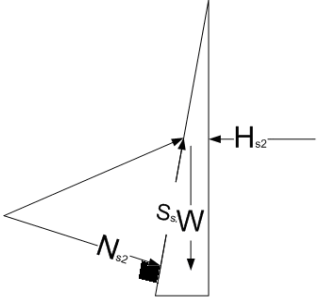
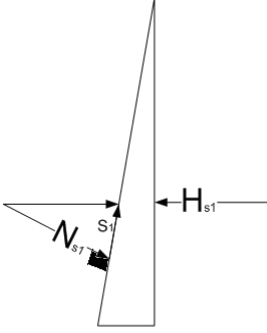
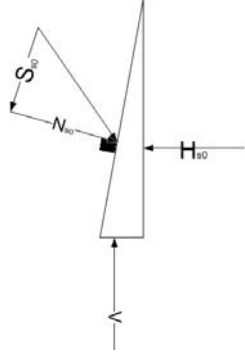
Table 6-10. Analytical and Numerical calculations

Parameter	R=1		R=5		R=10	
	Analytic	Numeric	Analytic	Numeric	Analytic	Numeric
Kn	79.4(MN/m)	9.19(Mpa/m)	397	45.95(Mpa/m)	794	91.9(Mpa/m)
Ks	79.4(MN/m)	9.19(Mpa/m)	79.4	9.19(Mpa/m)	79.4	9.19(Mpa/m)
δ (mm)	2.17	49.77	1.93	44.45	1.7	39.22
S'(MN)	2.23	2.01	2.21	1.6	2.19	1.2
N'(MN)	11.68	10.4	11.58	8.12	11.48	5.85
Model	0.8		0.65		0.45	

N' is the normal force to the joint after relaxation and S' is the shear force to the joint after relaxation.

Table 6-11 shows displacement and forces at different stages of relaxation in presence of in-situ stress (vertical and horizontal). Fig 6-9 shows the joint shear displacement about 0.06 mm at the stage before excavation. By excavating the tunnel, the vertical force disappears. The gravity force does not act in this stage. This stage could be called the first stage of relaxation (after excavation and before acting gravity force). In this stage, numerical solution shows a considerable amount of shear displacement in the joint. Fig 6-10 shows the joint shear displacement in the first stage of relaxation. The maximum amount of joint shear displacement is about 41mm. As it can be seen from Table 6-11, the normal force in this stage is reduced and the sign of shear force is changed. The changes in the sign of shear force mean that the direction of shear force has been changed due to the relaxation of the in-situ stress.

Table 6-11. Force and displacement in different stage of relaxation

 <p>Forces state after acting the gravity force</p>	 <p>Forces state after the excavation without acting gravity</p>	 <p>In-situ forces before the excavation</p>	Parameter	Kn/Ks
10.4	10.5	11.1	N(MN)	R=1
2.01	1.85	-1.84	S(MN)	
49.77	47.64	0	δ (mm)	
8.12	8.24	11.1	N(MN)	R=5
1.6	1.45	-1.84	S(MN)	
44.45	42.56	0	δ (mm)	
5.85	6.06	11.1	N(MN)	R=10
1.2	1.07	-1.84	S(MN)	
39.22	37.6	0	δ (mm)	

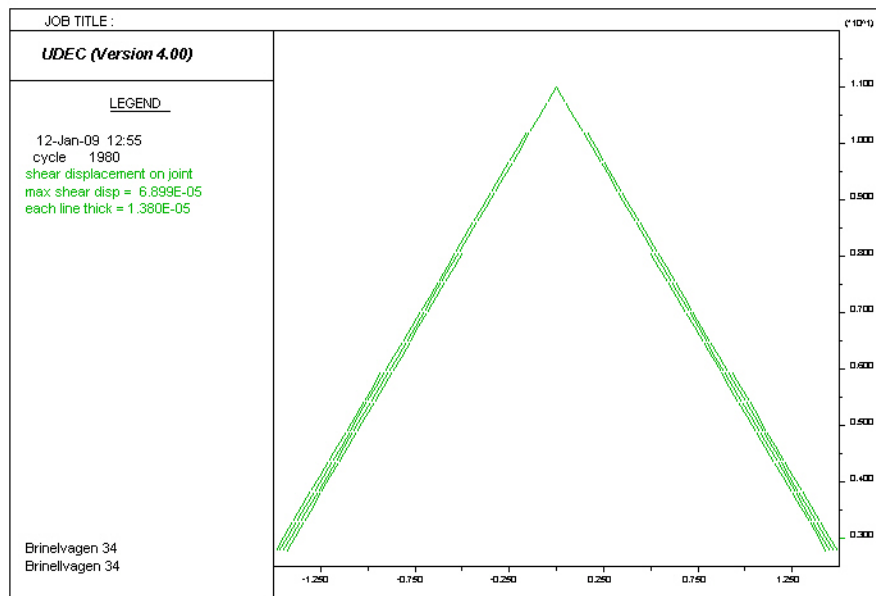


Fig. 6-9. Joint shear displacement in presence of in-situ stress without the excavation of tunnel for $R=5$

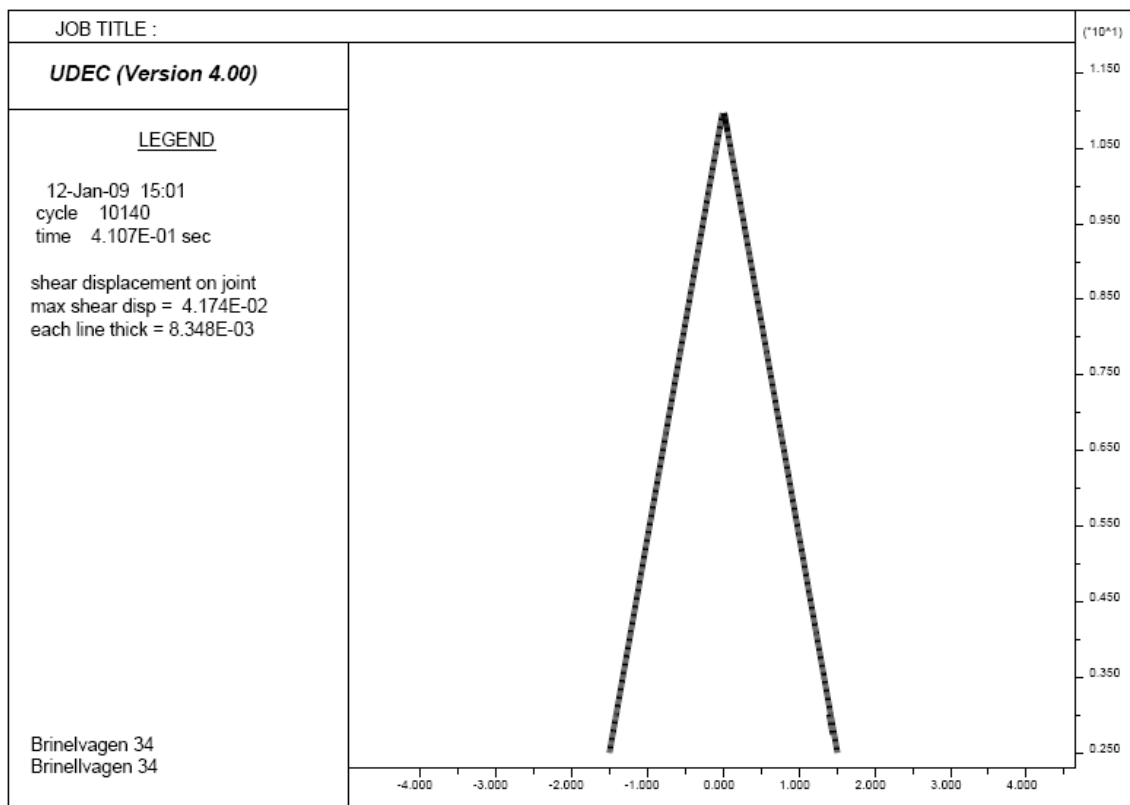


Fig. 6-10. Joint shear displacement after relaxing the in-situ stress without acting the gravity (stage 1 of relaxation)

The last column of Table 6-11 depicts the second stage of relaxation due to the acting of gravity force. The amount of normal force in this stage is reduced while the shear force increases according to the table 6-11. Fig. 6-11 shows the shear displacement at stage 2.

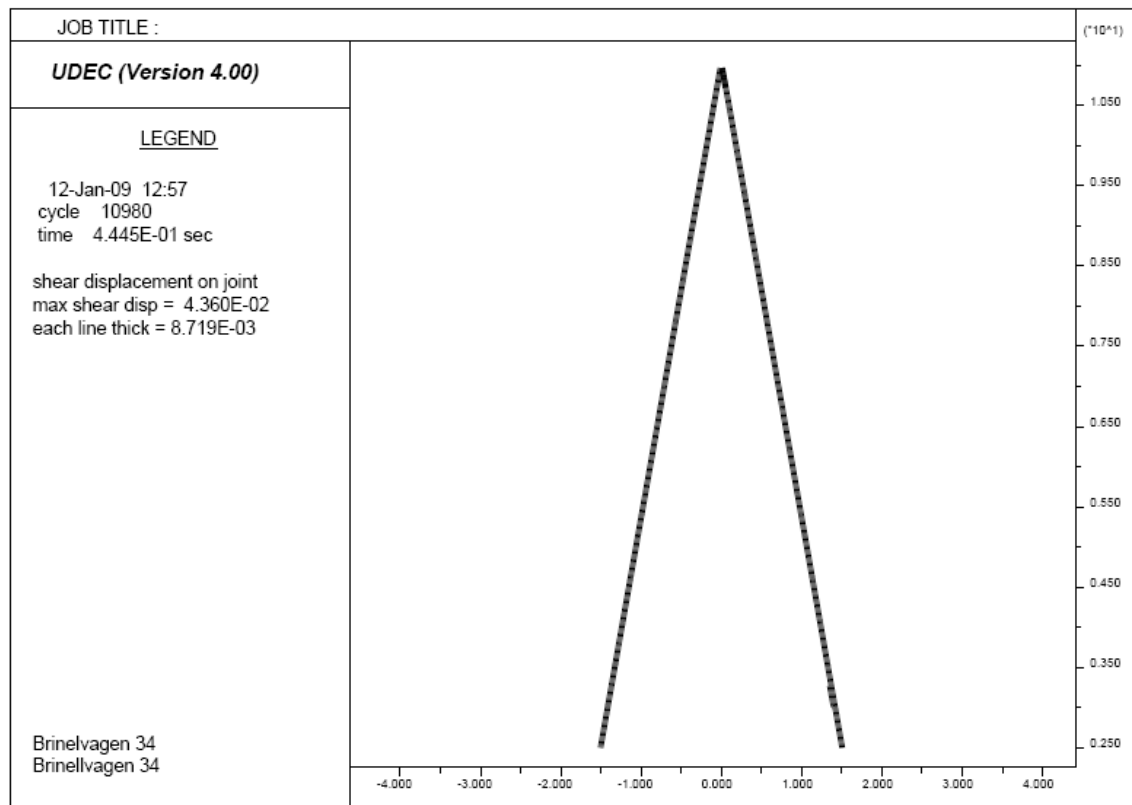


Fig. 6-11. Joint shear displacement after relaxing the in-situ load and gravity force (stage 2 of relaxation

The analytical solution proposed by Bray and Crawford cannot calculate the first stage of relaxation (relaxation of in-situ stress). The analytical solution could only calculate the relaxation of block from stage 1 to stage 2. The amount of relaxation in the first stage of relaxation is much higher compared to that of stage 2.

Table 6-12 shows the predicted displacement due to gravity acting by two methods of analytical and DEM. The values in the table for DEM calculated based on the difference between column 4 and 5 of table 6-11. Table 6-12 shows both DEM and analytical solution predict the displacement due to gravity force equally. But the analytical solution doesn't consider the displacement due to relaxation of in-situ stress and the analytical solution calculates the difference between two last stages of relaxation.

Table 6-12. Predicted displacement due to gravity force by DEM and analytical method

Predicted displacement due to weight by Analytic	Predicted displacement due to weight by DEM	Kn/Ks
2.17	2.13	R=1
1.93	1.9	R=5
1.7	1.62	R=10

The occurred shear displacement in the first stage of relaxation causes an increase in the amount of total displacement. Increasing total displacement decreases the normal force since the displacement of the block has to be vertical from the symmetrical reason. Getting the lower normal force to the joint means having lower safety, and the block is closer to failure. This is the reason why the DEM predicts lower safety for blocks

The vertical force at failure in analytical solution ($T_{y\text{analytic}}$) depends on 4 parameters (apical angle, friction angle, horizontal in-situ stress and ratio between joint normal and shear stiffness). DEM solution considers 6 parameters as in-data (vertical and horizontal in-situ stress, shear and normal joint stiffness, apical angle and friction angle). DEM requires not only the ratio between shear and normal joint stiffness but also values of shear and normal joint stiffness and vertical in-situ stress. Each of the neglected key parameters generates uncertainty in the model (Ditlevsen, 1982). Although the values of joint shear and normal stiffness is influence indirectly by vertical stresses but it is not considered in the analytical solution directly. Ignoring key parameters such as joint shear and normal stiffness together with first stage of relaxation lead to uncertainty in the model.

A sensitivity analysis has been run in order to assess the model precision and biased factor. Figure 6-12 shows the differences between precision, biased and accuracy (Stille, et al. 2003).

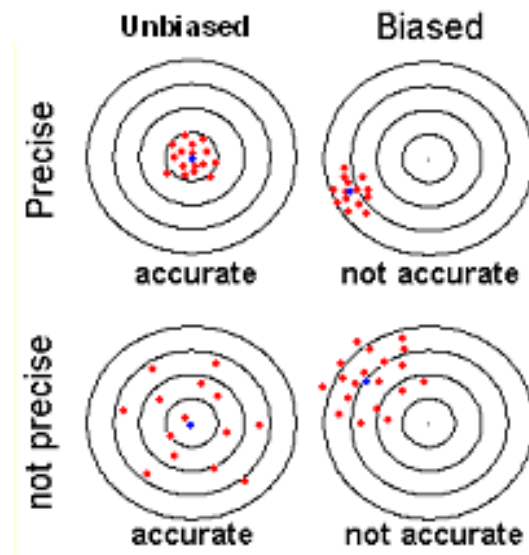


Figure 6-12 precision, biased and accuracy (Stille, et al. 2003).

As it could be seen from figure 6-7, if there is not any accessible information, the uncertainty in model varies substantially. In this case the precision is poor. In order to increase precision of the outcome of the analytical solution more information than depth is required (Fig. 6-13- 6-15).

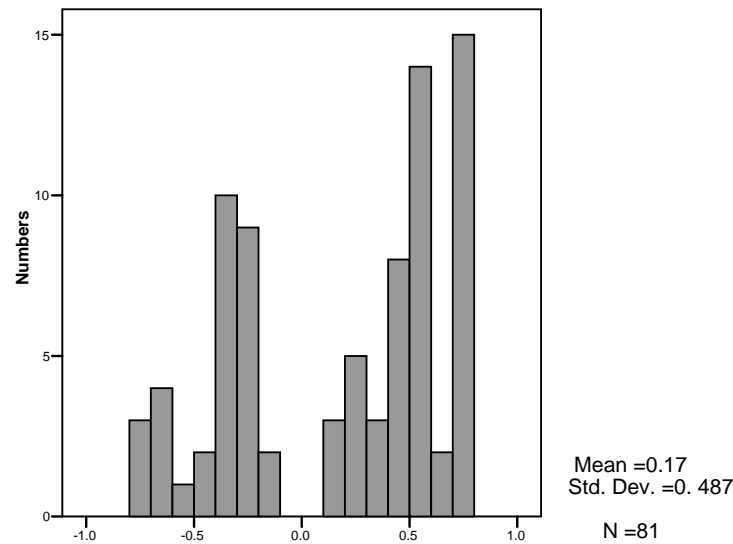


Fig. 6-13 Model uncertainty for depth of 20 m

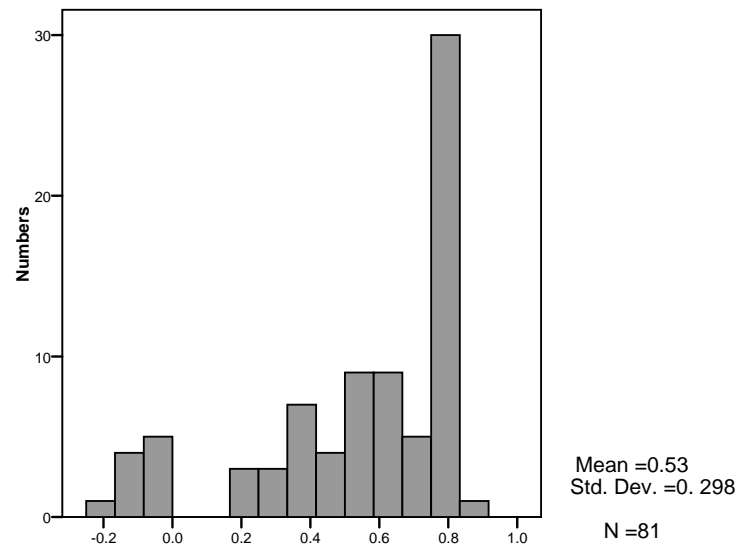


Fig. 6-14 Model uncertainty for depth of 100 m

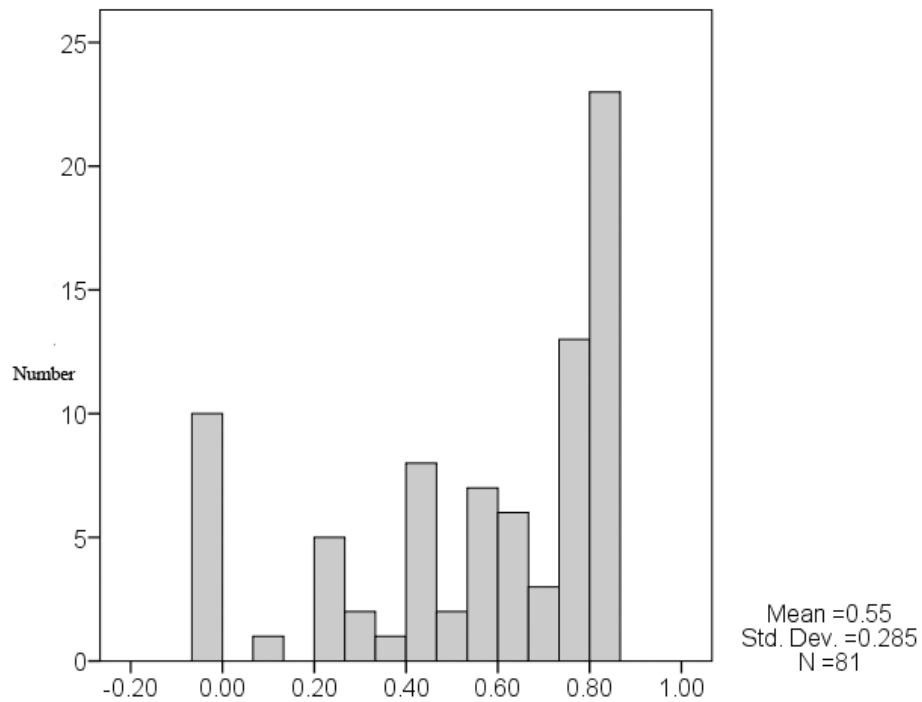


Fig. 6-15 Model uncertainty for depth of 400 m

The second useful piece of information is K_0 value. From figures 6-16- 6-18 it can be seen that for the analytical solution the case with $K_0=0.5$, is more uncertain than $K_0=1$ and $K_0=2$.

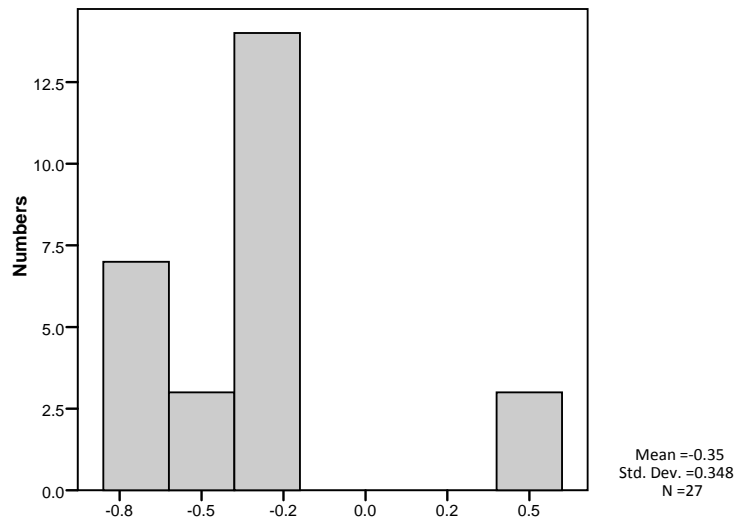


Fig. 6-16 Model uncertainty for depth of 20 m and $K=0.5$

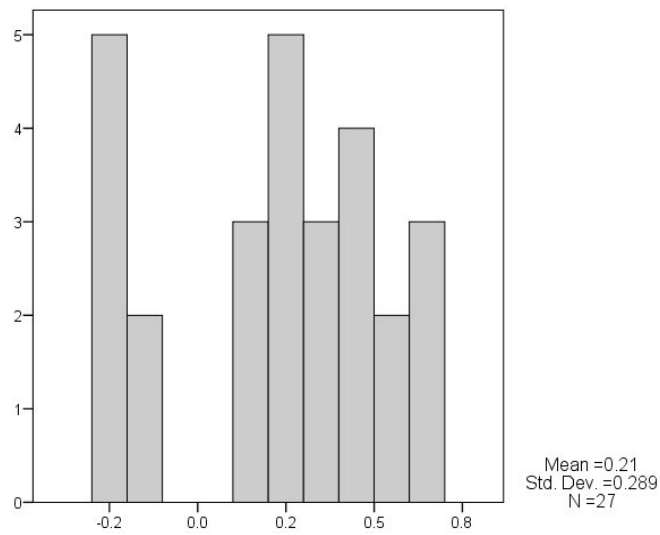


Fig. 6-17 Model uncertainty for depth of 20 m and $K=1$

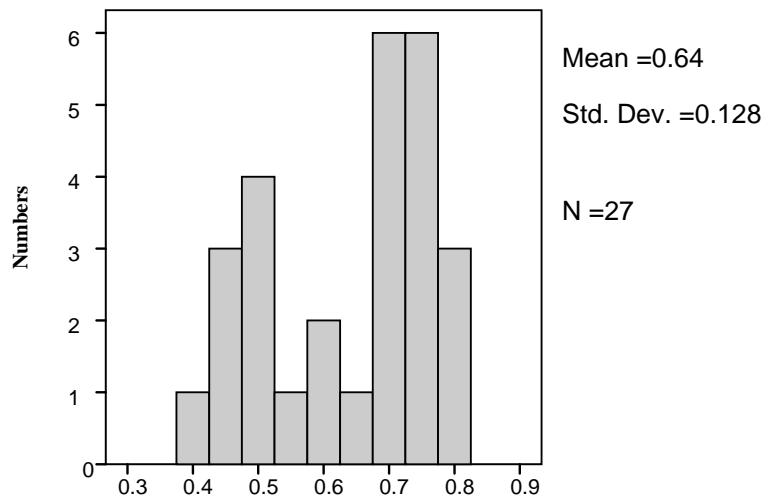


Fig. 6-18 Model uncertainty for depth of 20 m and K=2

The cases with $K_0=2$ has the lowest uncertainty in the analytical model, it is more precise than other cases. For this case, the model uncertainty varies from 40% to 80%.

The third information that is useful is the stiffness ratio. Figure 6-19- 6-21 show the model uncertainty in depth of 20m and $K_0=1$ with different R (ratio of normal stiffness to the shear stiffness) values and angle ratio (α / ϕ). From these figures, it could be understood that in the depth of 20 m and $K_0=1$, the outcome of analytical model is not precise.

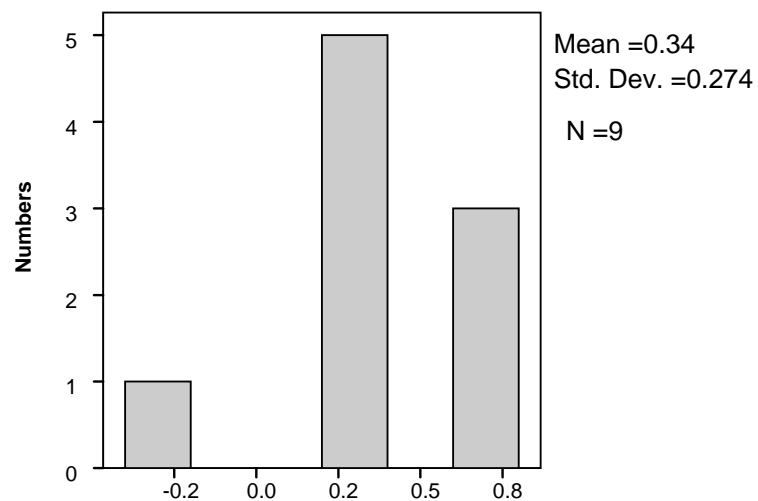


Fig.6-19 Model uncertainty for depth of 20 m and $K_0=1$ and R=10

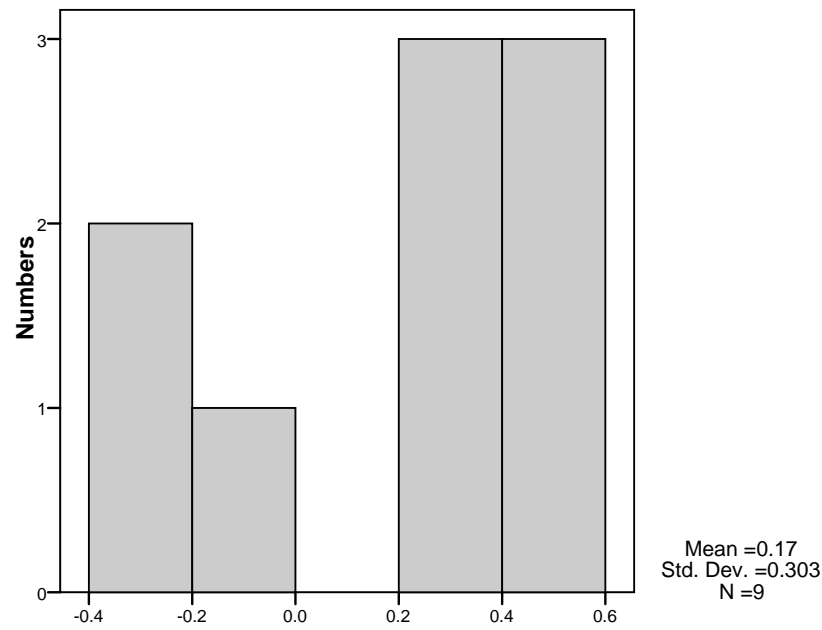


Fig.6-20 Model uncertainty for depth of 20 m and $K_0=1$ and $R=20$

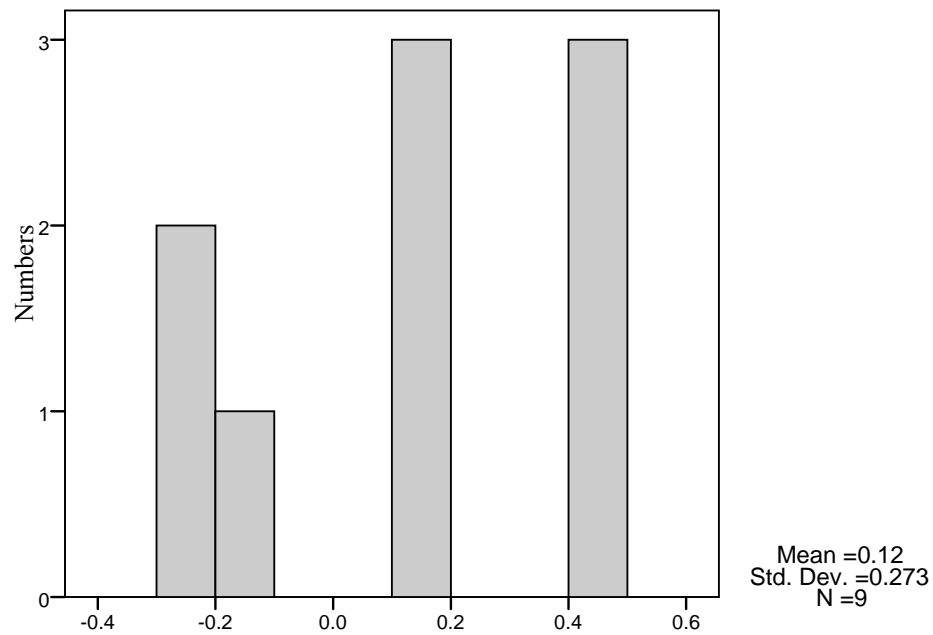


Fig. 6-21 Model uncertainty for depth of 20 m and $K_0=1$ and $R=30$

As it can be seen from Figure 6-19 - 6-21, the uncertainty in the model is increased by increasing of the stiffness ratio (ratio of normal stiffness to the shear stiffness). The fourth piece of

information that is useful to estimate model uncertainty is the angle ratio (ratio of semi-apical angle to the friction angle). Fig 6-22 - 6-25 show the model uncertainty for the cases of 20 m dept, $K_0=1$ and $R=10$ for different values of angle ratio between 0.2-0.8. All these figures (6-22 - 6-25) show a more precise estimation of model uncertainty and their coefficient of variation is lower than 10%. However in some cases the estimation is also biased (see fig 6-25). It becomes clear from the figure that, as angle ratio reaches to 1, the outcome of the model becomes more biased. By increasing the stiffness ratio, the outcome of the model becomes more biased too.

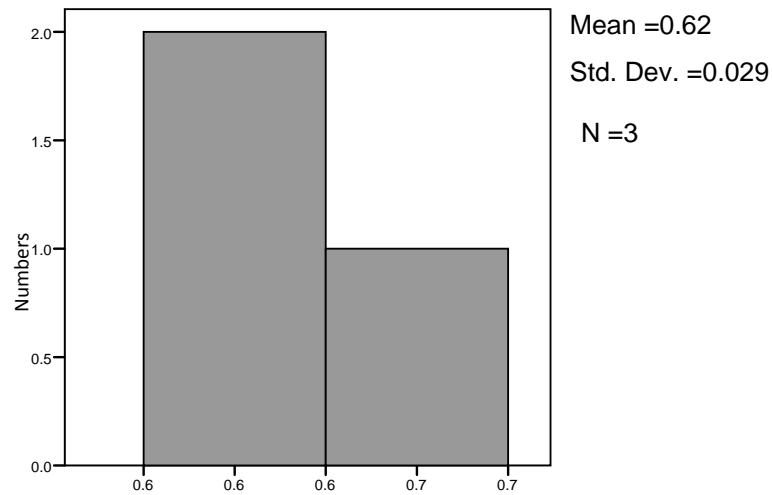


Fig 6-22 Model uncertainty for depth of 20 m, $K_0=1$, $R=10$ and angle ratio 0.32-0.2

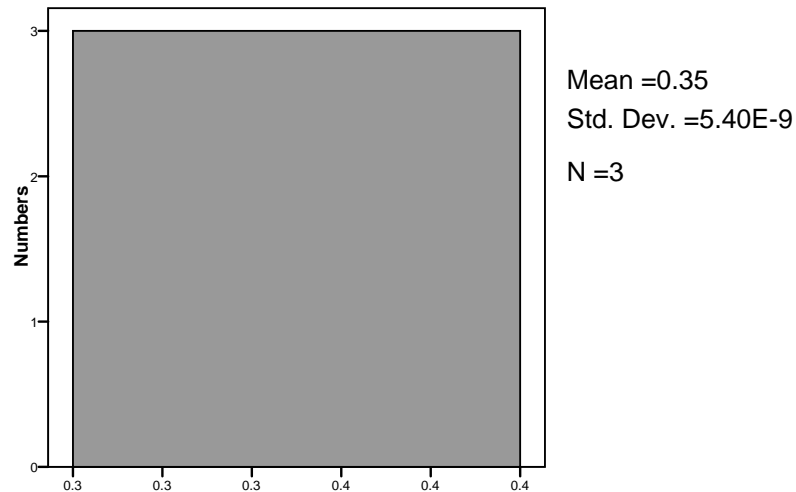


Fig 6-23 Model uncertainty for depth of 20 m, $K_0=1$, $R=10$ and angle ratio 0.6 -0.4

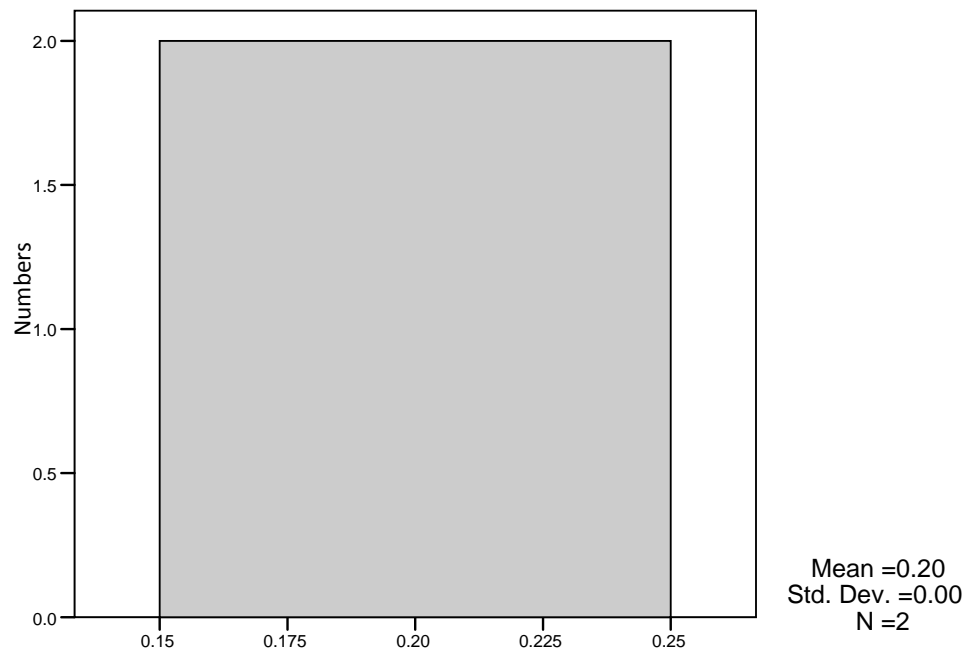


Fig 6-24 Model uncertainty for depth of 20 m, $K_0=1$, $R=10$ and angle ratio 0.75 -0.6

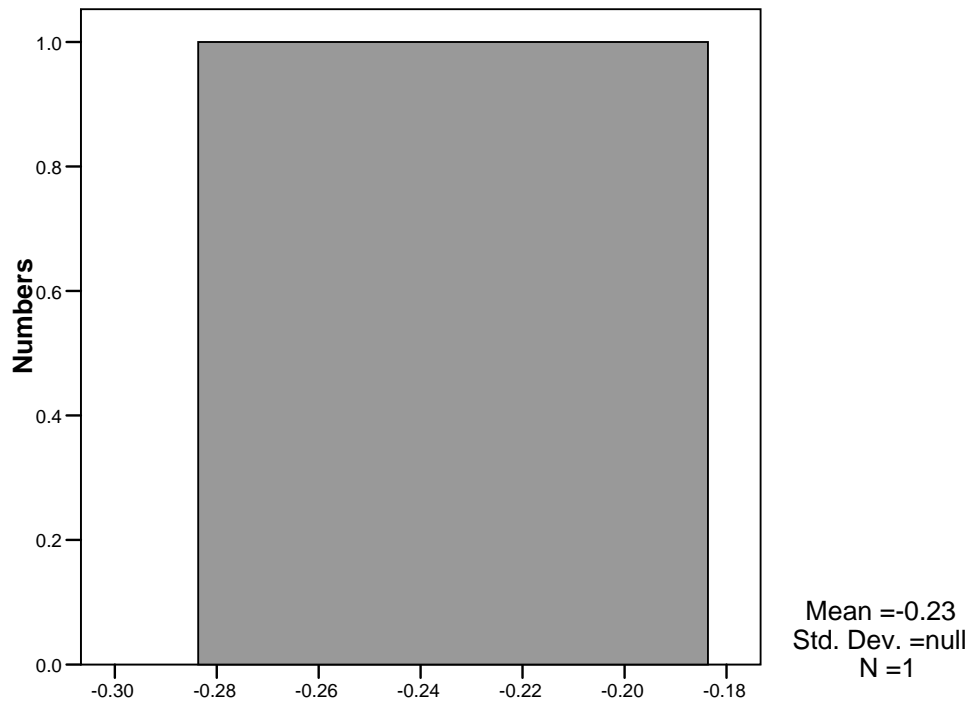


Fig 6-25 Model uncertainty for depth of 20 m, $K_0=1$, $R=10$ and angle ratio 0.8

For the sake of brevity, some diagrams were presented in here. Other condition of stresses, stiffness ratio and angle ratio are shown in appendix.

The designer needs to know both about precision and biased factor of the outcome of the model. The precision could be improved by having more information about more key parameters. In case of acceptable precision, the biased factor could be used to calibrate the analytical solution.

6-9. *Conclusions*

Model uncertainty of analytical solution based on joint relaxation has been assessed. The analyses show that Bray-Crawford solution has good accuracy for the tunnels with negligible vertical in-situ stress and high value of K_0 .

The DEM considers the relaxation of in-situ stress, while the analytical solution does not. The relaxation of in-situ stress gives the joint normal displacement which makes reduction of clamping force. This is not considered in analytical solution; therefore, the analytical solution overestimates the block stability.

With decreasing of K_0 , the mean value of model uncertainty factor decreases. This corresponds to that the outcome of the analytical solution is more biased. The standard deviation of model uncertainty factor increases with decreasing of K_0 . Neglecting key parameters such as vertical stress, joint shear and normal stiffness together with relaxation of in-situ stress generates model uncertainty. Thus the analyses show that the vertical stress plays important role in estimation of block stability in crown of openings.

Three important parameters to identify model uncertainty have been recognized. They are K_0 , ratio between joint normal and shear stiffness, and ratio between block semi-apical angle and friction angle. As the amount of information about the in-situ stress state, joint stiffness, apical and friction angle increases, the variation of model uncertainty factor decreases and the model uncertainty factor could be determined more precisely. Information about the all identified key parameters is required in order to assess acceptable precision.

The results of the analyses indicate that, by increasing the ratio between joint, normal stiffness, and shear stiffness, or the ratio between semi-apical angle and joint friction angle the outcome of model is more biased. Cases with higher value of vertical in-situ stress than horizontal stresses - especially for the shallow depth tunnels or the cases in which the friction angle is closed to semi-apical angle, the analytical solution overestimates the block stability. By having biased factor in an acceptable precision, the outcome of analytical model could be modified. The analytical solution could be used in combination with the tables for determining model uncertainty factor.

Chapter 7

Remarks and Conclusions

The purpose of this research has been to quantify the model uncertainties of different design tools in order to calculate block stability. The author has described different design tools to estimate block volume such as kinematic analysis and DFN, and also design tools to estimate block stability such as analytical solutions and DEM.

Different approaches of Kinematic limit equilibrium with various assumptions in the joint length, stresses, and joint orientation have been applied to a cavern. These results have been compared to those of DFN-DEM, which show that the conventional KLE (unlimited joint length and without field stress) overestimate the unstable block volume. However, while by applying the joint length, the unstable block volume is reduced. By considering the joint length and field stresses around the largest unstable block, its volume is reduced. Monte Carlo could be used to define a representative value for joint length and the orientation which could be used in a Kinematics limit equilibrium which considers the clamping forces from in-situ stress. The comparison between this approach and DFN-DEM shows that this approach predicts the unstable block volume lower than DFN-DEM.

Another conclusion of KLE analysis is that the information about joint length and stresses could lead to a better design. Once again, the costs for obtaining the information about the joint length and stresses must be compared with the costs for overdesign. As an example that relates to the case study in conventional KLE analysis, the support must be design for a 5779 m^3 of block per 1 meter of tunnel length. While considering the joint length and stress field, it is reduced to 22 m^3 per tunnel length.

The analytical solution based on joint relaxation could be used together with kinematic analysis in order to estimate the stability of block. Model uncertainty of the analytical solution has been assessed. The analyses show that Bray solution has good accuracy for the tunnels with negligible vertical in-situ stresses and high value of K_0 .

The DEM considers the relaxation of in-situ stress, while the analytical solution does not. The relaxation of in-situ stress gives the joint normal displacement which makes reduction of clamping force. This is not considered in analytical solution; therefore, the analytical solution overestimates the block stability.

With decreasing of K_0 , the mean value of model uncertainty factor decreases. This corresponds to that the outcome of the analytical solution is more biased. The standard deviation of model uncertainty increases with decreasing of K_0 . Neglecting the vertical stress, values of joint shear and normal stiffness together with relaxation of in-situ stress generate model uncertainty. Thus the analyses show that the vertical stress plays important role in estimation of block stability in crown of openings.

Three important parameters to identify model uncertainty have been recognized. They are K_0 , ratio between joint normal and shear stiffness, and ratio between block semi-apical angle and friction angle. As the amount of information about the in-situ stress state, joint stiffness, apical and friction angle increases, the variation of model uncertainty factor decreases and the model uncertainty factor could be determined more precisely. Information about all the identified key parameters is required in order to assess acceptable precision.

The results of the analyses indicate that, by increasing the ratio between joint normal stiffness and shear stiffness, or the ratio between semi-apical angle and joint friction angle the outcome of model is more biased. Cases with higher value of vertical in-situ stress than horizontal stresses - especially for the shallow depth tunnels or the cases in which the friction angle is closed to semi-apical angle, the analytical solution overestimates the block stability. By having biased factor in an acceptable precision, the outcome of analytical model could be modified. The analytical solution could be used in combination with the tables for determining model uncertainty factor.

Further Research

Although block failure is a common failure mode in underground openings, there is still a need for more research on the probabilistic design against block failure. Further research could perform to analyze the effects of key parameters such as K_0 , angle ratio, and stiffness ratio on the reliability index.

The analyses show that there is a systematic error in Bray-Crawford solution. The solution needs to be improved in order to consider the effects of in-situ stress relaxation. The analytical solution

based on joint relaxation could be revised in order to consider the joint stiffness changes due to changes of loading.

Moreover, current available commercial software cannot perform the probabilistic approach. More work is needed to develop the software that could be helpful in research and practice.

References

1. Ang A. and Tang W. 2007, *Probability concepts in engineering*. Volume I, Basic Principles, 2nd Ed. John Wiley & Sons, New York.
2. Baecher G. Christian J. 2003, *Reliability and statistics in geotechnical engineering*, Wiley: London.
3. Baghbanan A, Jing L. 2007, Hydraulic Properties of Fractured Rock Masses with Correlated Fracture Length and Aperture. *Int J Rock Mech Min Sci* ;44(5):704-719.
4. Baghbanan A, Jing L. 2008, Stress Effects on Permeability in Fractured Rock Mass with Correlated Fracture Length and Aperture– a Numerical Study. *Int J Rock Mech Min Sci.*; 45(8):1320-1334.
5. Bandis S. C. Lumsden A. C. Barton, N. R. 1983, Fundamentals of Rock Joint Deformation *Int. J. Rock Mech. Min. Sci. & Geomech. Abstr.* 20, No. 6, pp. 249-268.
6. Barton N. Choubey V. 1977, The shear strength of rock joints in theory and practice, *Rock Mechanics and Rock Engineering*, 10 PP 1-54
7. Barbour L. and Krahn J. 2004, Numerical modeling prediction or process? *Geo Spec*, PP 44-52
8. Barton N. 1971, A relationship between joint roughness and joint shear strength. *Proc. Int. Symp. On Rock Mech. Rock fracture*. Nancy. Paper I-8,
9. Barton N., Lien R. and Lunde J. 1974, Engineering classification of rock masses for the design of rock support. *Rock Mechanics and Rock Engineering*, 6, pp. 189-236.
10. Batschelet E. 1981. *Circular statistics in biology*. 1st Ed. New York: Academic Press.
11. Berglund J. 2001. Clab2 etapp 2 Byggnadsgeologisk dokumentation, SKB, Rapportnummer 0519001-045.
12. Bieniawski Z.T. 1989, *Engineering rock mass classifications*. John Wiley & Sons, New York, 251 pp.
13. Boontun A. 1998, The effect of joint parameters on rock block size and key block size distributions, PhD thesis, Michigan tech. Uni.
14. Brady BHG. and Brown ET. 1985, *Rock Mechanics for Underground Mining*, Allen & Unwin;, London
15. Cartney, S.A. 1977, The ubiquitous joint method cavern design at Dinorwic power station, *Tunnels and Tunneling*, P 54-57

16. Chan HC. and Einstein H. 1981, Approach to Complete Limit Equilibrium Analysis for Rock Wedges - The Method of "Artificial Supports", *Rock Mechanics and Rock Engineering* 14, 59-86
17. Cheng Y. M. and Zhang Y. H. 2000, Rigid body rotation and block internal discretization in DDA analysis, *Int. J. Numer. Anal. Meth. Geomech.*; 24:567-578
18. Chihsen T.L. Amadai B. Jung J. Dwyer J. 1996. Extension of discontinuous deformation analysis for jointed rock masses, *Int. J. Rock Mech. Min. Sci. & Geomech. Abstr.* 33 (7) PP 671-694
19. Crawford A. M. 1982, Rock wedge Stability, 23rd Symposium on Rock Mech. PP 1057-1064.
20. Crawford A. M. Bray J. W. 1983, Influence of in-situ stress field and joint stiffness on rock wedge stability in underground openings, *Can Geotech. J.* 20, pp 1990-2001,
21. Cundall P. 1971, a computer model for simulating progressive large scale movements in blocky rock system. In: Proc., Intern. Soc. of Rock Mechanics, Nancy, Vol. 1.
22. Curran J.H., Corkum B. and Hammah R.E. 2004, three dimensional analysis of underground wedges under the influence of stresses, Proc. Gulf Rock 04 conf. Elsevier Science Publisher.
23. Curran J.H., and Corkum B.T. 1995, Examine2D—A 2D boundary element program for calculating stresses around underground excavations in rock. Version 5. Rock Engineering Group, University of Toronto, Toronto, Canada.
24. Delin P. Stille H. 1993, Field and Laboratory testing of rock, SKB technical note
25. Dershowitz W. S. 1984. Rock Joint Systems, Ph.D. Dissertation, Massachusetts Institute of Technology, Cambridge, MA.
26. Dershowitz W.S. Einstein H. 1988, Characterizing rock joint geometry with joint system models. *Rock Mech. and Rock Engn.*, Vol 21, 1988, pp 21 - 51.
27. Diederichs M. S. Espley C. Langille, Hutchinson D.J. 2000, A semi-empirical hazard assessment approach to wedge instability in underground mine openings, In *GeoEng*, Melbourne, CD-ROM, 8pgs,
28. Dinis Da Gamma, C. 1977, computer model for block size analysis of jointed rock masses, Proc. 15th APCOM. Brisbane, Australia, P. 305-315
29. Ditlevsen O. 1982, Model uncertainty in structural reliability, *Structural Safety J.* 1(1)

- 73-86.
30. Draper D. 1995, Assessment and propagation of model uncertainty, *J. R. Statist. Soc. B* 57 No 1. PP 45-97
 31. Eberhardt E. Stead D. Reeves M. J. and Connors C. 1997, Design of tabular excavation in foliated rock: an integrated numerical modeling approach, *Geotech. & Geological Eng.* Vol 15, 47-85
 32. Eberhardt E. Stead D. Coggan J. Willenberg H. 2002, An integrated numerical analysis approach to the Randa rock slide, 1st European Conf. on landslides, Prague, PP 355-362.
 33. Elsworth D. 1986, Wedge stability in the roof of a circular tunnel: plane strain condition, *Int. J. Rock Mechanics and Mining Sci. & Geomech. Abs.* 23(2), PP 181-181
 34. Eurocode 1997-1:2004. Eurocode 7: Geotechnical design – Part 1: General rules. European Committee for Standardization
 35. Fredriksson A. Hässler, L. Söderberg L. Extension of CLAB, numerical modeling, deformation measurements and comparison of forecast with outcome, *Rock Mechanics a challenge for society*, Särkkä & Eloranta (Ed.) 2001, Swets&Zeitlinger Lisse PP. 743-747
 36. Goodman R. Shi. G.H. 1985, *Block theory and its application to rock engineering*. 1st Ed. London: Prentice-Hall.
 37. Goodman, R. 1989, *Introduction to the rock mechanics*, 2nd Ed, New York: John Wiley and Sons
 38. Goodman R. John C. 1976, Finite element analysis for discontinuous rock. In *numerical Methods in Geotechnical Engineering*. McGraw-Hill, Newyork.
 39. Goodman R. Shi G. H. 1982, Calculation of support for hard, jointed rock using the keyblock principle, PROC. 23RD US. Symposium on Rock Mechanics, PP 883-893, California
 40. Hadjigeorgiou J. Grenon M. 2005 Rock slope analysis using fracture systems, *Int. J. of surface Mining, Reclamation and Enviroment*, 19(2), PP 87-99
 41. Hammett R.D. and Hoek E. 1981. Design of large underground caverns for

42. Hencher S.R. 1985, Limitations of stereographic projections for rock slope stability analysis, *J. Hong Kong Institution of Engineers*, 13(7). PP 37-41.
43. Hermanson J. 1996, Visualization of the fracture network in rock blocks along the Äspö HRL tunnel using a DFN model approach, SKB, HRL-96-08.
44. Hoek E. and Brown, E.T. 1980, *Underground excavations in rock*. London: Instn Min. Metall.
45. Hoek E., Grabinsky M .W. and Diederichs M.S. 1991, Numerical modelling for underground excavation design, *Transactions of the Institution of Mining and Metallurgy (Section A: Mining Industry)*, 100, A22–A30,
46. Hwang J. Y. 2004, Kinematic and stability analysis method of rock blocks considering finite discontinuity persistence, *KSCE journal of civil Eng.* 8(4), PP 397-402.
47. ISRM International Society for Rock Mechanics, Commission on Standardization of Laboratory and Field Test. 1978, Suggested methods for the quantitative description of discontinuities in rock masses, *Int. J. Rock Mechanics & Mining Sci.* Vol 15 PP319-68.
48. Itasca Consulting Group, 2005, *UDEC Manuel*, Minneapolis, Minnesota
49. Jing L., Stephansson O. 2007, *Fundamentals of discrete element methods for rock engineering: Theory and applications (developments in geotechnical engineering)*. 1st Ed. Amsterdam; Elsevier Science BV.
50. Kemeny D. J. M. A. Hagaman R. M. and Wu X. 1993, Analysis of rock fragmentation using digital image processing *J. Geotech. Engng* 199, 1144-1160
51. Kim B. H. Cai M. Kaiser P. K. and Yang H. S. 2007, Estimation of Block Sizes for Rock Masses with Non-persistent Joints, *Rock Mech. Rock Engng.* 40 (2), 169–192
52. Kirsch G. Die , 1898, Theorie der Elastizität und die Bedürfnisse der Festigkeitslehre. Veit Ver Deut Ing, 42:797-807
53. Kleine T. 1988. A mathematical model of rock breakage by blasting, PhD thesis, Uni. Of Queensland, Australia
54. Ronold K. O. and Bjerager P. 1992. Model Uncertainty Presentation in geotechnical reliability analyses, *J. Geotech. Eng. Div. ASCE.* 118 (3) PP. 636-377.

55. Krahn J. 2003, the 2001 R.M. Hardy lecture: the limits of limit equilibrium analyses, *Can Geotech J*, 40 643-660
56. Kulatilake P.H.S.W, Ucpirti H. Wang S. Radberg G., Stephansson O. 1992, Use of Distinct Element Method to perform stress analysis in rock with non-persistent joints and to study the effect of joint geometry parameters on the strength and deformability of rock masses. *Rock Mech. Rock Eng.* 25(4) PP 253-274.
57. Lambe T. W. Whitman R. V. 1969, *Soil Mechanics*, John Wiley & Sons, New York
58. Lanaro F. and Fredriksson A. 2005, Rock Mechanics Characterization of the rock mass-summary of primary data, SKB, R05-21
59. Mardia K.V. 1972. *Statistics of Directional Data*. 1st Ed. London: Academic Press.
60. Mauldon M., Goodman R. 1990, Rotational kinematic and equilibrium of blocks in rock mass. *Int. J. Rock Mech Min Sci.* 27 (4), 291-301
61. Mauldon M., Goodman R. 1996, Vector analysis of keyblock rotations, *Journal of Geotechnical Eng.* 122 (12) PP 976-987
62. Mauldon M., Chou K.C. and Wu Y. 1997, Uncertainty analysis of tunnel roof stability. *Transportation research record.* 1582, 53-59.
63. Mauldon M., Zhao M. 1995, Stability of key blocks under self-weight and surface forces, Proc. 35th US. Symposium on Rock Mech. P 113-118.
64. Miller D. R. 1979, Stability of backs walls and pillars in Dolphin Mine, King Island^d, Division of Applied geomechanics, Technical rept, No 41, Commonwealth Scientific and Industrial Research Organization, Melbourne, Australia,
65. Min KB, Jing L, Stephansson O. 2004. Determining the equivalent permeability tensor for fractured rock masses using a stochastic REV approach: Method and application to the field data from Sellafield, UK. *Hydrogeol J*;12(5):497-510.
66. Nicholas D. E. 1981, Mining selection- A numerical approach. In design and operation of caving and sublevel stoping mines ,Edited by Hustrulid W. A. PP 39-53. AIME, Newyork
67. Nomikos P.P. Soianos A.I. Tsoutrelis C. E. 1999, stability of symmetric wedge formed in the roof of a circular tunnel: non-hydrostatic natural stress field, *Int. J. Rock Mech. & Mining Sci.* 36, 687-691

68. Nomikos P.P., Soianos A.I. Tsoutrelis C. E. 2002, Symetric wedge in the roof of a tunnel excavated in an inclined stress field, *Int. J. Rock Mech., & Min. Sci.* 39:59-67
69. Nomikos P.P., Yiouta –Mitra P.V. Soianos A.I. 2006 , stability of asymeric roof wedge under non-symeric loading, *Rock Mech, Rock Engng*, 39(2), 121-129
70. Nomikos PP. Sofianos AI. 2008, Progressive failure of 2D symmetric roof rock wedges, 5th Asian Rock Mechanics Symposium, Tehran,;
71. Nord G., Bagheri M., Baghbanan A., Stille H. 2007. Design consideration of large caverns by using advanced drilling equipment, *Felsbau*, 5, P 131-136.
72. Oda M., Yamabe T., Ishizuka Y., Kumasaka H., Tada H. and Kimura K. Elastic Stress and Strain in Jointed Rock Masses by Means of Crack Tensor Analysis, *Rock Mech. Rock Engng.* (1993) 26 (2), 89—112
73. Ohnishi Y. Nagano K. and Fujikawa T. 1985, evaluation of stability of excavated jointed rock mass by block theory. *J. Geotech. Engrg., JSCE*, No 364/III, PP 209-218
74. Ohnishi Y., Nishiyama S., and Sasaki T. 2006, Development and application of discontinuous deformation analysis, In: Leung, C, F, and Zhou, Y, X, (eds.), *Rock Mechanics in Underground Constructions* (Proc, of 4th Axia Rock Mechanics Symp. Singapore), p, 59-70, Keynote lecture,
75. Pahl P.J. 1981, Estimating the mean length of discontinuity traces, *Int. J. Rock Mech. Min. Sci. & Geomech. Abstr.* 18, PP 221-228
76. Palmström A. 1995, RMi - a rock mass characterization system for rock engineering purposes, PhD thesis, University of Oslo, Norway;
77. Park H., West. T.R. 2001. Development of probabilistic approach for rock wedge failure, *Engineering Geology*, 59, 233-251.
78. Pine R. J. , Owen D.R. J. Coggan J. S. and Rance J.M. 2007, A new discrete fracture modeling approach for rock masses, *Geotechnique* 57, No. 9, 757-766
79. Priest SD.1993, *Discontinuity analysis for rock engineering*, Chapman & Hall, London
80. Priest, S. D. 1980, The use of inclined hemisphere projection methods for the determination of kinematic feasibility, slide direction and volume of rock blocks, *Int. J. Rock Mech. Min. Sci. & Geomech. Abstr.* Vol. 17, pp. 1 to 23

81. Pötsch M. Shubert W. 2005, From documentation to prediction- a computer based method for discontinuity analysis and block stability assessment in tunneling, Proceeding of 31st ITA-AITES, World tunneling congress, Istanbul
82. Rockscience, *Theory Manuel for underground wedge stability analysis*, Unwedge v 3.0(Available at www.rockscience.com)
83. Röshoff K. Stephansson O. Larsson H. Stanfors R. Eriksson K. 1983, Clab-an intermediate for spent nuclear fuel in Sweden, 5th International congress on rock mechanics, Melbourne, Australia
84. Shi G. H. Goodman R. E. 1985, Two dimensional discontinuous deformation analysis, *Int. J. Numerical and Analytical methods in geomechanics*, Vol 9, 541-556
85. Shi G.H. 1989, PhD thesis, "Block system modeling by discontinuous deformation analysis, Univ. of California", Berkeley, Dept, of Civil Eng.
86. Shi G.H. 2008, Recent application of discontinuous deformation analysis and Manifold method, ARMA, Sanfrancisco
87. Sofianos A.I. 1986, Stability of Rock Wedges in Tunnel Roofs, *In. J. Rock Mech. Min. Sci. & Geomech. Abst.*, Vol, 23, No, 2, pp, 119-130,
88. Sofianos A.I. 1984, Numerical simulation of underground excavations within jointed rock of infinite extent, PhD thesis, Uni, of London
89. Starzec P. Anderson J. 2002, Application of two level fractorial design to sensitivity analysis of key block statistics from fracture geometry *In. J. Rock mechanics and mining sciences*, 39 PP 234-255
90. Stille H. Fredriksson A. 1996, bergmekanisk utredning av stabilitet och inverkan på befintlig Bergum, SKB PR-96-06
91. Stille H. Andersson J. and Olsson L. 2003, Information based design in rock engineering. SveBeFo Rapport no 61. Stockholm
92. Strafield A. M. and Cundall P. A. 1988, Towards a methodology for rock mechanics modelling, *Int. J. Rock Mech. Min. Sci. Gemech. Abstr.* Vol 25, No. 3, PP 99-106
93. Terzaghi K. 1946. *Rock defects and loads on tunnel supports*. In: Proctor, R.V., White, T.L. (Eds.), In: Rock tunneling with steel supports, vols. 1, 17-99. Commercial Shearing and Stamping Company, Youngstown, OH, pp. 5-153.

94. Vanmarcke E.H. 1977, Probabilistic modelling of soil properties, *ASCE. Journal of the geotechnical Eng. Div.* pp 1227-1265
95. Vaughan D. and Isenberg J. 1991, application brief stability of openings in jointed rock, *Int. J. for Numerical and analytical methods in Geomech.* 15, 433-442
96. Villaescusa E. and Brown E. T. 1991, Stereological estimations of in-situ block size distributions, Proc. 7th Congress, ISRM, Aachen, W.Wittke Ed. Vol 1, PP. 361-365, A. A. Balkema, Rotterdam.
97. Villaescusa. E. and E.T. Brown. 1991, Sterological estimation of in-situ block size distributions, In *Proceedings of 7th Congress, ISRM Aachen*, Ed. W. Wittke, 1991, Vol 1. 361-365. Balkema. Rotterdam.
98. Warburton P.M. 1987, Implications of keystone action for rock bolt support and block theory, *Int. J. Rock Mech. & Geomech. Abstr.* 24,(5) PP 283-290.
99. Warburton P. M. 1990, Laboratory Test of a Blocky Rock *Int. J. Rock Mech. Min. Sci. & Geomech. Abstr.* 27.(5), pp. 445-152
100. Warburton P.M. 1981, Vector Stability Analysis of an Arbitrary Polyhedral Rock Block with any Number of Free Faces *Int. J. Rock Mech. Min. Sci. & Geomech. Abstr.* Vol. 18, pp. 415-427
101. Warburton P.M. 1985, A computer program for reconstructing blocky rock geometry and analyzing single block, *Computers & Geosciences* 11(6), pp 707-712
102. Warburton P.M. 1987, Implications of keystone action for rock bolt support and block Theory, *Int. J. Rock Mech. And Mining Sci. & Geomech. Abstr.* 24(5), 283-290
103. Weibel E. R. 1980, *Stereological methods*, academic press, London
104. Wu J. H. Ohnishi, Y. Nishiyama, S. A. 2005, development of the discontinuous deformation analysis for rock fall analysis, *Int. J. Numer. Anal. Meth. Geomech.*, 29, PP 971–988

Appendix

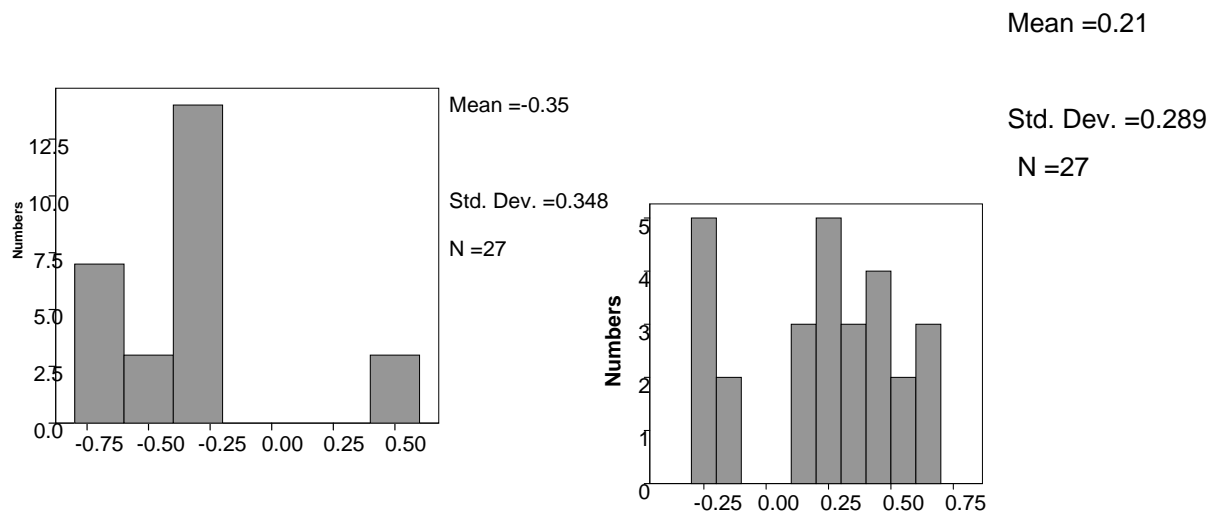


Fig. A-1 Model uncertainty for depth of 20 m and K=0.5

Fig. A-2 Model uncertainty for depth of 20 m and K=1

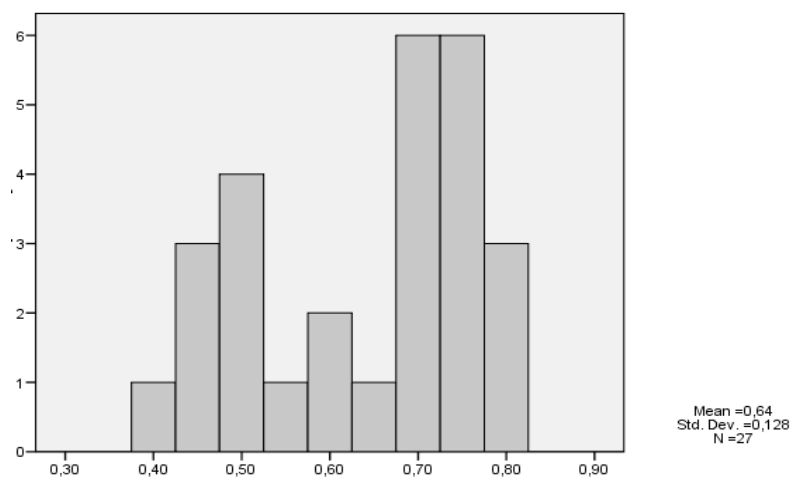


Fig. A-3 Model uncertainty for depth of 20 m and K=2

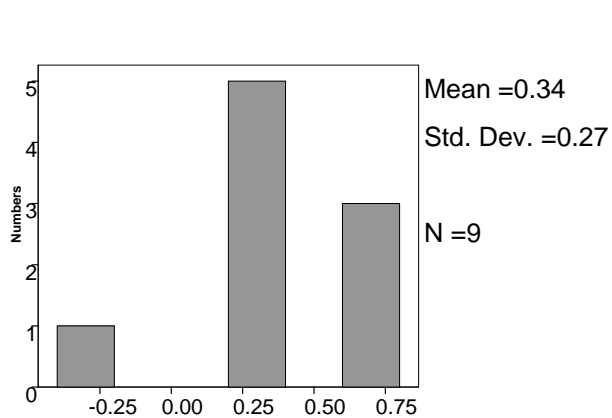


Fig. A- 4 Model uncertainty for depth of 20 m and K=1 and R=10

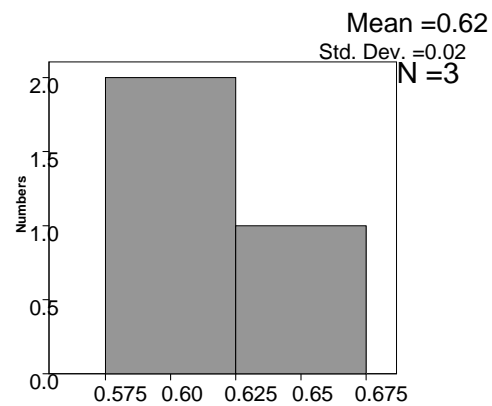


Fig. A-5 Model uncertainty for depth of 20 m and K=1 and R=10, Angle ratio 0.3-0.2

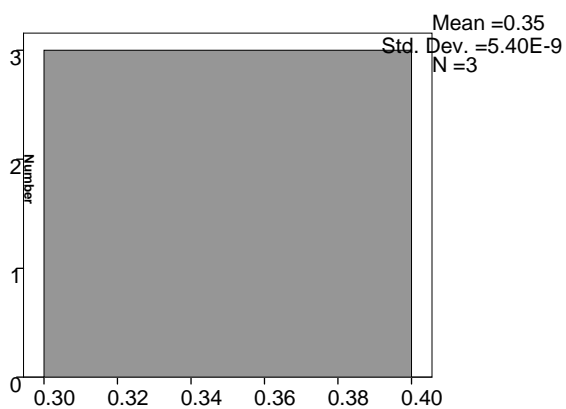


Fig. A-6 Model uncertainty for depth of 20 m and K=1 and R=10, Angle ratio 0.6-0.4

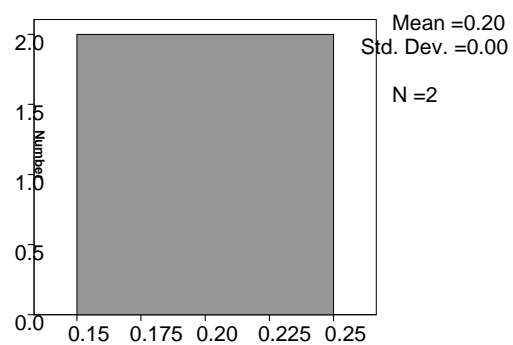


Fig. A-7 Model uncertainty for depth of 20 m and K=1 and R=10, Angle ratio 0.75-0.6

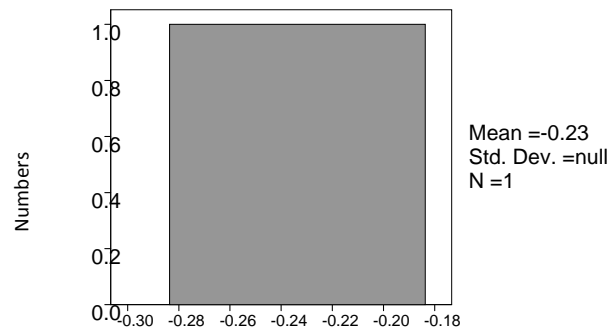


Fig. A-8 Model uncertainty for depth of 20 m and K=1 and R=10, Angle ratio 0.8

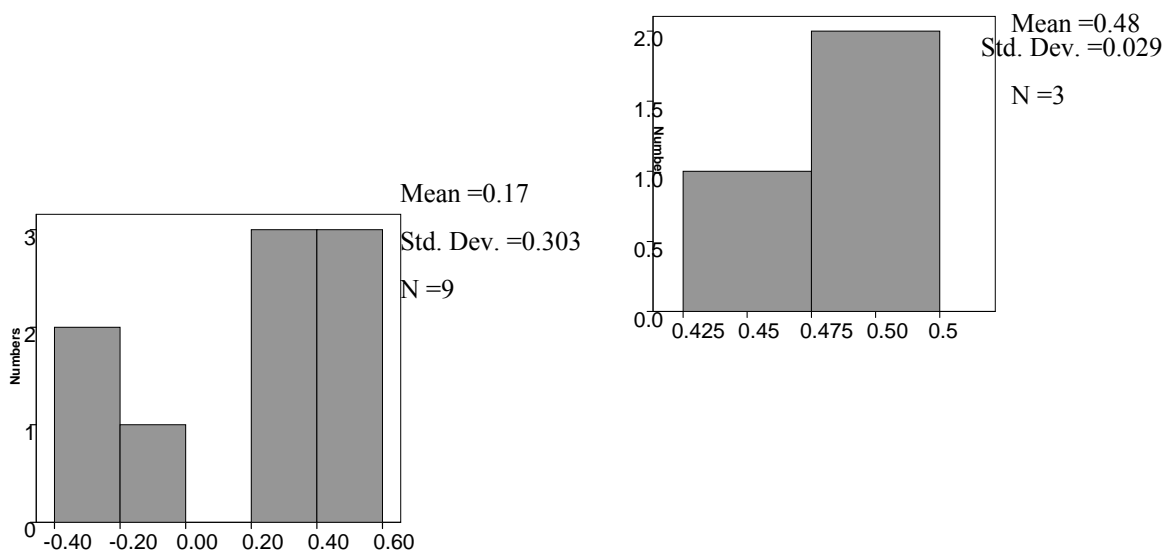


Fig. A-9 Model uncertainty for depth of 20 m and K=1 and R=20

Fig. A-10 Model uncertainty for depth of 20 m and K=1 and R=20, Angle ratio 0.3-0.2

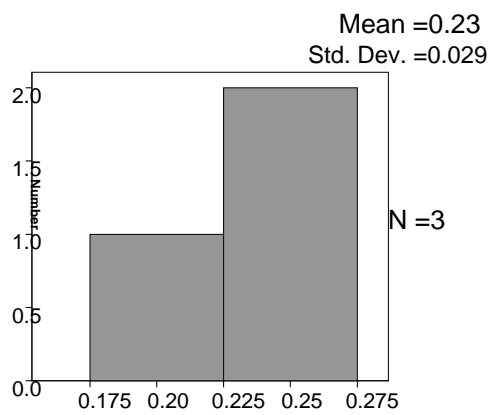


Fig. A-11 Model uncertainty for depth of 20 m and K=1 and R=20, Angle ratio 0.6-0.4

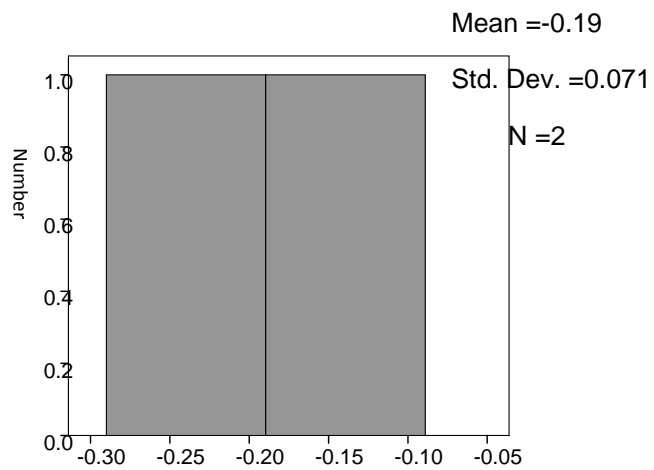


Fig. A-12 Model uncertainty for depth of 20 m and K=1 and R=20, Angle ratio 0.75-0.6

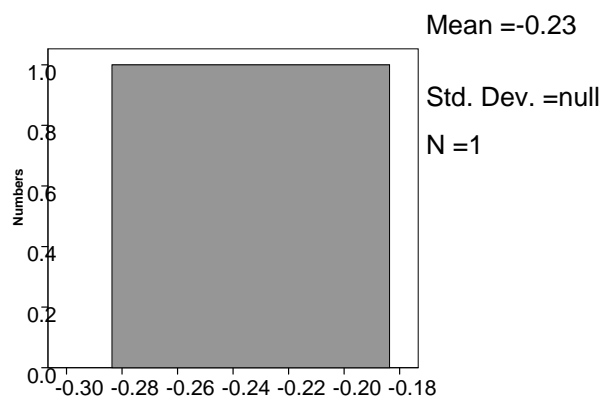


Fig. A-13 Model uncertainty for depth of 20 m and K=1 and R=20, angle ratio 0.8

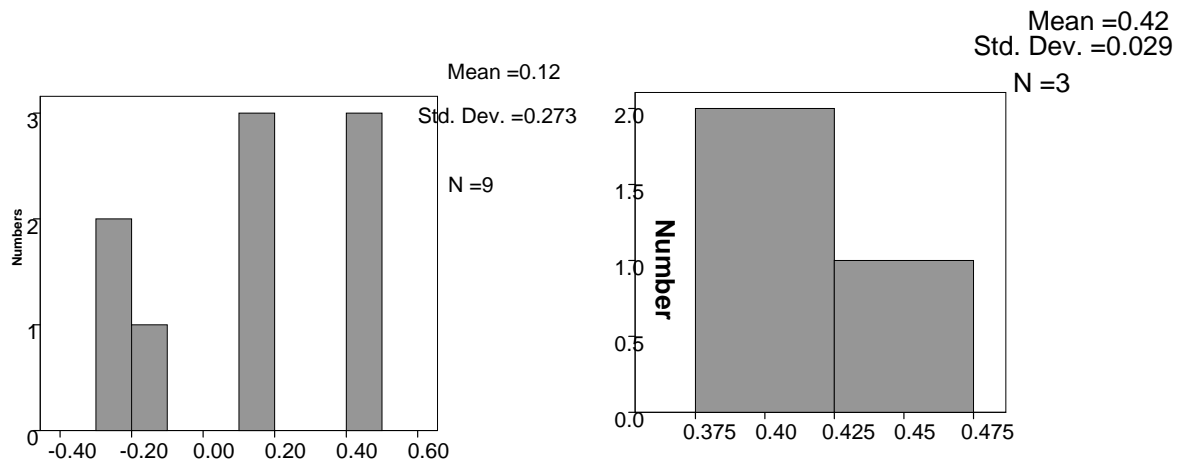


Fig. A-14 Model uncertainty for depth of 20 m and K=1 and R=30

Fig. A-15 Model uncertainty for depth of 20 m and K=1 and R=30, Angle ratio 0.3-0.2

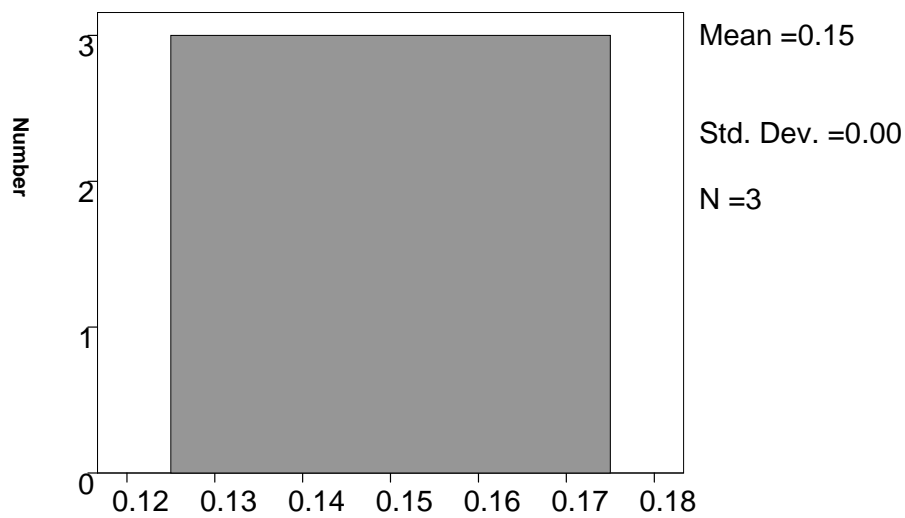


Fig. A-16 Model uncertainty for depth of 20 m and K=1 and R=30, Angle ratio 0.6-0.4

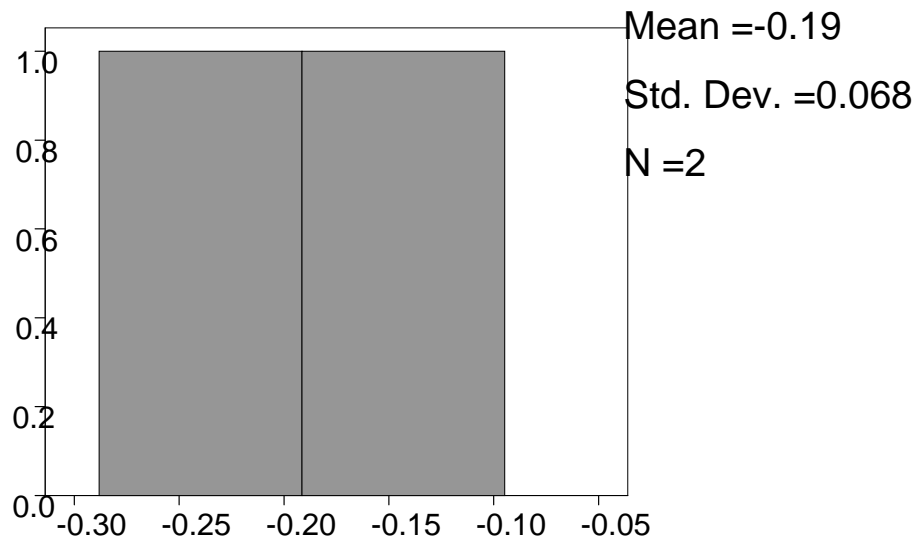


Fig. A-17 Model uncertainty for depth of 20 m and K=1 and R=30, Angle ratio 0.75-0.6

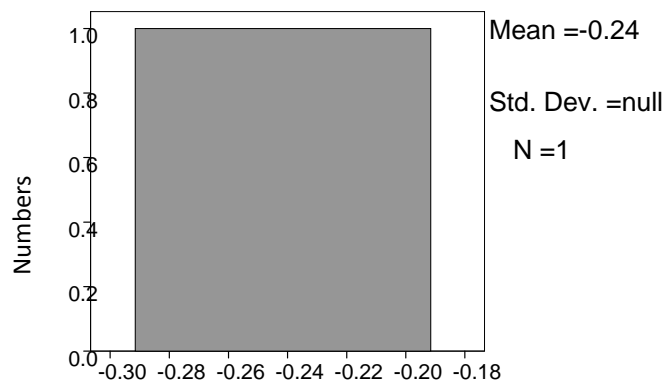


Fig. A-18 Model uncertainty for depth of 20 m and K=1 and R=30, angle ratio 0.8

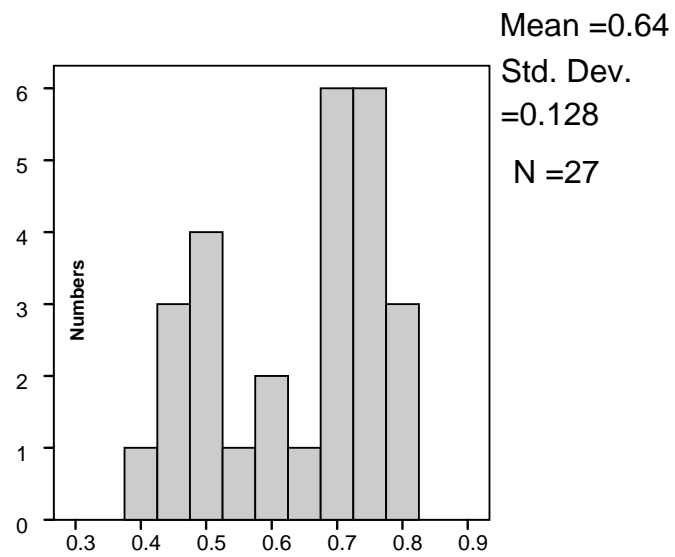


Fig. A-19 Model uncertainty for depth of 20 m and K=2

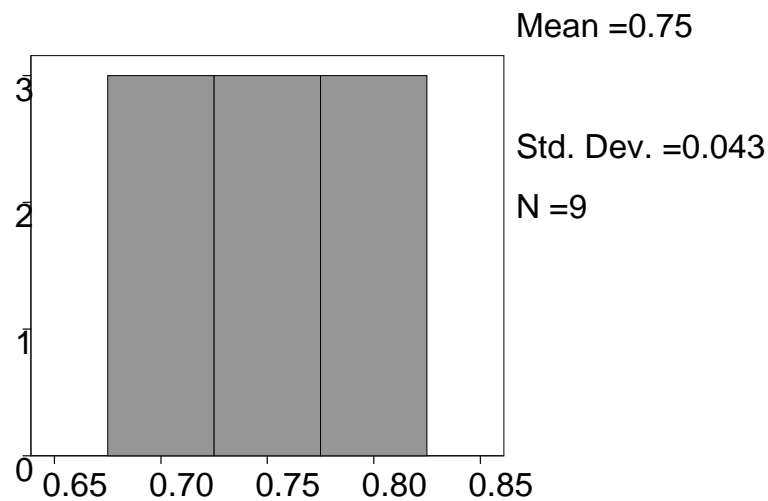


Fig. A-20 Model uncertainty for depth of 20 m and K=2 , R=1

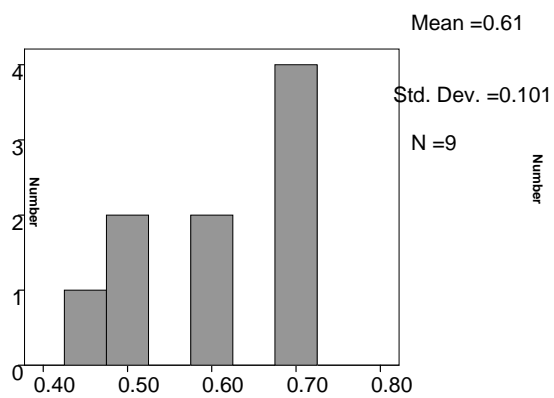


Fig. A-21 Model uncertainty for depth of 20 m and K=2 , R=5

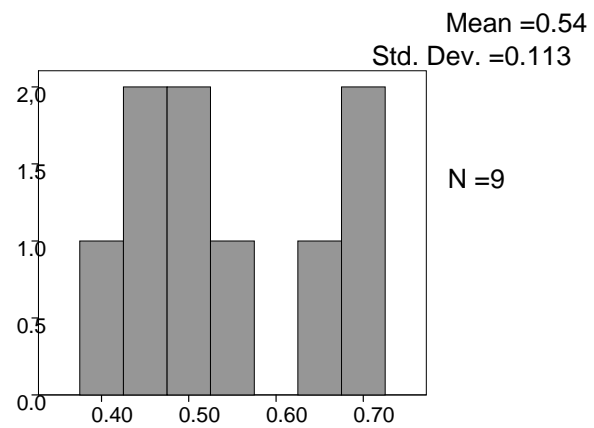


Fig. A-22 Model uncertainty for depth of 20 m and K=2 , R=10

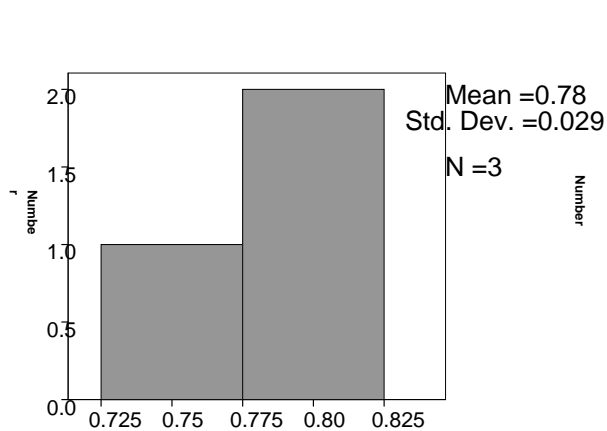


Fig. A-23 Model uncertainty for depth of 20 m and K=2 , R=1, Angle ratio 0.3-0.2

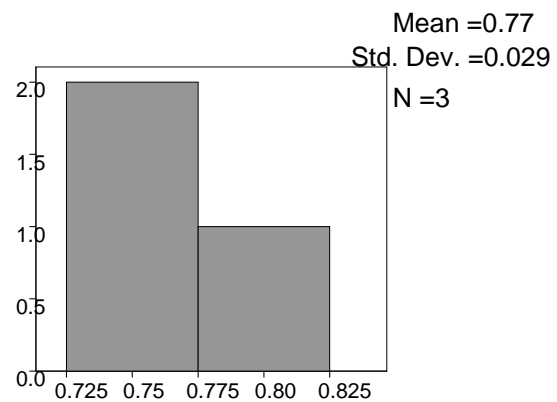


Fig. A-24 Model uncertainty for depth of 20 m and K=2 , R=1, Angle ratio 0.4-0.6

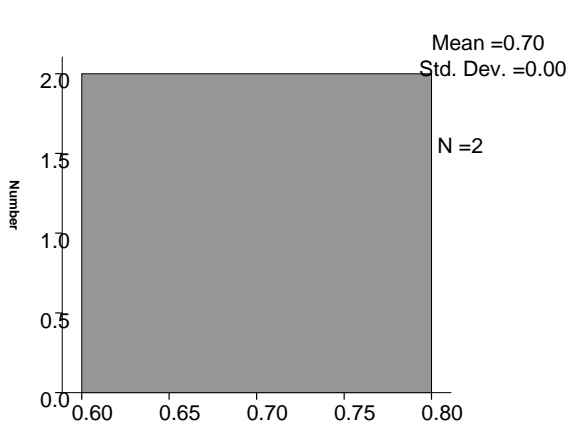


Fig. A-25 Model uncertainty for depth of 20 m and K=2 , R=1, Angle ratio 0.75-0.6

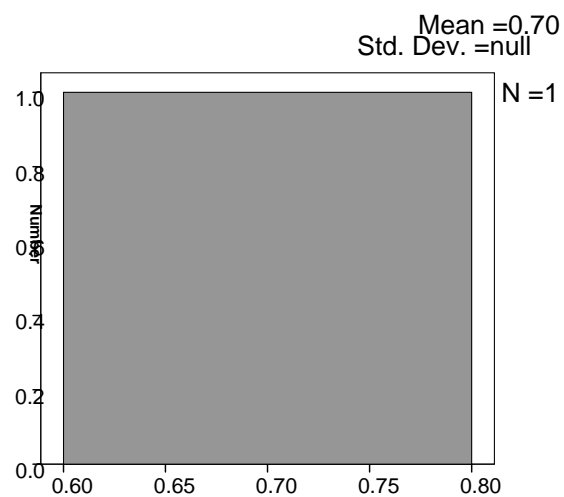


Fig. A-26 Model uncertainty for depth of 20 m and K=2 , R=1, Angle ratio 0.8

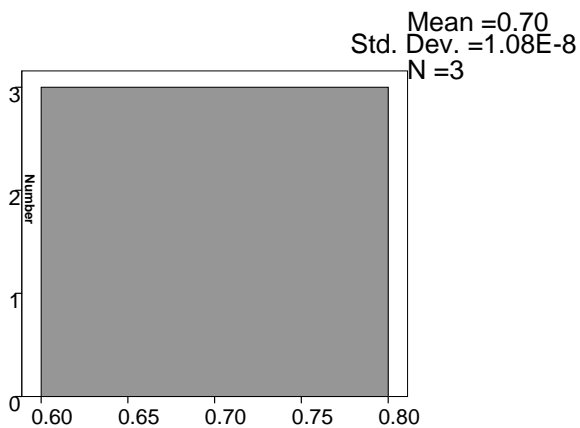


Fig. A-27 Model uncertainty for depth of 20 m and K=2 , R=5, Angle ratio 0.3-0.2

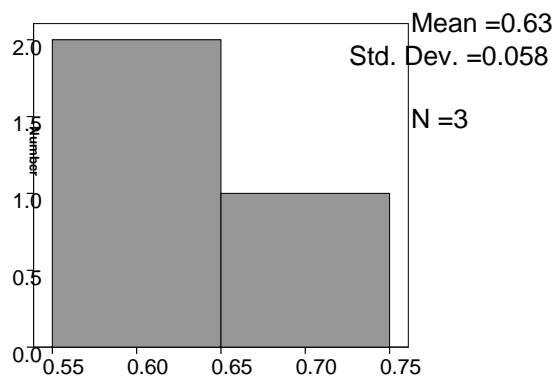


Fig. A-28 Model uncertainty for depth of 20 m and K=2 , R=5, Angle ratio 0.6-0.4

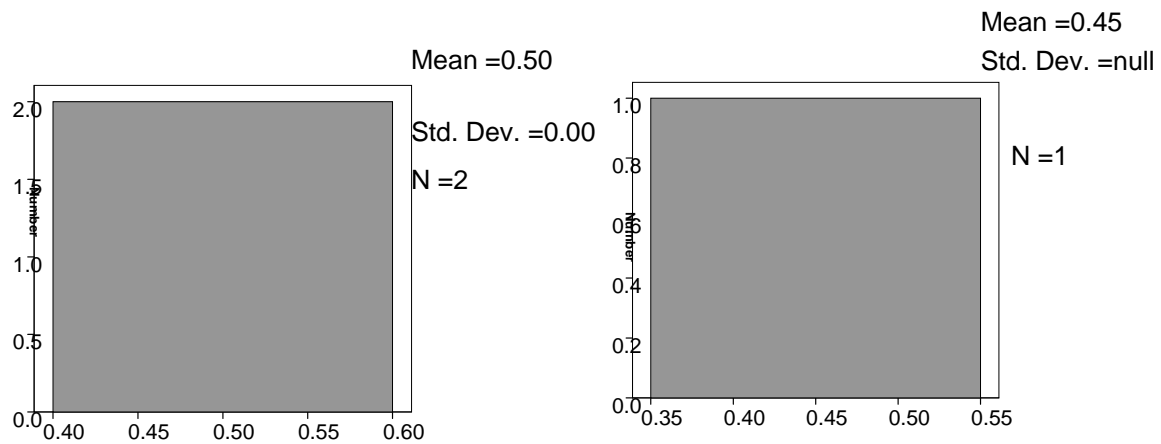


Fig. A-29 Model uncertainty for depth of 20 m and K=2 , R=5, Angle ratio 0.75-0.6

Fig. A-30 Model uncertainty for depth of 20 m and K=2 , R=5, Angle ratio 0.8

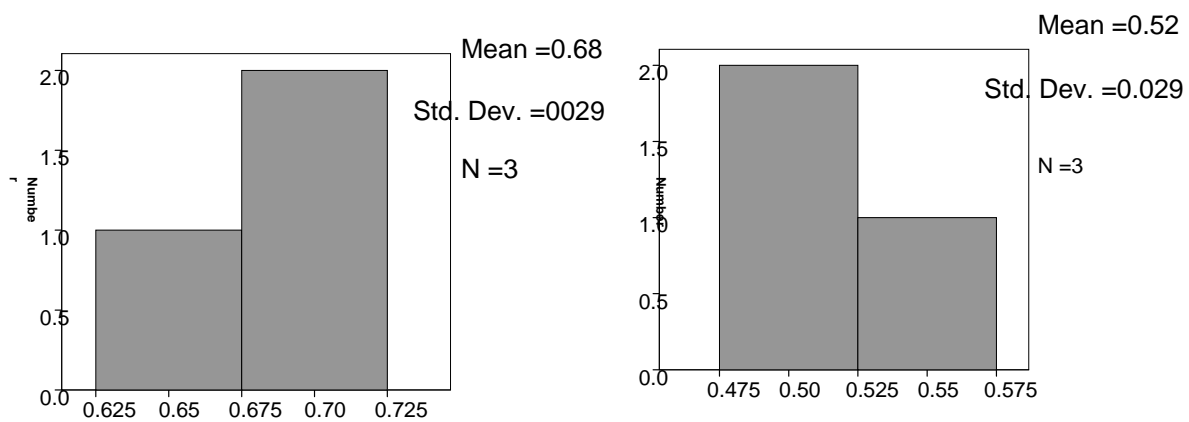


Fig. A-31 Model uncertainty for depth of 20 m and K=2 , R=10, Angle ratio 0.3-0.2

Fig. A-32 Model uncertainty for depth of 20 m and K=2 , R=10, Angle ratio 0.6-0.4

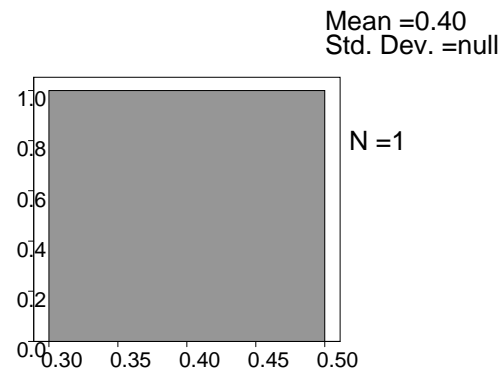
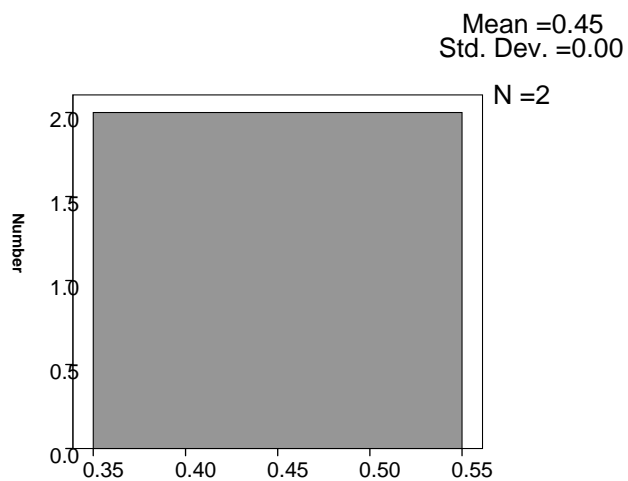


Fig. A-33 Model uncertainty for depth of 20 m and K=2 , R=10, Angle ratio 0.75-0.6

Fig. A-34 Model uncertainty for depth of 20 m and K=2 , R=10, Angle ratio 0.8

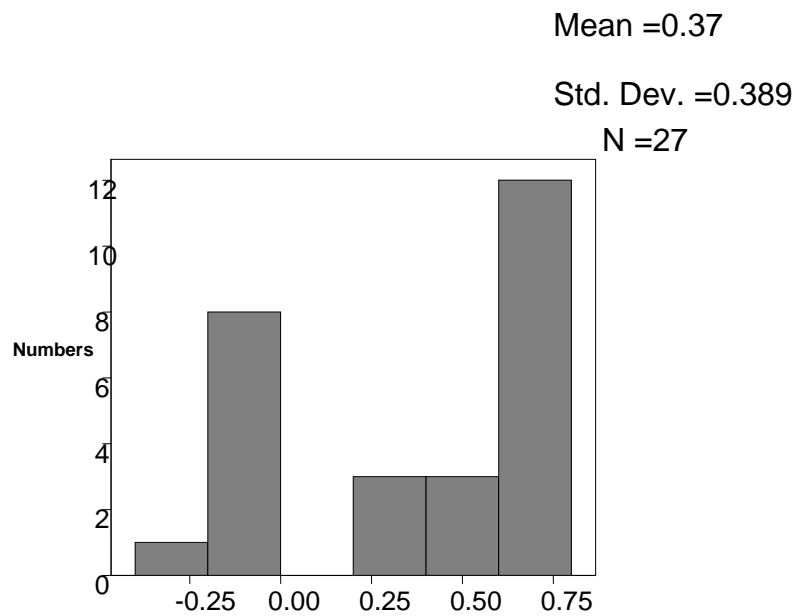


Fig. A-35 Model uncertainty for depth of 100 m and K=0.5

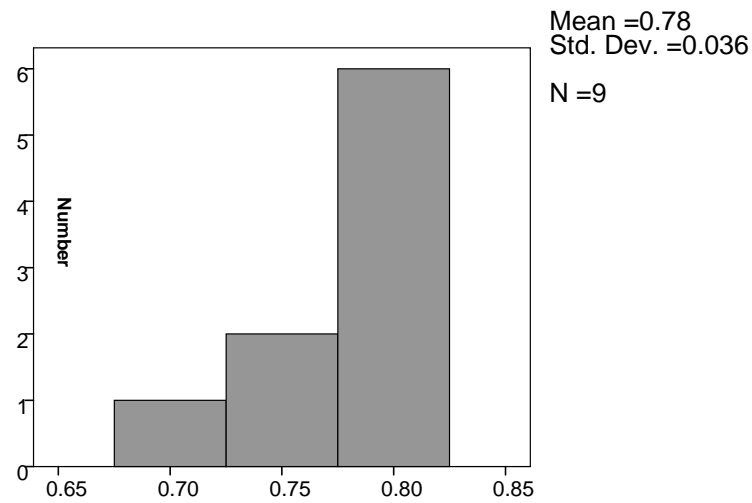


Fig. A-36 Model uncertainty for depth of 100 m and $K=0.5$, $R=1$

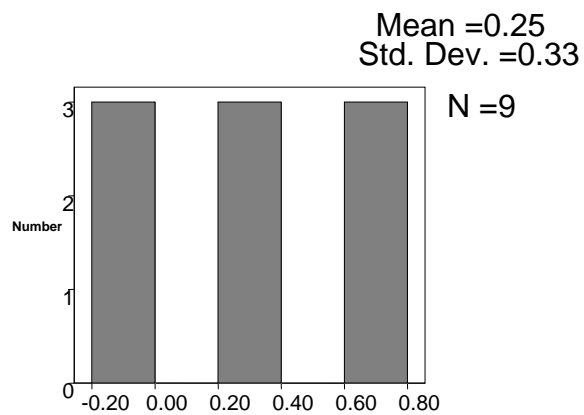


Fig. A-37 Model uncertainty for depth of 100 m and $K=0.5$, $R=5$

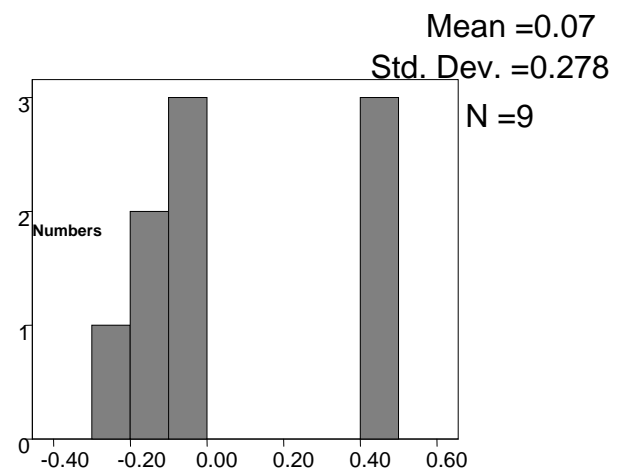


Fig. A-38 Model uncertainty for depth of 100 m and $K=0.5$, $R=10$

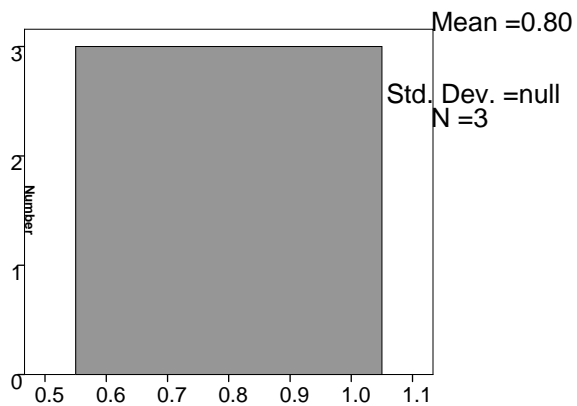


Fig. A-39 Model uncertainty for depth of 100 m and K=0.5 , R=1, Angle ratio 0.3-0.2

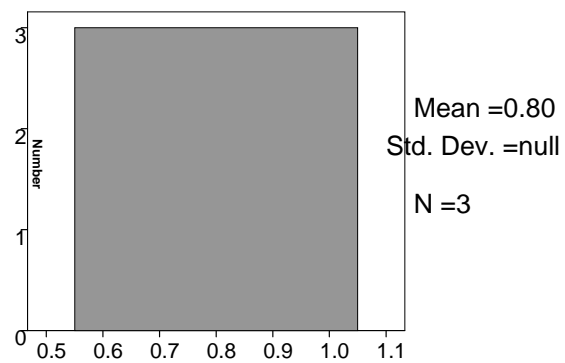


Fig. A-40 Model uncertainty for depth of 100 m and K=0.5 , R=1, Angle ratio 0.4-0.6

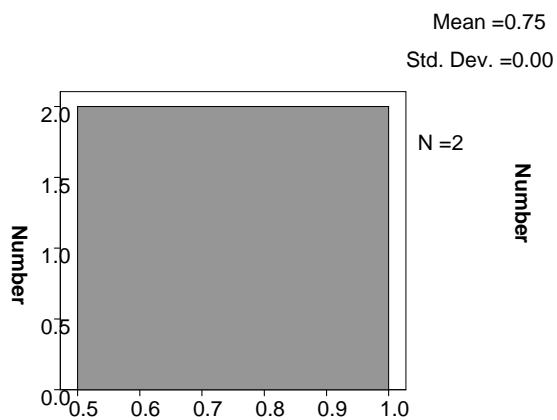


Fig. A-41 Model uncertainty for depth of 100 m and K=0.5 , R=1, Angle ratio 0.75-0.6

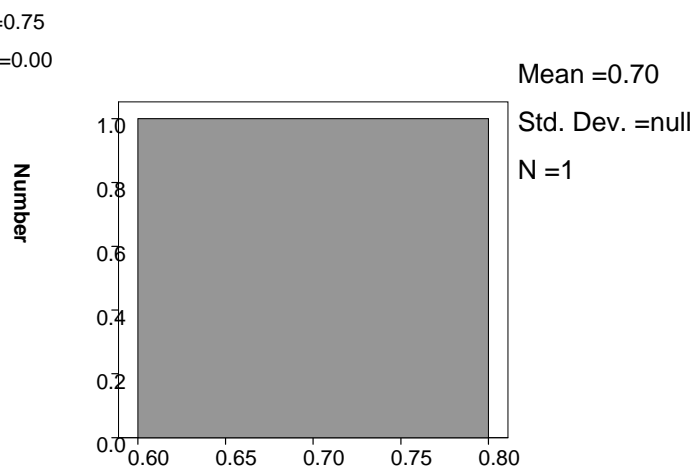


Fig. A-42 Model uncertainty for depth of 100 m and K=0.5 , R=1, Angle ratio 0.8

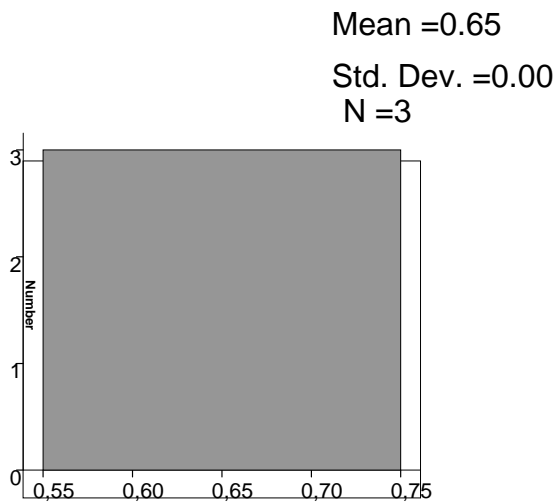


Fig. A-43 Model uncertainty for depth of 100 m and K=0.5 , R=5, Angle ratio 0.3-0.2

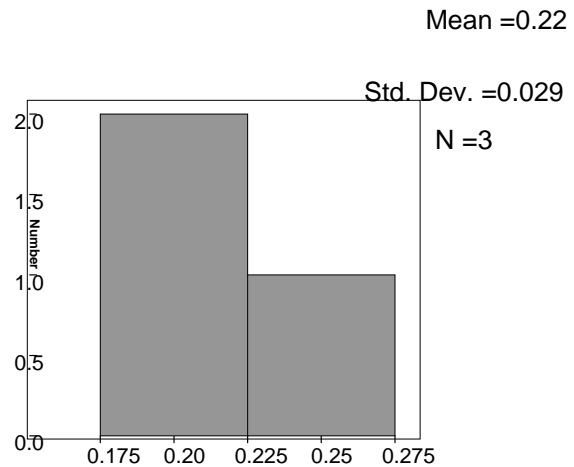


Fig. A-44 Model uncertainty for depth of 100 m and K=0.5 , R=5, Angle ratio 0.6-0.4

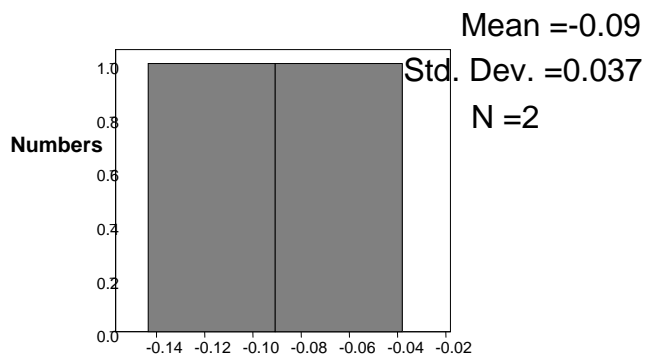


Fig. A-45 Model uncertainty for depth of 100 m and K=0.5 , R=5, Angle ratio 0.75-0.6

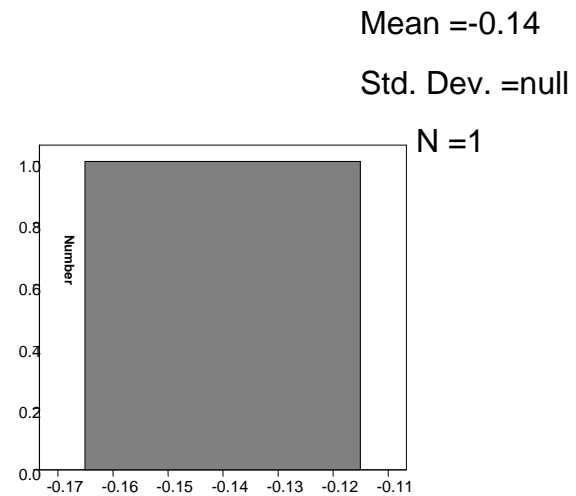


Fig. A-46 Model uncertainty for depth of 100 m and K=0.5 , R=5, Angle ratio 0.8

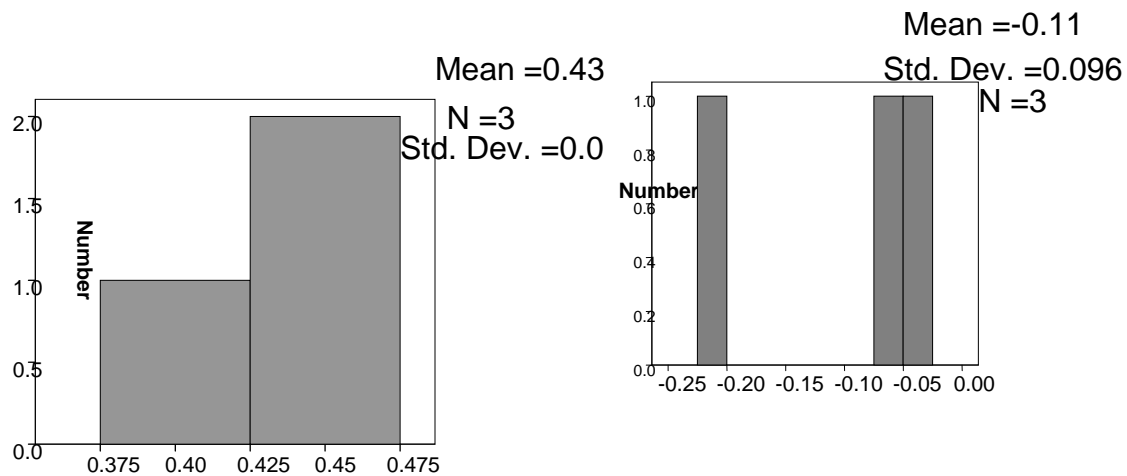


Fig. A-47 Model uncertainty for depth of 100 m and $K=0.5$, $R=10$, Angle ratio 0.3-0.2

Fig. A-48 Model uncertainty for depth of 100 m and $K=0.5$, $R=10$, Angle ratio 0.6-0.4

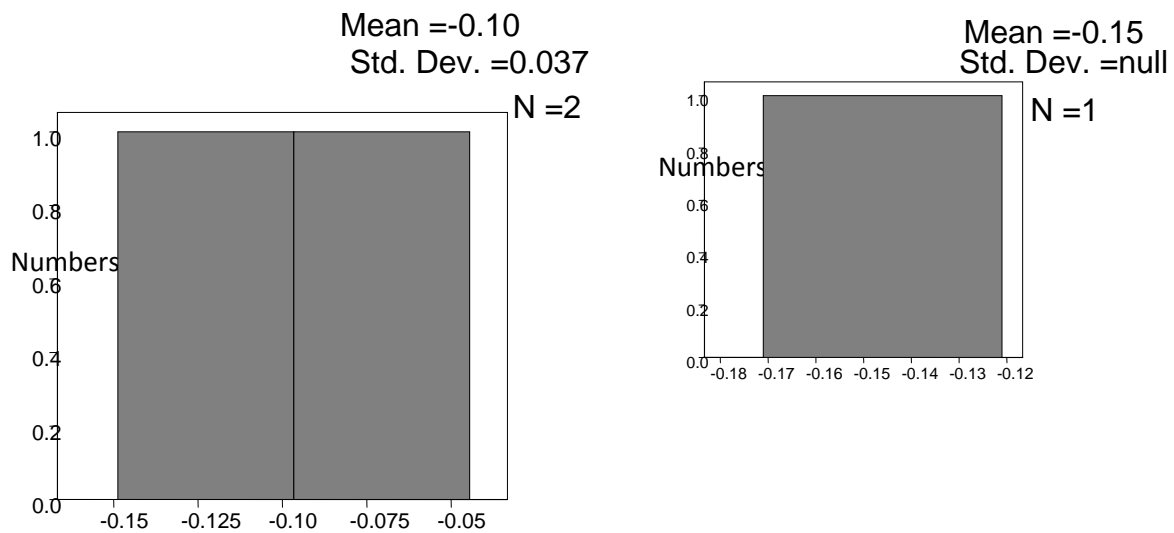


Fig. A-49 Model uncertainty for depth of 100 m and $K=0.5$, $R=10$, Angle ratio 0.75-0.6

Fig. A-50 Model uncertainty for depth of 100 m and $K=0.5$, $R=10$, Angle ratio 0.8

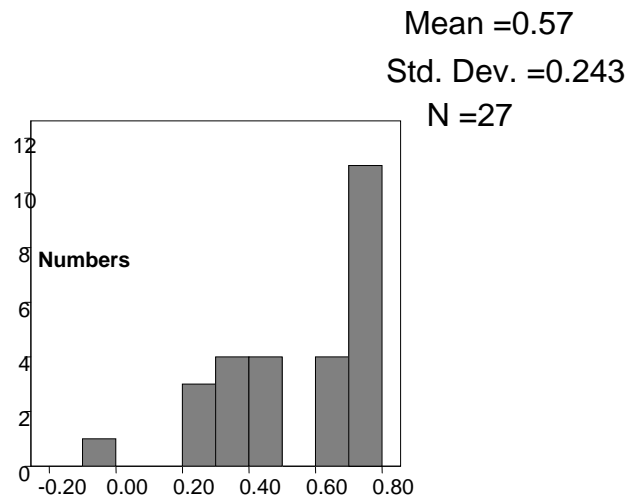


Fig. A-51 Model uncertainty for depth of 100 m and K=1

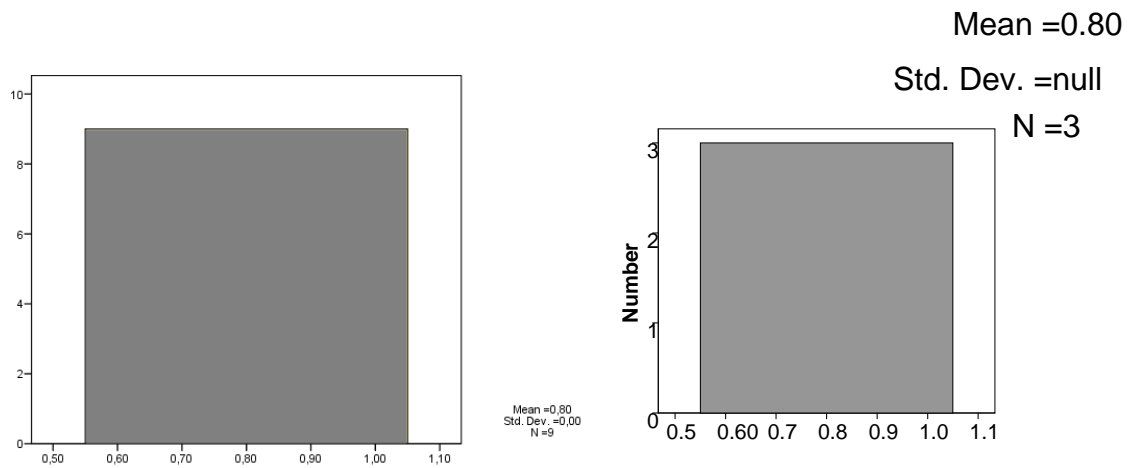


Fig. A-52 Model uncertainty for depth of 100 m and K=1 and R=1

Fig. A-53 Model uncertainty for depth of 100 m and K=1 and R=1, Angle ratio 0.3-0.2

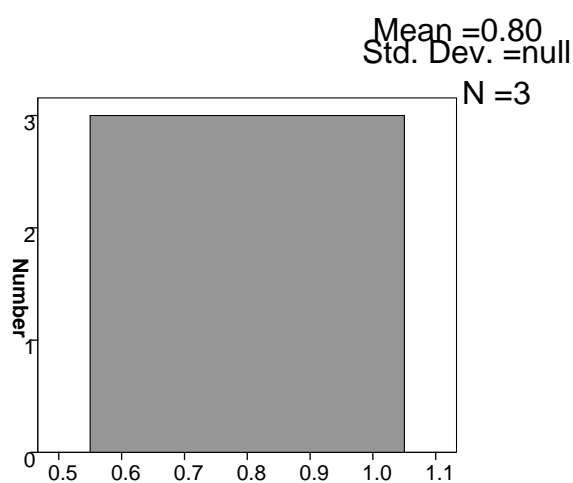


Fig. A-54 Model uncertainty for depth of 100 m and K=1 and R=1, Angle ratio 0.6-0.4

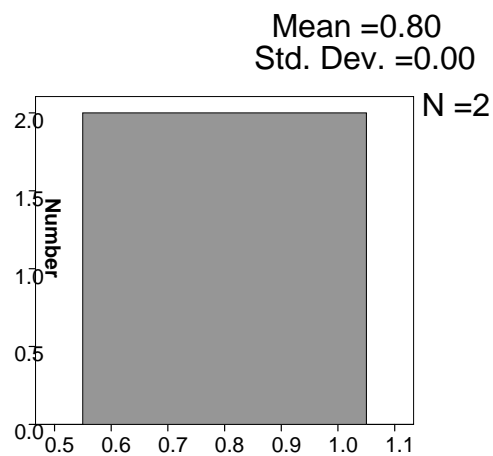


Fig. A-55 Model uncertainty for depth of 100 m and K=1 and R=1, Angle ratio 0.75-0.6

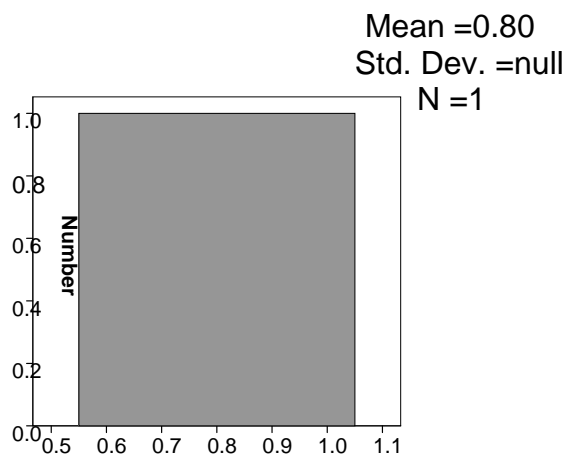


Fig. A-56 Model uncertainty for depth of 100 m and K=1 and R=1, Angle ratio 0.8

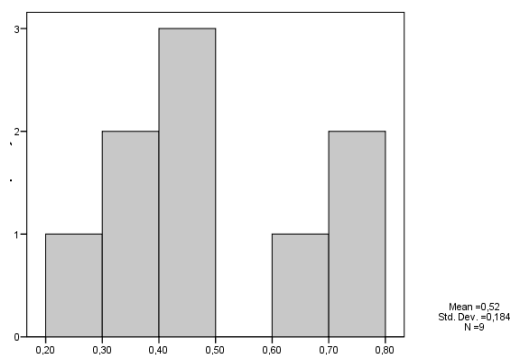


Fig. A-57 Model uncertainty for depth of 100 m and K=1 and R=5

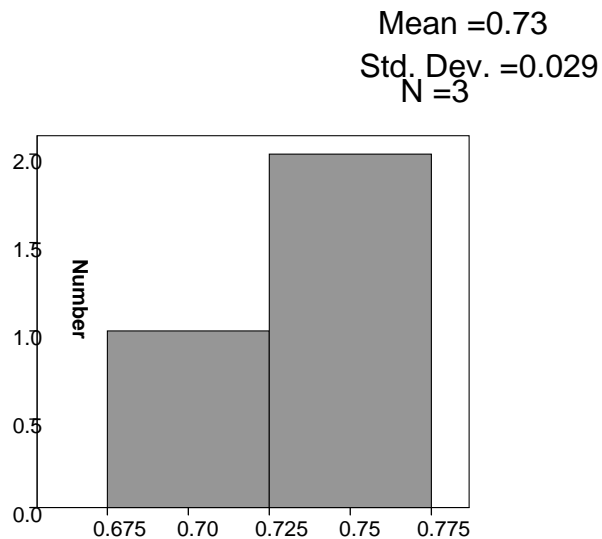


Fig. A-58 Model uncertainty for depth of 100 m and K=1 and R=5, angle ratio 0.3-0.2

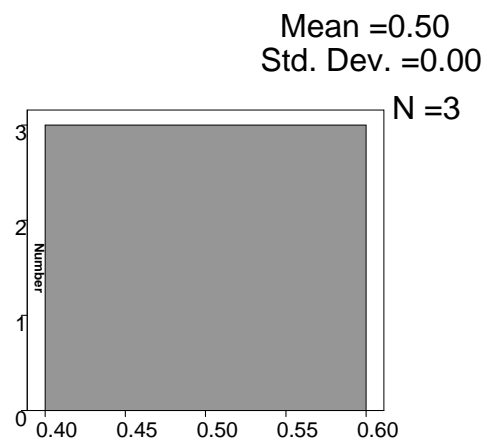


Fig. A-59 Model uncertainty for depth of 100 m and K=1 and R=5 Angle ratio 0.6-0.4

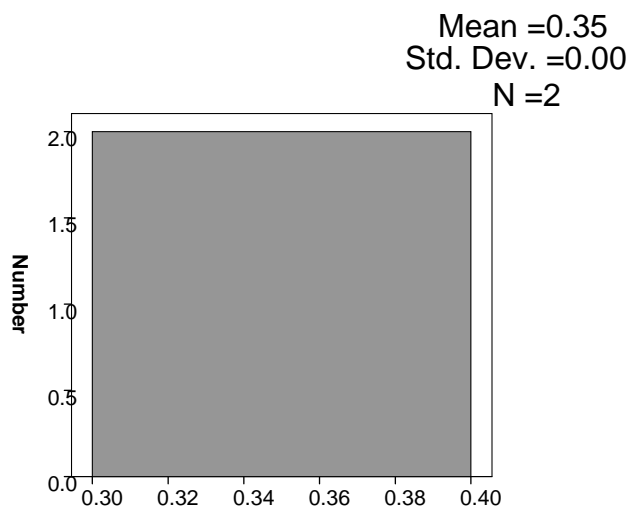


Fig. A-60 Model uncertainty for depth of 100 m and K=1 and R=5, angle ratio 0.75-0.6

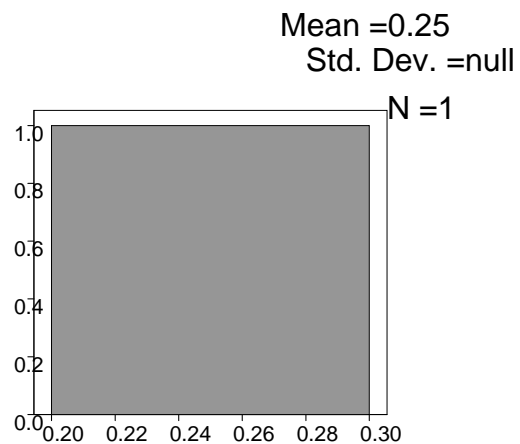


Fig. A-61 Model uncertainty for depth of 100 m and K=1 and R=5, Angle ratio 0.8

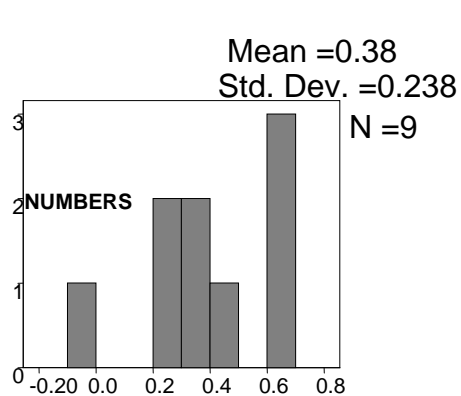


Fig. A-62 Model uncertainty for depth of 100 m and K=1 and R=10

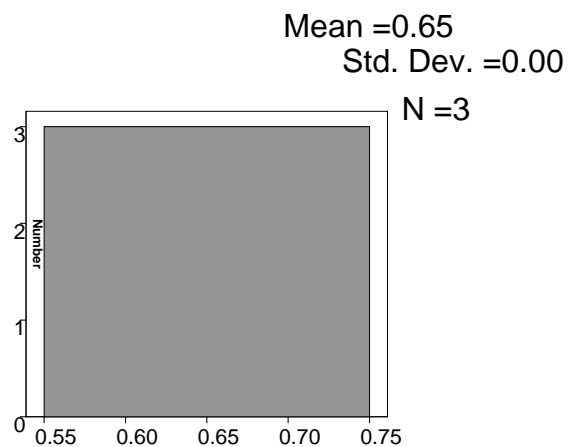


Fig. A-63 Model uncertainty for depth of 100 m and K=1 and R=10, Angle ratio 0.3-0.2

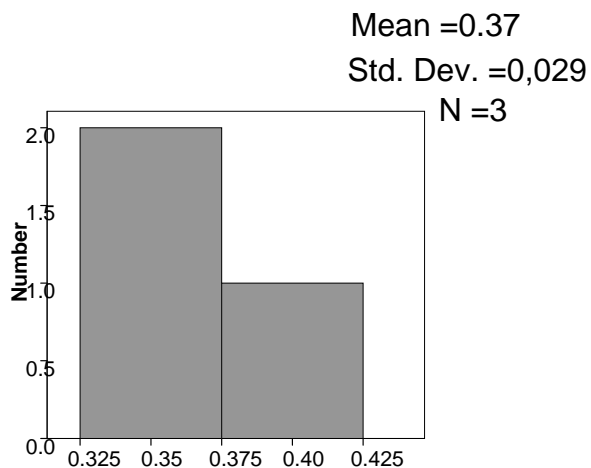


Fig. A-64 Model uncertainty for depth of 100 m and K=1 and R=10, angle ratio 0.6-0.4

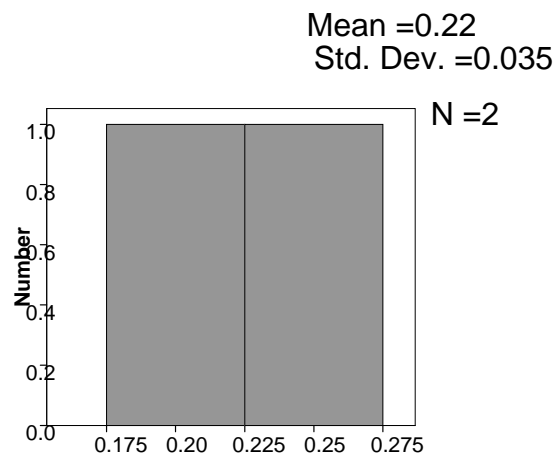


Fig. A-65 Model uncertainty for depth of 100 m and K=1 and R=10, angle ratio 0.75-0.6

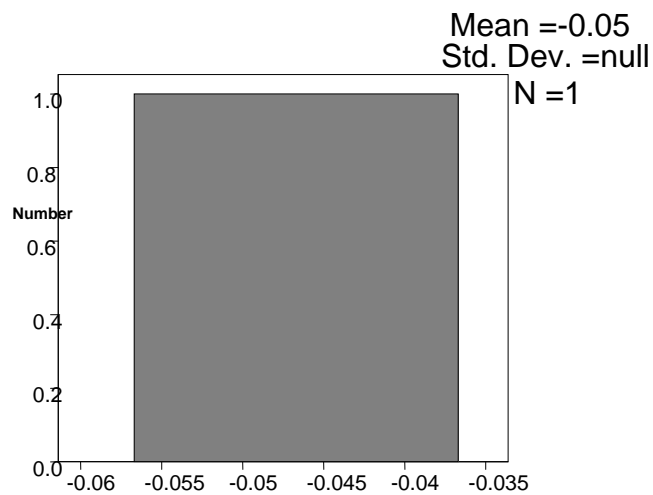


Fig. A-66 Model uncertainty for depth of 100 m and K=1 and R=10, angle ratio 0.8

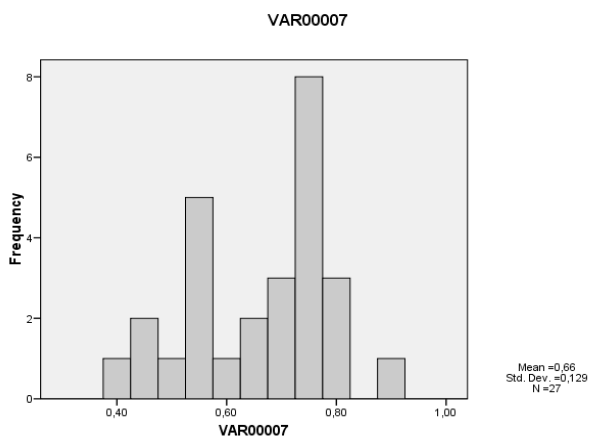


Fig. A-67 Model uncertainty for depth of 100 m and K=2

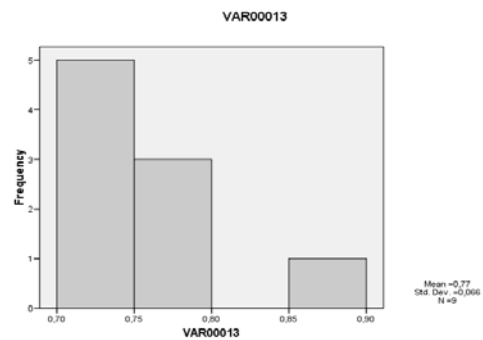


Fig. A-68 Model uncertainty for depth of 100 m and K=2, R=1

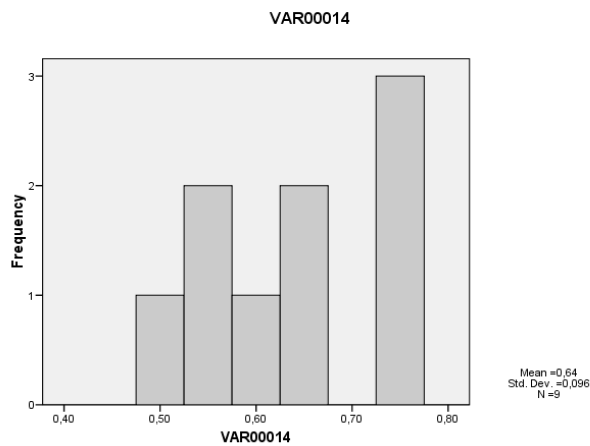


Fig. A-69 Model uncertainty for depth of 100 m and K=2 , R=5

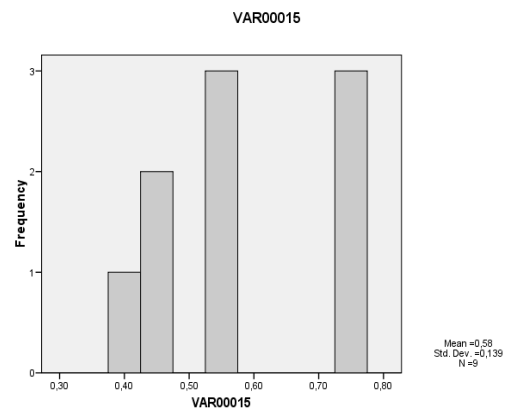


Fig. A-70 Model uncertainty for depth of 100 m and K=2 , R=10

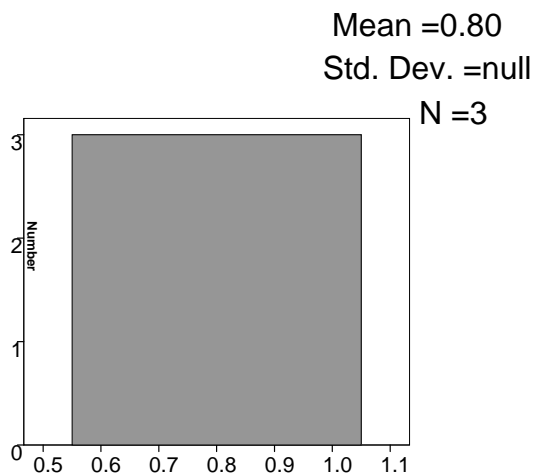


Fig. A-71 Model uncertainty for depth of 100 m and K=2 , R=1, Angle ratio 0.3-0.2

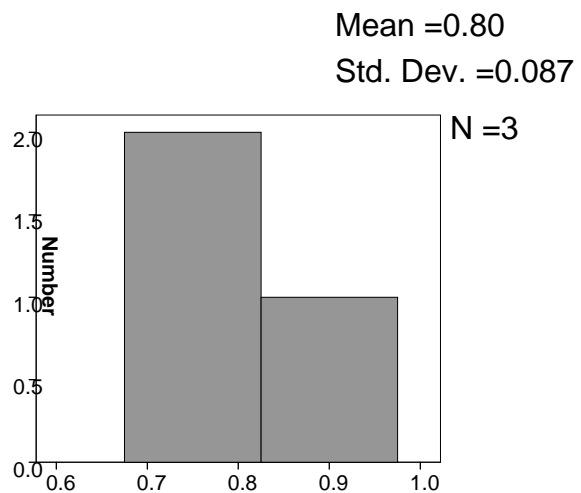


Fig. A-72 Model uncertainty for depth of 100 m and K=2 , R=1, Angle ratio 0.4-0.6

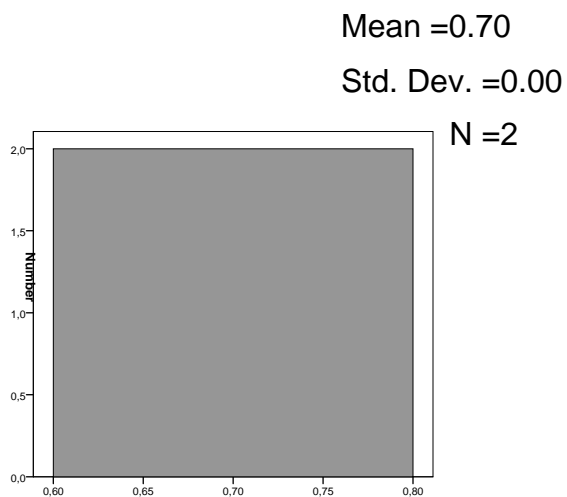


Fig. A-73 Model uncertainty for depth of 100 m and K=2 , R=1, Angle ratio 0.75-0.6

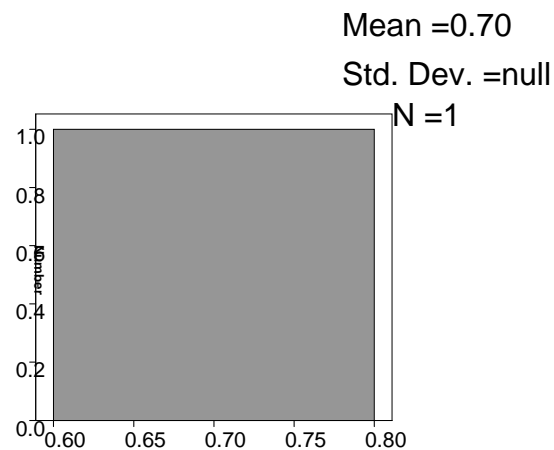


Fig. A-74 Model uncertainty for depth of 100 m and K=2 , R=1, Angle ratio 0.8

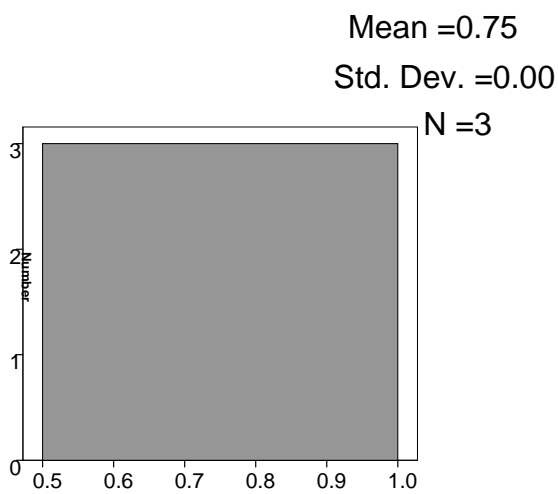


Fig. A-75 Model uncertainty for depth of 100 m and K=2 , R=5, Angle ratio 0.3-0.2

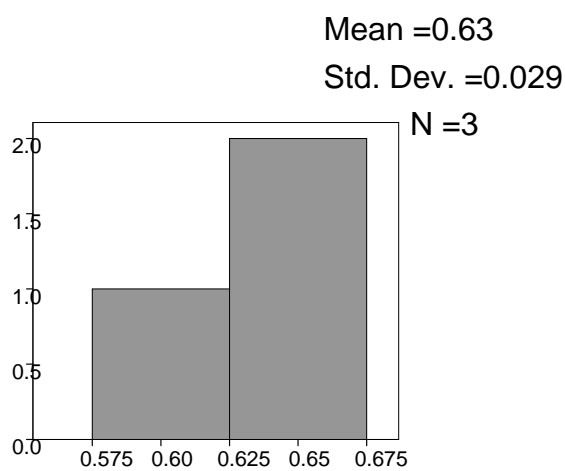


Fig. A-76 Model uncertainty for depth of 100 m and K=2 , R=5, Angle ratio 0.6-0.4

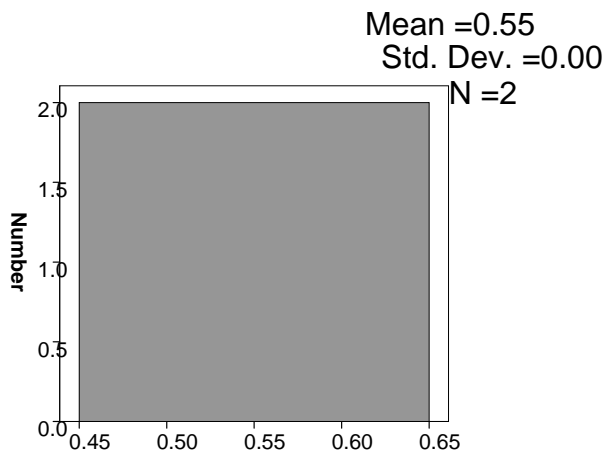


Fig. A-77 Model uncertainty for depth of 100 m and K=2 , R=5, Angle ratio 0.75-0.6

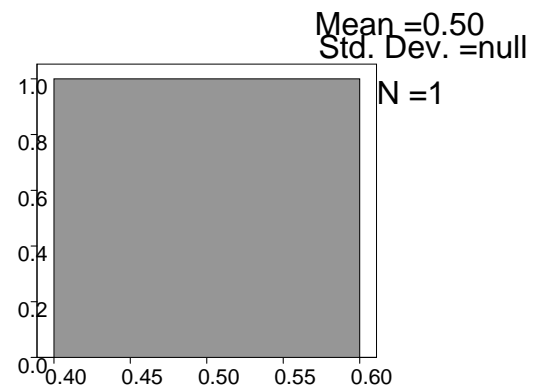


Fig. A-78 Model uncertainty for depth of 100 m and K=2 , R=5, Angle ratio 0.8

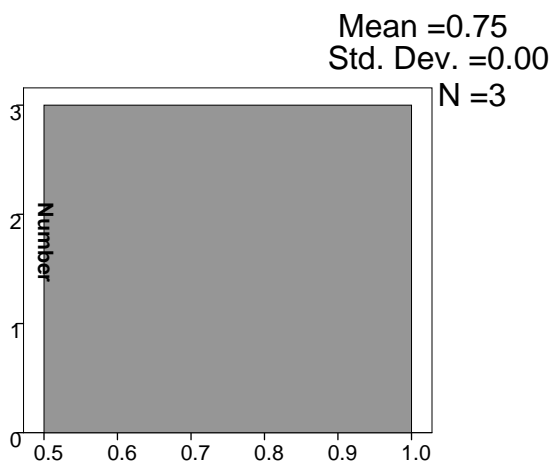


Fig. A-79 Model uncertainty for depth of 100 m and K=2 , R=10, Angle ratio 0.3-0.2

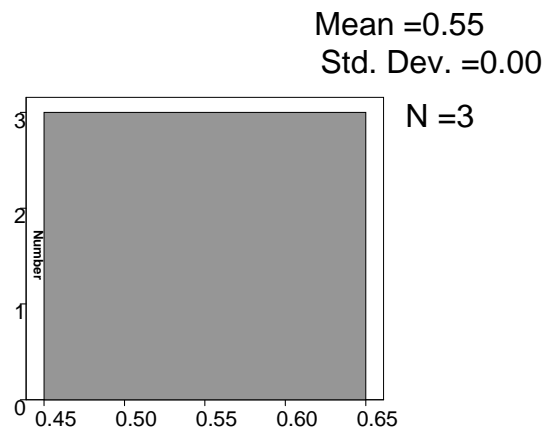


Fig. A-80 Model uncertainty for depth of 100 m and K=2 , R=10, Angle ratio 0.6-0.4

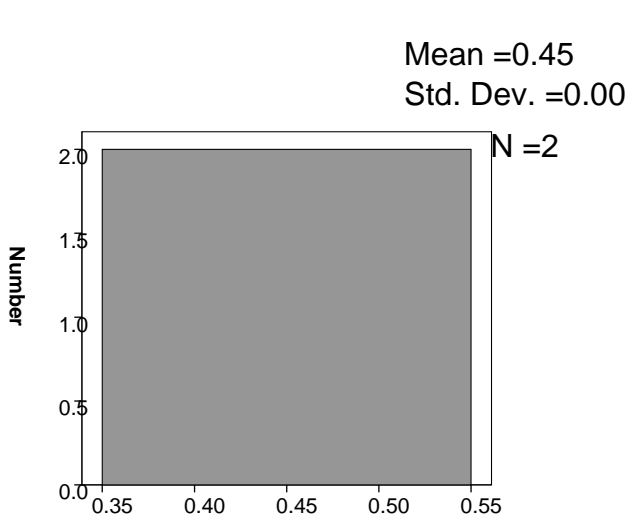


Fig. A-81 Model uncertainty for depth of 100 m and K=2 , R=10, Angle ratio 0.75-0.6

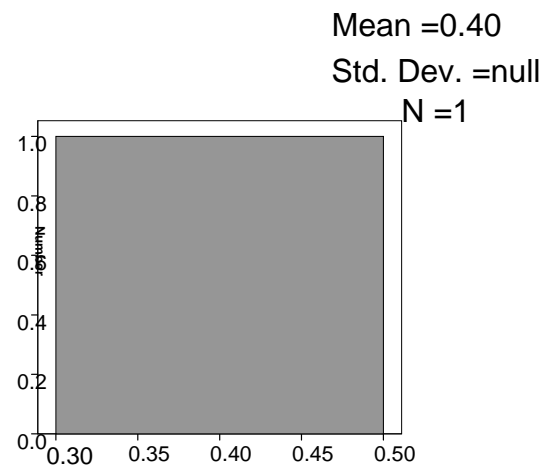


Fig. A-82 Model uncertainty for depth of 100 m and K=2 , R=10, Angle ratio 0.8

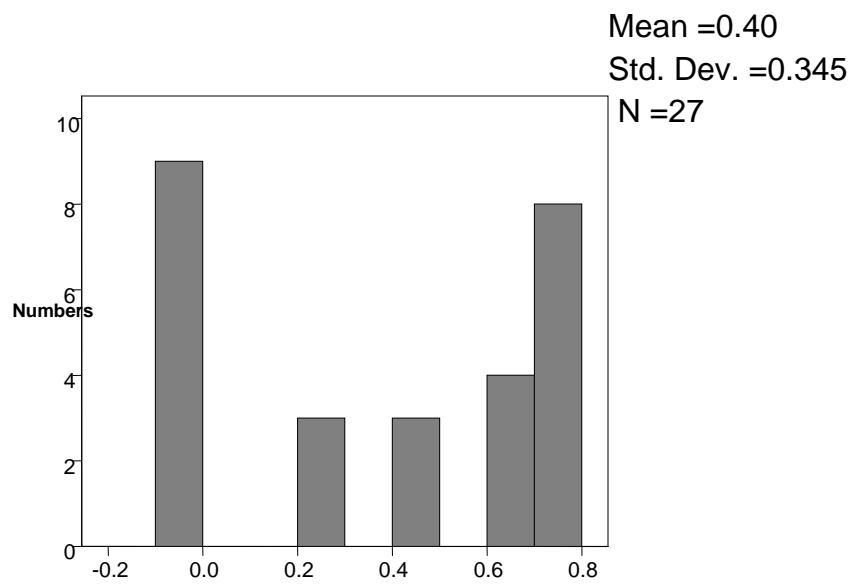


Fig. A-83 Model uncertainty for depth of 400 m and K=0.5

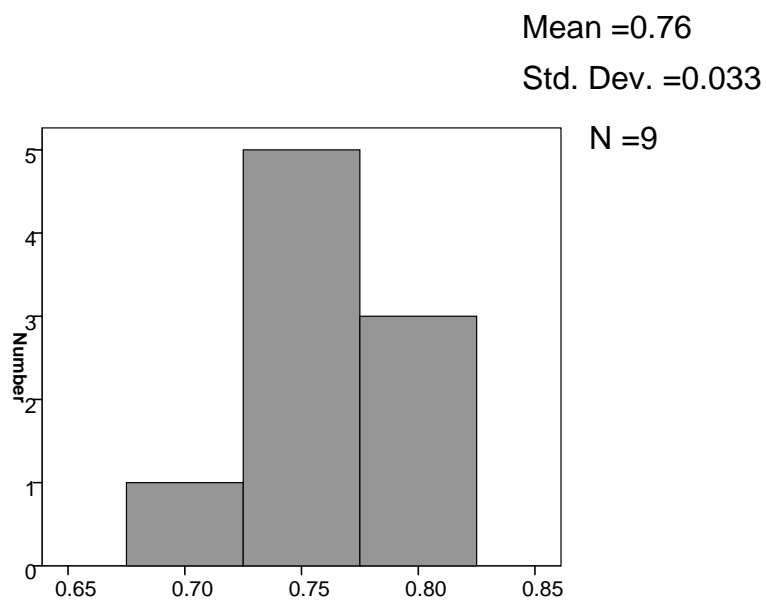


Fig. A-84 Model uncertainty for depth of 400 m and K=0.5 , R=1

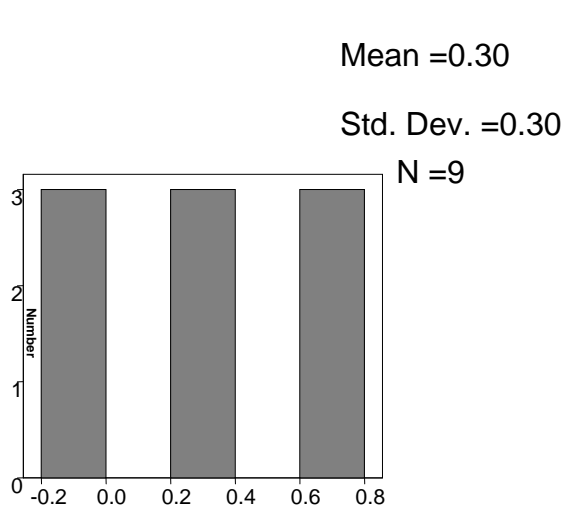


Fig. A-85 Model uncertainty for depth of 400 m and K=0.5 , R=5

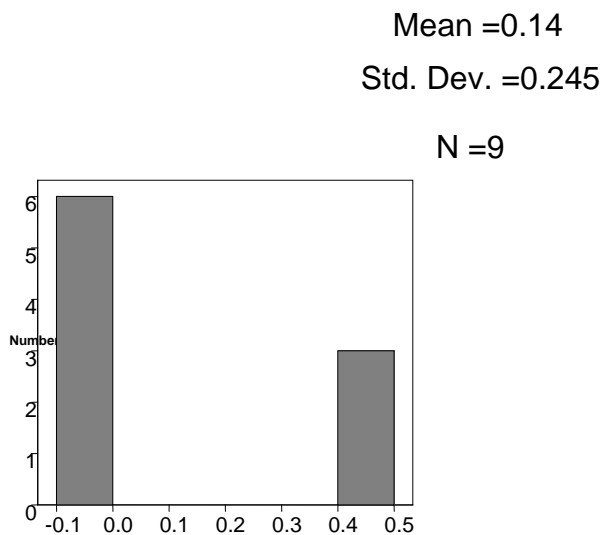


Fig. A-86 Model uncertainty for depth of 400 m and K=0.5 , R=10

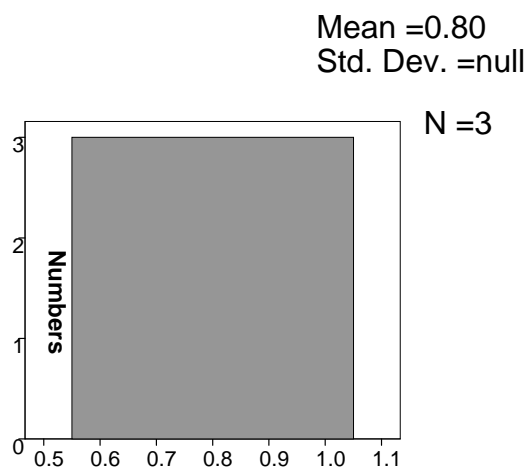


Fig. A-87 Model uncertainty for depth of 400 m and K=0.5 , R=1, Angle ratio 0.3-0.2

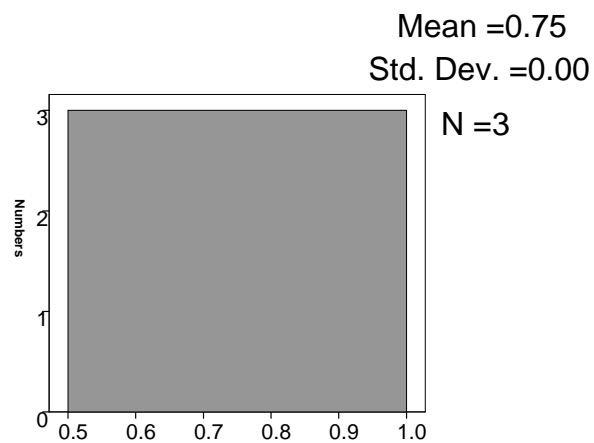


Fig. A-88 Model uncertainty for depth of 400 m and K=0.5 , R=1, Angle ratio 0.4-0.6

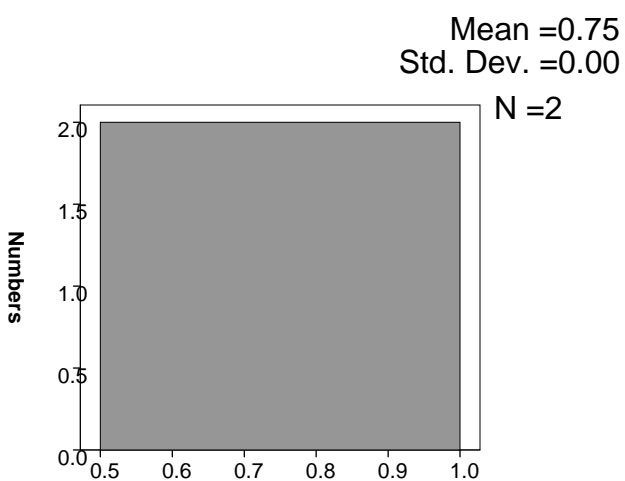


Fig. A-89 Model uncertainty for depth of 400 m and K=0.5 , R=1, Angle ratio 0.75-0.6

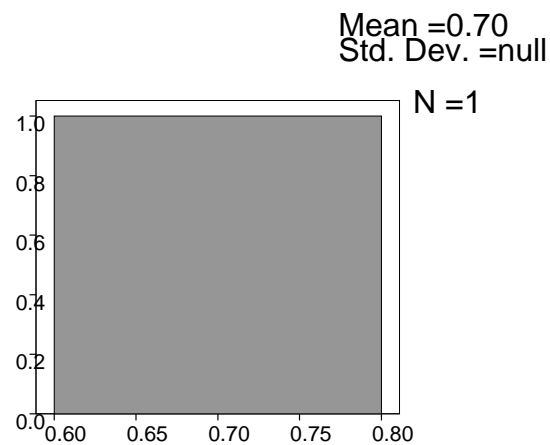


Fig. A-90 Model uncertainty for depth of 400 m and K=0.5 , R=1, Angle ratio 0.8

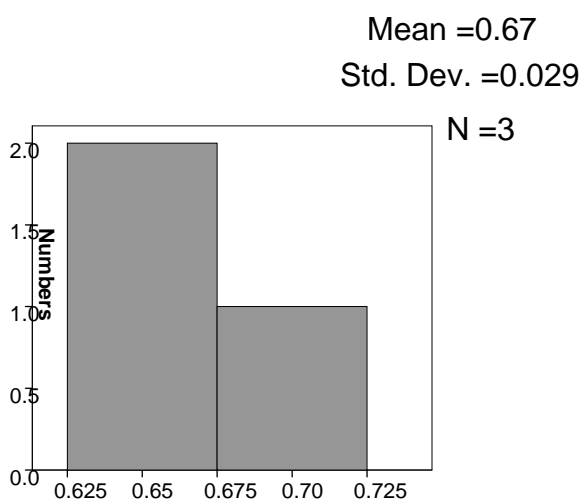


Fig. A-91 Model uncertainty for depth of 400 m and K=0.5 , R=5, Angle ratio 0.3-0.2

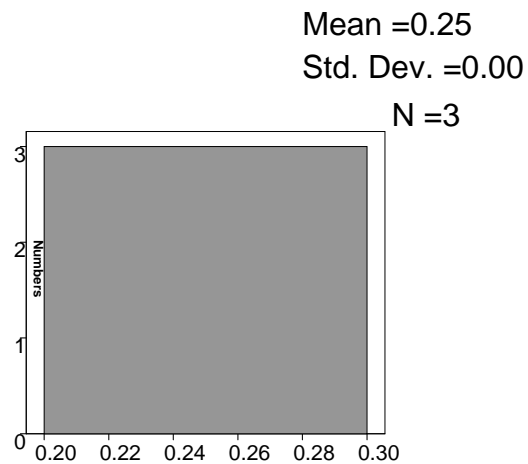


Fig. A-92 Model uncertainty for depth of 400 m and K=0.5 , R=5, Angle ratio 0.6-0.4

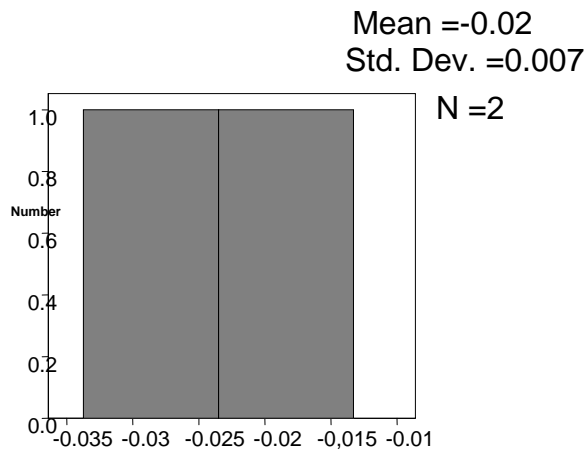


Fig. A-93 Model uncertainty for depth of 400 m and K=0.5 , R=5, Angle ratio 0.75-0.6

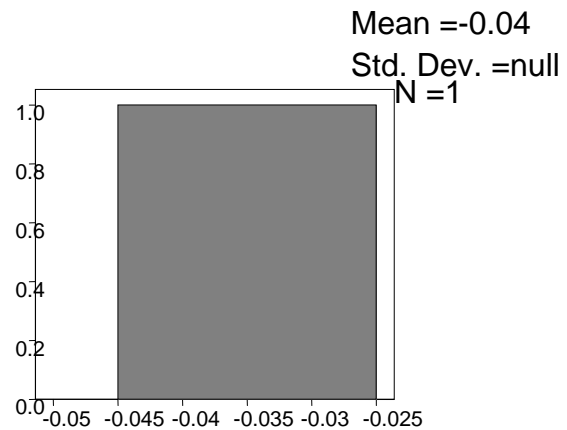


Fig. A-94 Model uncertainty for depth of 400 m and K=0.5 , R=5, Angle ratio 0.8

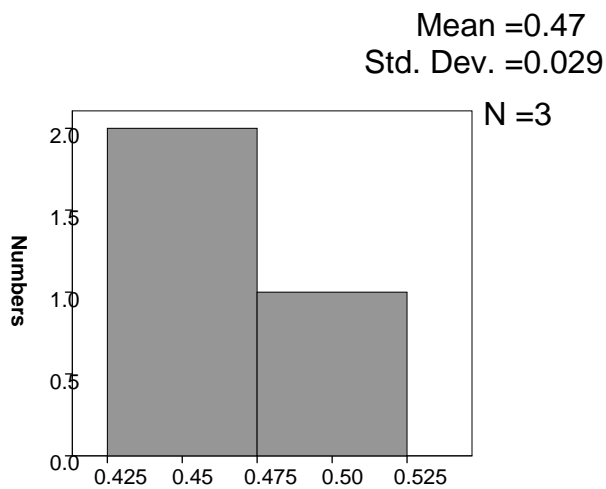


Fig. A-95 Model uncertainty for depth of 400 m and K=0.5 , R=10, Angle ratio 0.3-0.2

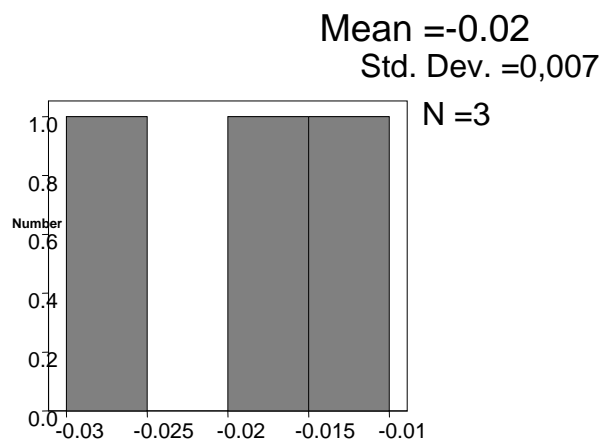


Fig. A-96 Model uncertainty for depth of 400 m and K=0.5 , R=10, Angle ratio 0.6-0.4

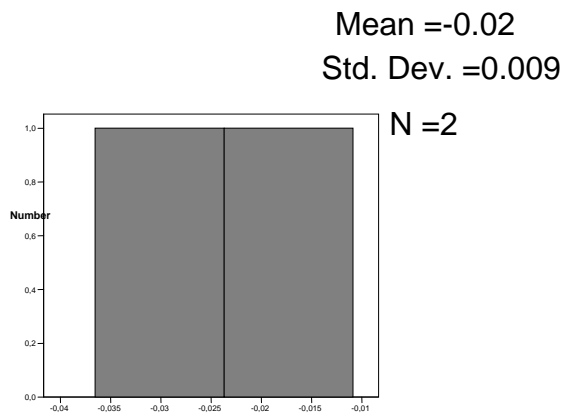


Fig. A-97 Model uncertainty for depth of 400 m and K=0.5 , R=10, Angle ratio 0.75-0.6

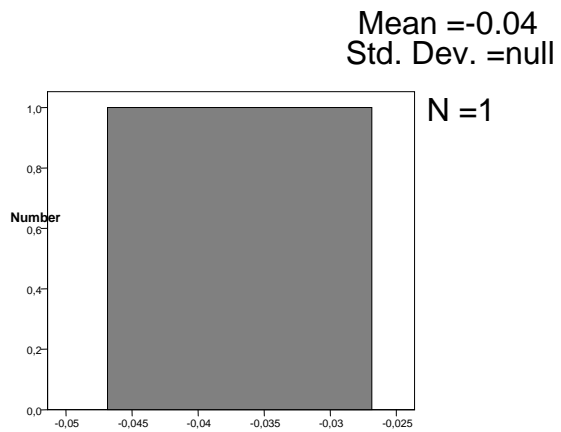


Fig. A-98 Model uncertainty for depth of 400 m and K=0.5 , R=10, Angle ratio 0.8

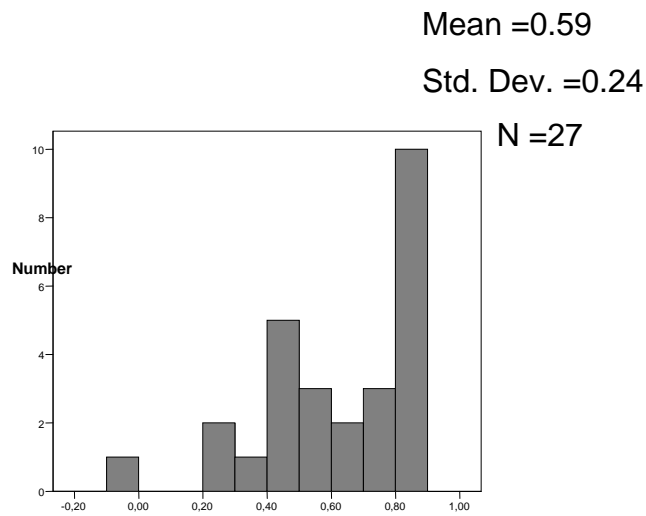


Fig. A-99 Model uncertainty for depth of 400 m and K=1

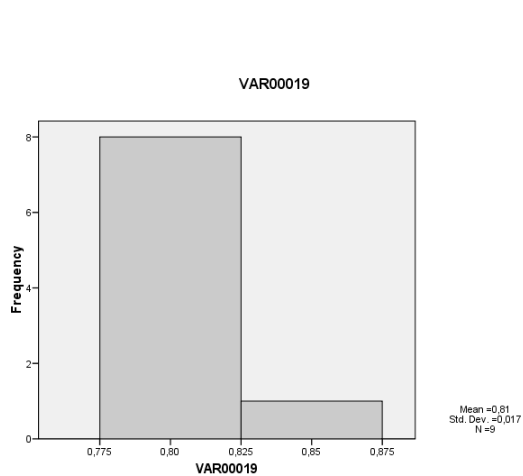


Fig. A-100 Model uncertainty for depth of 400 m and K=1 and R=1

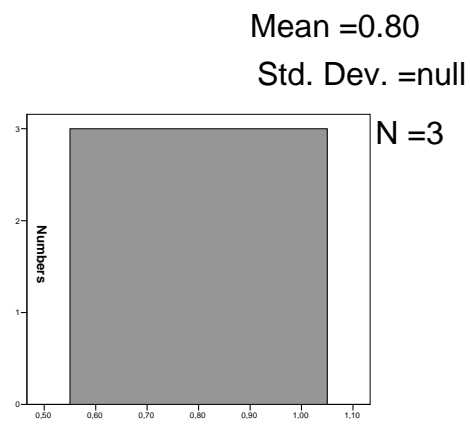


Fig. A-101 Model uncertainty for depth of 400 m and K=1 and R=1, Angle ratio 0.3-0.2

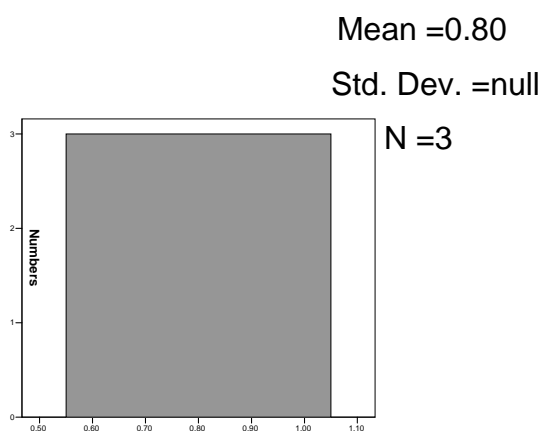


Fig. A-102 Model uncertainty for depth of 400 m and K=1 and R=1, Angle ratio 0.6-0.4

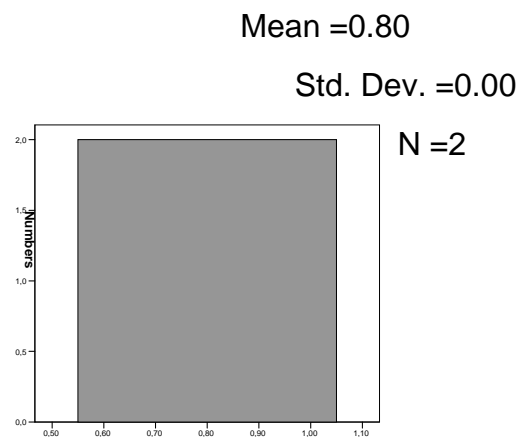


Fig. A-103 Model uncertainty for depth of 400 m and K=1 and R=1, Angle ratio 0.75-0.6

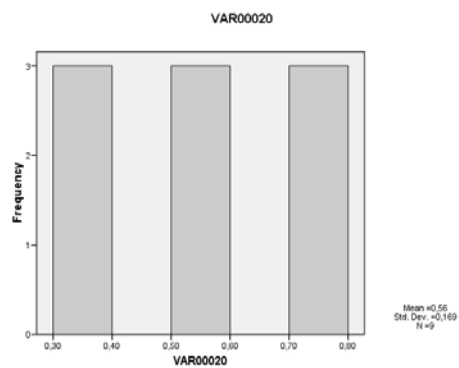
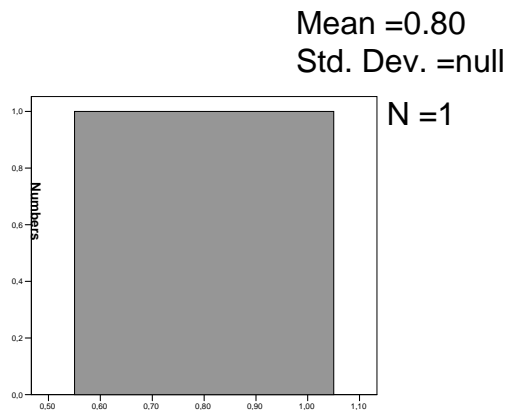


Fig. A-104 Model uncertainty for depth of 400 m and K=1 and R=1, Angle ratio 0.8

Fig. A-105 Model uncertainty for depth of 400 m and K=1 and R=5

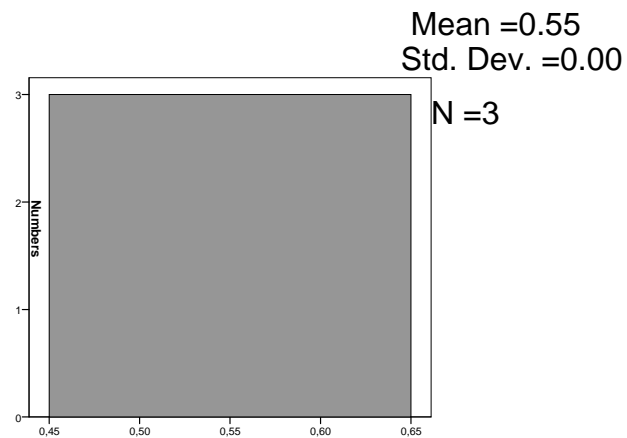
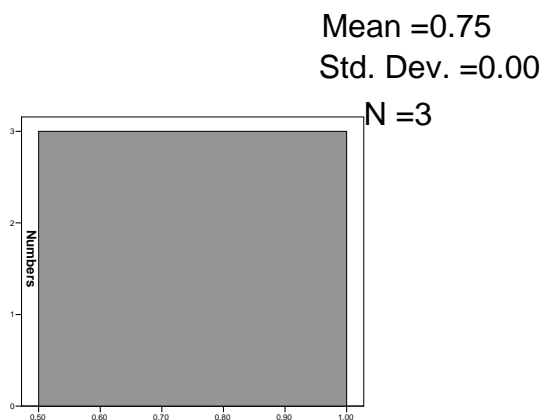


Fig. A-106 Model uncertainty for depth of 400 m and K=1 and R=5, angle ratio 0.3-0.2

Fig. A-107 Model uncertainty for depth of 400 m and K=1 and R=5 Angle ratio 0.6-0.4

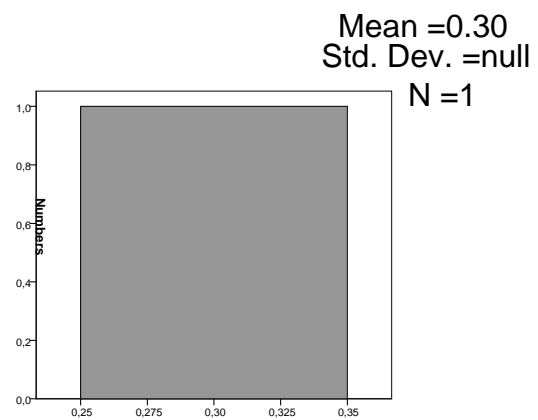
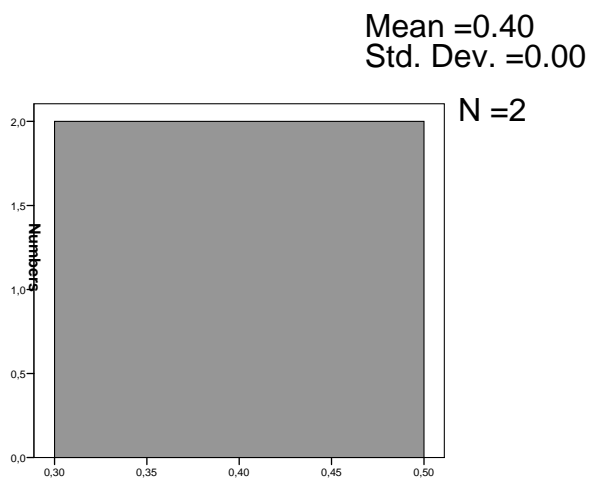


Fig. A-108 Model uncertainty for depth of 400 m and K=1 and R=5, angle ratio 0.75-0.6

Fig. A-109 Model uncertainty for depth of 400 m and K=1 and R=5, Angle ratio 0.8

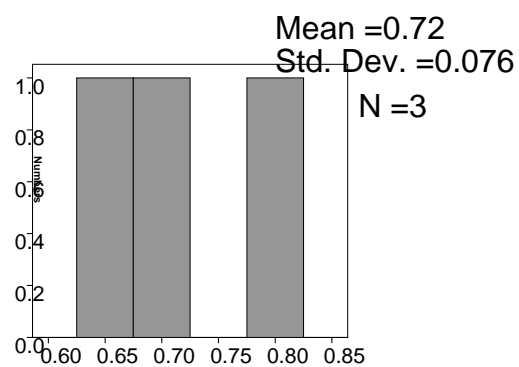
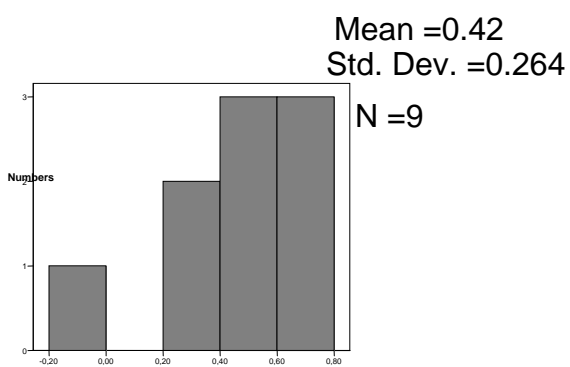


Fig. A-110 Model uncertainty for depth of 400 m and K=1 and R=10

Fig. A-111 Model uncertainty for depth of 400 m and K=1 and R=10, Angle ratio 0.3-0.2

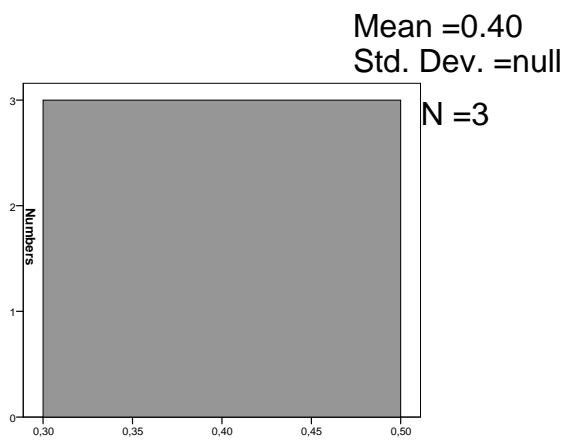


Fig. A-112 Model uncertainty for depth of 400 m and K=1 and R=10, angle ratio 0.6-0.4

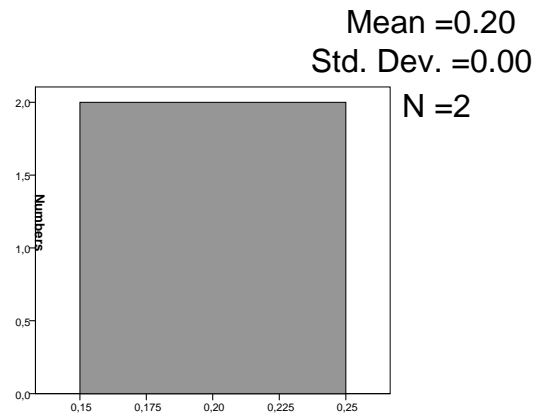


Fig. A-113 Model uncertainty for depth of 400 m and K=1 and R=10, angle ratio 0.75-0.6

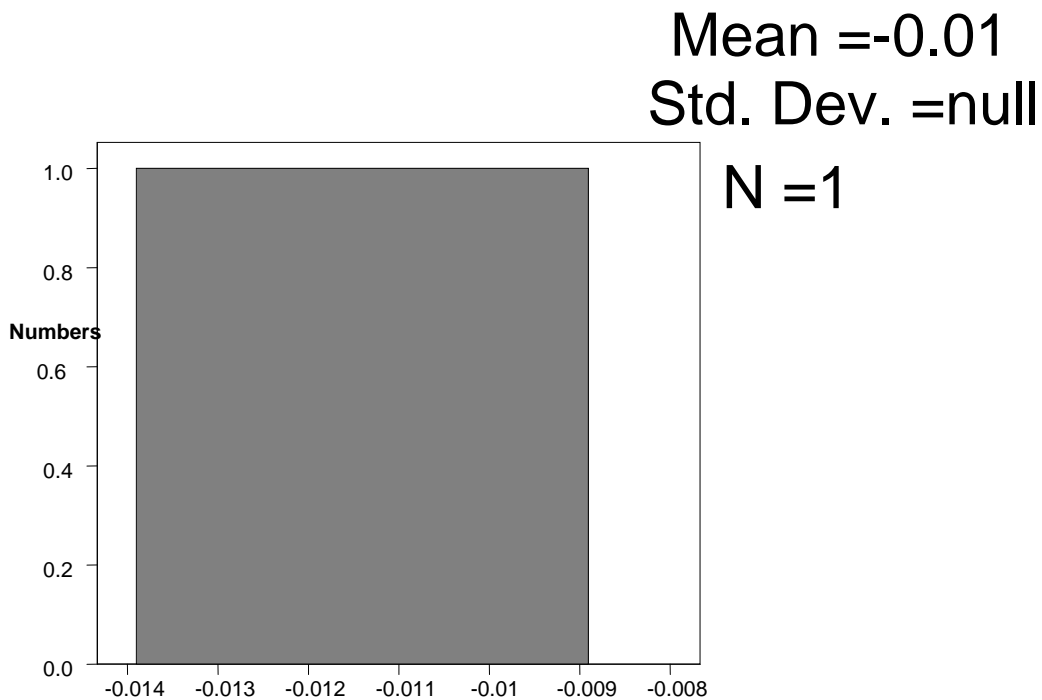


Fig. A-114 Model uncertainty for depth of 400 m and K=1 and R=10, angle ratio 0.8

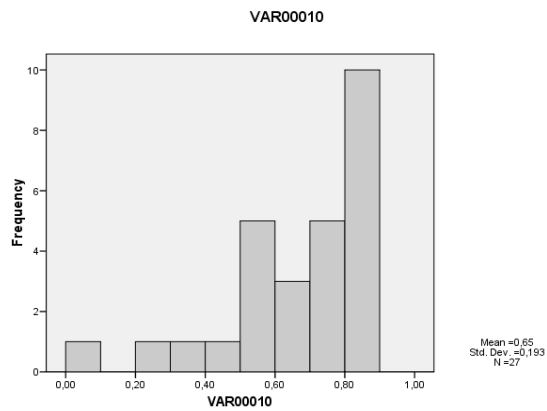


Fig. A-115 Model uncertainty for depth of 400 m and K=2

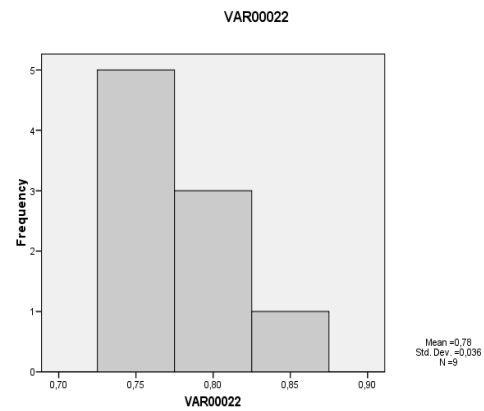


Fig. A-116 Model uncertainty for depth of 400 m and K=2 , R=1

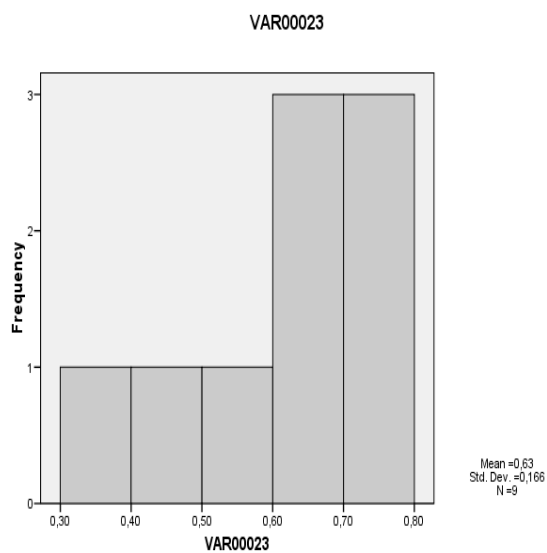


Fig. A-117 Model uncertainty for depth of 400 m and K=2 , R=5

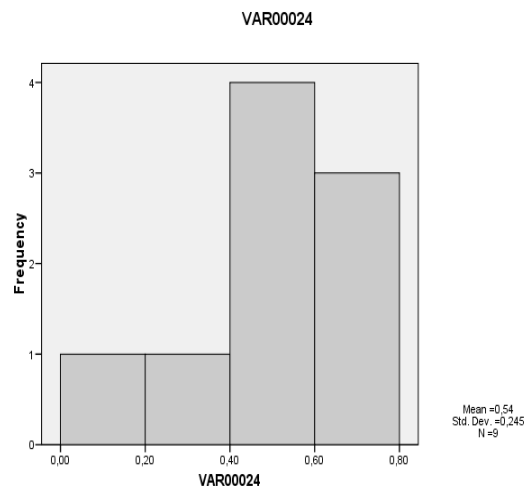


Fig. A-118 Model uncertainty for depth of 400 m and K=2 , R=10

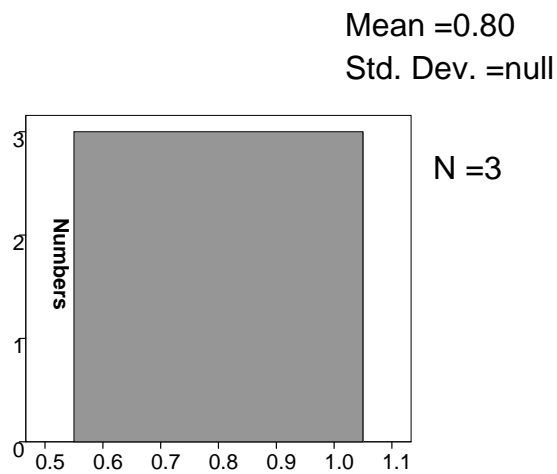


Fig. A-119 Model uncertainty for depth of 400 m and K=2 , R=1, Angle ratio 0.3-0.2

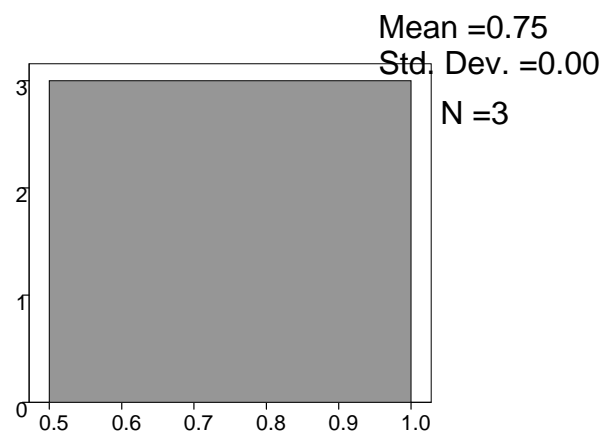


Fig. A-120 Model uncertainty for depth of 400 m and K=2 , R=1, Angle ratio 0.4-0.6

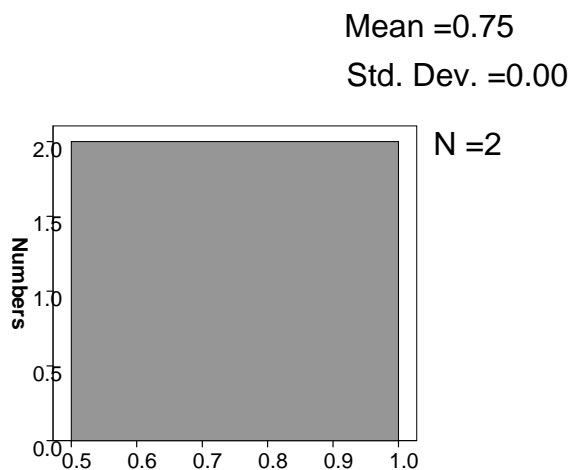


Fig. A-121 Model uncertainty for depth of 400 m and K=2 , R=1, Angle ratio 0.75-0.6

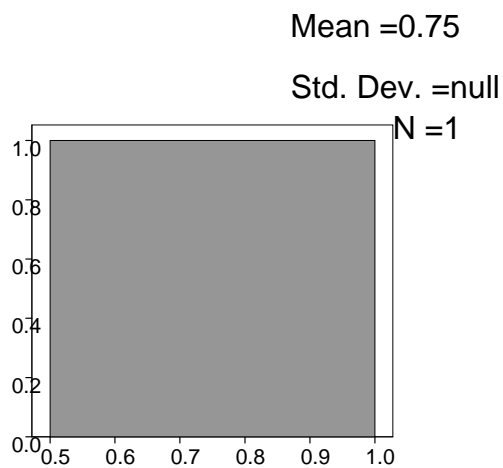


Fig. A-122 Model uncertainty for depth of 400 m and K=2 , R=1, Angle ratio 0.8

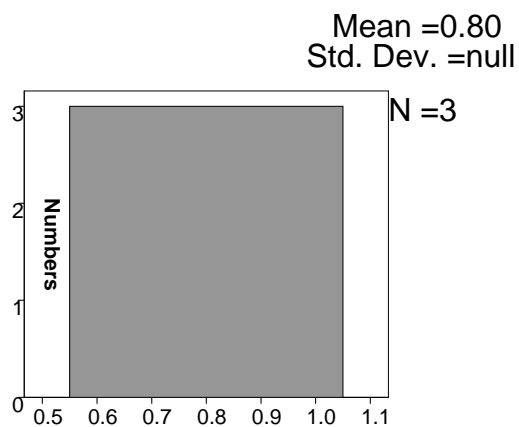


Fig. A-123 Model uncertainty for depth of 400 m and K=2 , R=5, Angle ratio 0.3-0.2

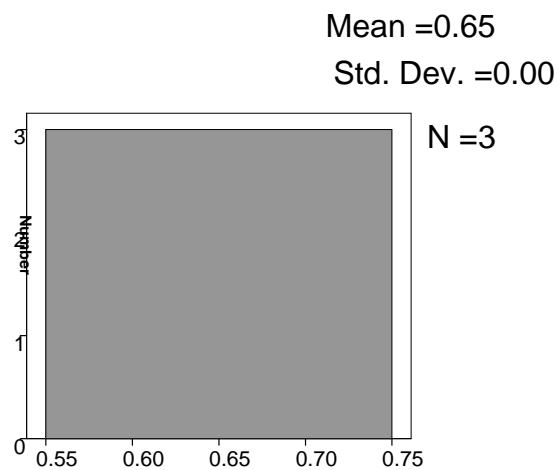


Fig. A-124 Model uncertainty for depth of 400 m and K=2 , R=5, Angle ratio 0.6-0.4

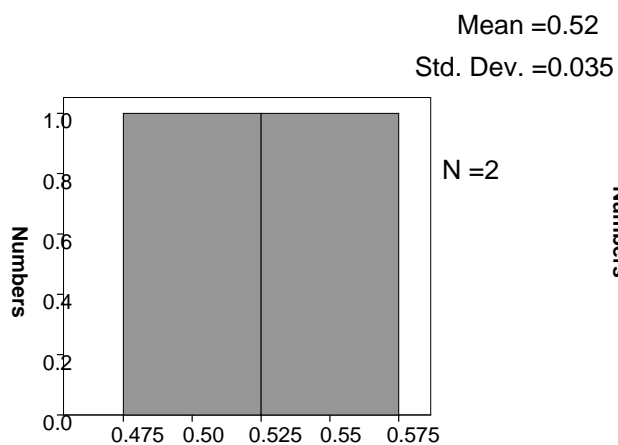


Fig. A-125 Model uncertainty for depth of 400 m and K=2 , R=5, Angle ratio 0.75-0.6

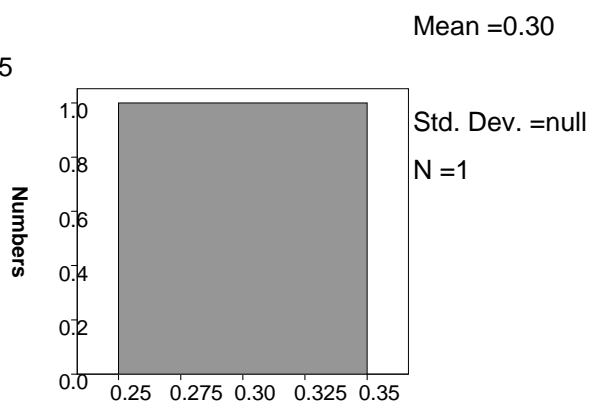


Fig. A-126 Model uncertainty for depth of 400 m and K=2 , R=5, Angle ratio 0.8

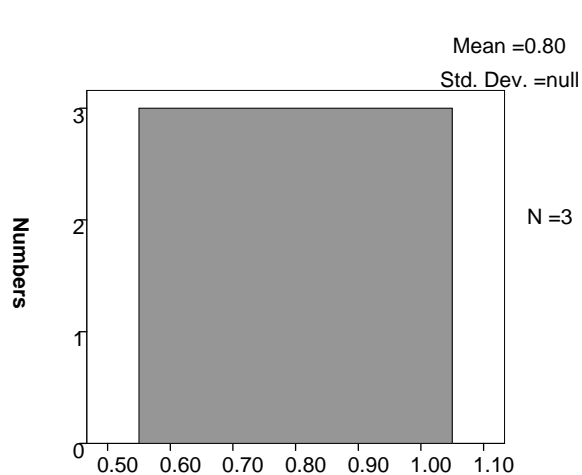


Fig. A-127 Model uncertainty for depth of 400 m and K=2 , R=10, Angle ratio 0.3-0.2

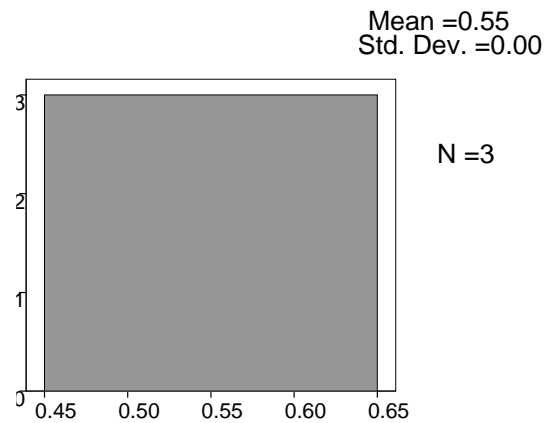


Fig. A-128 Model uncertainty for depth of 400 m and K=2 , R=10, Angle ratio 0.6-0.4

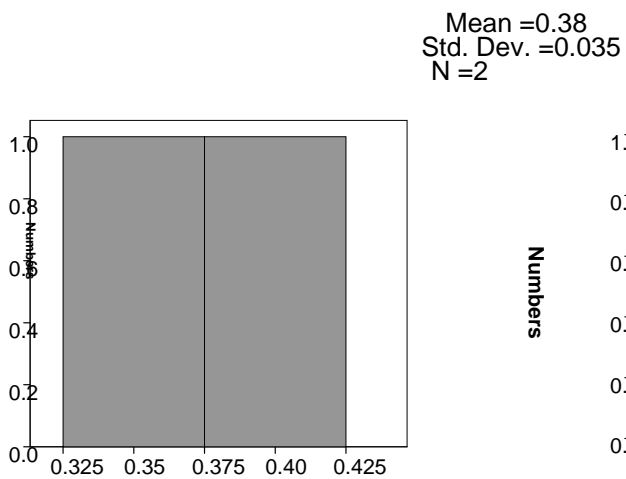


Fig. A-129 Model uncertainty for depth of 400 m and K=2 , R=10, Angle ratio 0.75-0.6

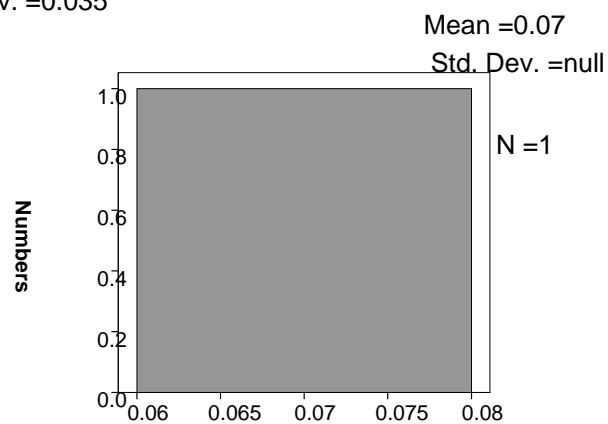


Fig. A-130 Model uncertainty for depth of 400 m and K=2 , R=10, Angle ratio 0.8